

Complex Nanostructures in Triblock Terpolymer Thin Films

Dissertation

Zur Erlangung des akademischen Grades eines
Doktors der Naturwissenschaften (Dr. rer. nat.)
im Fach Chemie der Fakultät für Biologie, Chemie und Geowissenschaften
der Universität Bayreuth

vorgelegt von

Sabine Ludwigs

geboren in Köln

Bayreuth, 2004

Die vorliegende Arbeit wurde in der Zeit von März 2002 bis Mai 2004 an der Universität Bayreuth am Lehrstuhl für Physikalische Chemie II unter der Betreuung von Herrn Prof. Dr. Georg Krausch angefertigt.

Vollständiger Abdruck der von der Fakultät für Biologie, Chemie und Geowissenschaften der Universität Bayreuth genehmigten Dissertation zur Erlangung des akademischen Grades eines Doktors der Naturwissenschaften (Dr. rer. nat.)

Promotionsgesuch eingereicht am: 12.05.2004

Wissenschaftliches Kolloquium am: 28.07.2004

Prüfungsausschuß

Prof. Dr. G. Krausch (Erstgutachter)

Prof. Dr. M. Ballauff (Zweitgutachter)

Prof. Dr. A. H. E. Müller

Prof. Dr. R. Schobert

Prof. Dr. H.-W. Schmidt (Vorsitzender)

Dekan: Prof. Dr. O. Meyer

Table of Contents

1. Introduction.....	1
1.1. Microphase separation in block copolymers.....	1
1.2. Thin film phase behavior of block copolymers.....	2
1.3. Polymer-analogous reactions to amphiphilic block copolymers.....	4
1.4. Synthesis and bulk phase behavior of investigated polymers.....	5
1.5. Objectives of this thesis.....	7
1.6. References.....	8
2. Overview of thesis – Results.....	11
2.1. Experiments on thin film phase behavior.....	11
2.1.1. Methods.....	11
2.1.2. Results.....	14
2.2. Comparison of mesoscale simulations with experiments.....	17
2.2.1. Methods.....	17
2.2.2. Results.....	17
2.3. From functional nanostructures towards possible applications.....	20
2.3.1. Methods.....	20
2.3.2. Results.....	21
2.4. pH-dependent nanostructures.....	24
2.4.1. Methods.....	24
2.4.2. Results.....	26
2.5. Individual contributions of joint publications.....	29
2.6. References.....	31
3. Publications.....	33
3.1. Combinatorial mapping of the phase behavior of ABC triblock terpolymers in thin films: experiments.....	33
3.1.1. Results and discussion.....	39
3.1.2. Conclusion.....	55
3.2. Phase behavior of ABC triblock terpolymers in thin films: mesoscale simulations.....	59
3.2.1. Results and discussion.....	64
3.2.2. Conclusion.....	79
3.3. Self-assembly of functional nanostructures from ABC triblock copolymers.....	83

3.4. pH-dependent nanostructures in thin films.....	93
3.4.1. Results and discussion.....	98
3.4.2. Conclusion.....	107
4. Summary / Zusammenfassung.....	111
5. Appendix.....	117
5.1. Publication on bulk phase behavior of the investigated polymers.....	117
5.2. Curriculum vitae.....	135
5.3. List of publications.....	137
5.4. Presentations at international conferences.....	138

1. Introduction

In this thesis a systematic and general scheme is presented to study the fundamentals of microdomain formation of ABC triblock terpolymers in thin films. Via controlling the structure formation process tailored nanostructures are formed. These structures might be a promising material for lithographic masks, nanoporous membranes, or pH-responsive nanostructures.

1.1. Microphase separation in block copolymers

Block copolymers consist of two or more chemically different polymer blocks which are covalently linked together to form a larger, more complex macromolecule. If the constituent polymers are immiscible, microphase separation is induced on a scale that is related to the size of the copolymer chains. Depending on the segmental interactions, the polymer molecular weight, and the volumetric composition, different microdomain structures are formed with typical length scales in the range between 10 and 100 nm.^{1,2} Diblock copolymers which have blocks of comparable volume fractions exhibit a lamella structure. Upon decreasing or increasing the volume fraction of one block gyroid, cylindrical, and spherical microdomains are formed, Figure 1.

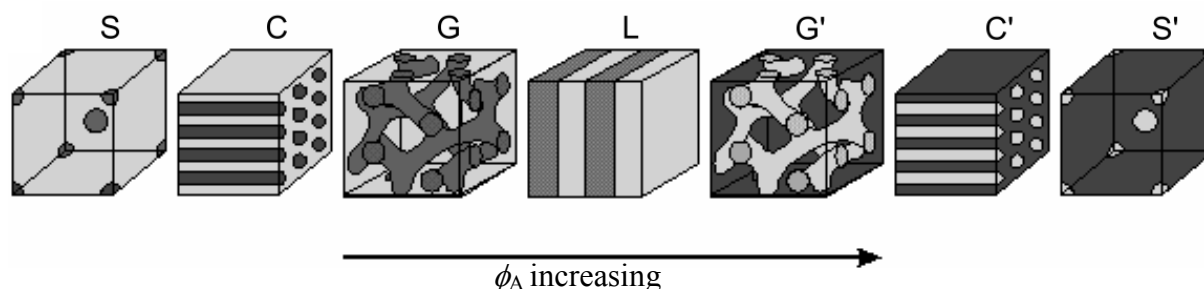


Figure 1. Thermodynamic equilibrium morphologies in AB diblock copolymers depending on the volume fraction of component A (ϕ_A). S: spheres, arranged in a body centered cubic lattice; C: cylinders, arranged on a hexagonal lattice; G: gyroid, bicontinuous double-gyroid phase; L: lamella structure.

While much of the previous work has been concentrated on block copolymers consisting of two components, the insertion of a third block widely enlarges the structural diversity.^{1,3,4} The morphology of ABC triblock terpolymers is influenced by the molecular weight, three interaction parameters ϵ_{AB} , ϵ_{AC} , ϵ_{BC} , and two independent composition variables ϕ_A and ϕ_B ($\phi_C = 1 - (\phi_A + \phi_B)$). Also the chain topology has been shown to control the phase behavior in the bulk.^{5,6,7,8,9} Due to this large number of independent molecular parameters triblock terpolymers show a large variety of morphologies.

As an example, the different morphologies in poly(styrene)-*block*-poly(butadiene)-*block*-poly(methyl methacrylate) triblock terpolymers discovered by Stadler and coworkers are summarized in Figure 2.^{10,11,12,13,14,15}

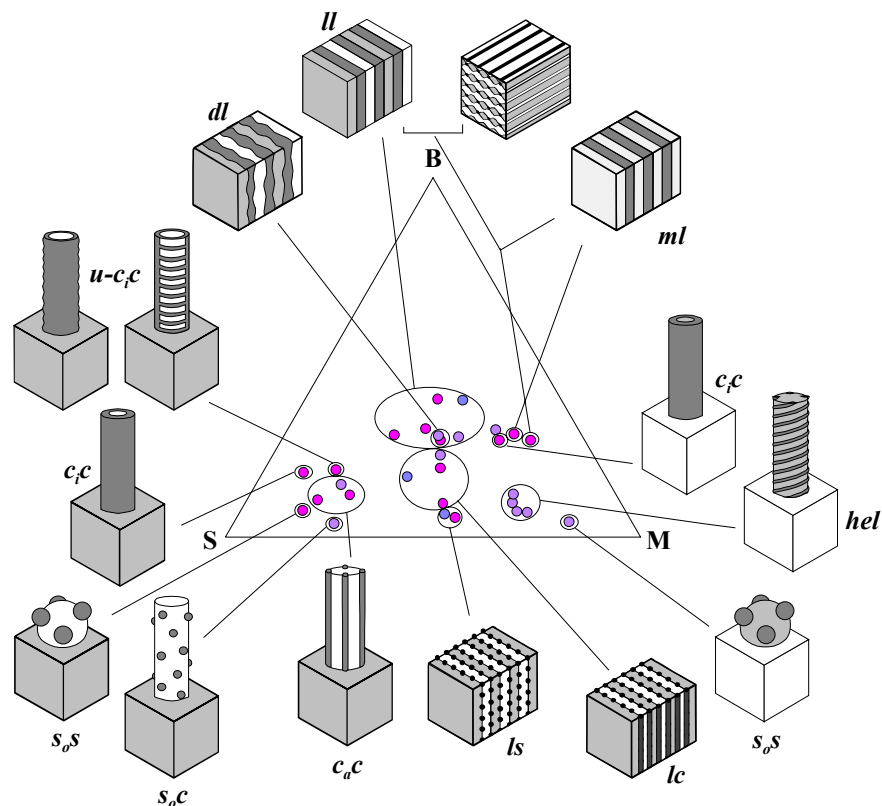


Figure 2. Ternary phase diagram of poly(styrene)-*block*-poly(butadiene)-*block*-poly(methyl methacrylate) triblock terpolymers. The color code corresponds to staining with OsO_4 . Poly(styrene): grey; poly(butadiene): black; poly(methyl methacrylate): white. (from Reference [16]. Copyright 2000, Wiley VCH).

1.2. Thin film phase behavior of block copolymers

In the presence of boundary surfaces and confined to a thickness comparable to the characteristic bulk domain spacing, the microdomain structures of block copolymers can significantly differ from the respective bulk structures. Both large scale alignment of the microdomains as well as the formation of novel microdomain structures has been observed.^{17,18,19,20,21}

In particular the aligning effect makes thin film structures suitable for applications in the area of nanotechnology.^{22,23,24} Thin films of diblock copolymers, for example, have been used as self-organized templates for the synthesis of various inorganic materials with a periodic order on the nanometer scale.^{25,26,27}

Knoll *et al.* have recently presented a detailed experimental phase diagram for thin films of a poly(styrene)-*block*-poly(butadiene)-*block*-poly(styrene) (SBS) triblock copolymer.^{28,29} Computer

simulations of a corresponding $A_3B_{12}A_3$ triblock copolymer film showed matching coincidence with the experimental results.^{28,30,31} In the bulk, this polymer forms hexagonally ordered poly(styrene) cylinders in a matrix of poly(butadiene). Though showing a well-defined morphology in bulk, the thin film phase behavior of this polymer is very complex. With increasing film thickness, the following thin film phases could be identified both in experiments and in simulations (Fig. 3): a disordered phase for the smallest film thickness (dis), very short upright standing cylinders (C_{\perp}), cylinders oriented parallel to the film plane ($C_{\parallel,1}$), a perforated lamella (PL), parallel oriented cylinders with an elongated cross section and necks, perpendicular oriented cylinders and finally two layers of parallel oriented cylinders ($C_{\parallel,2}$).

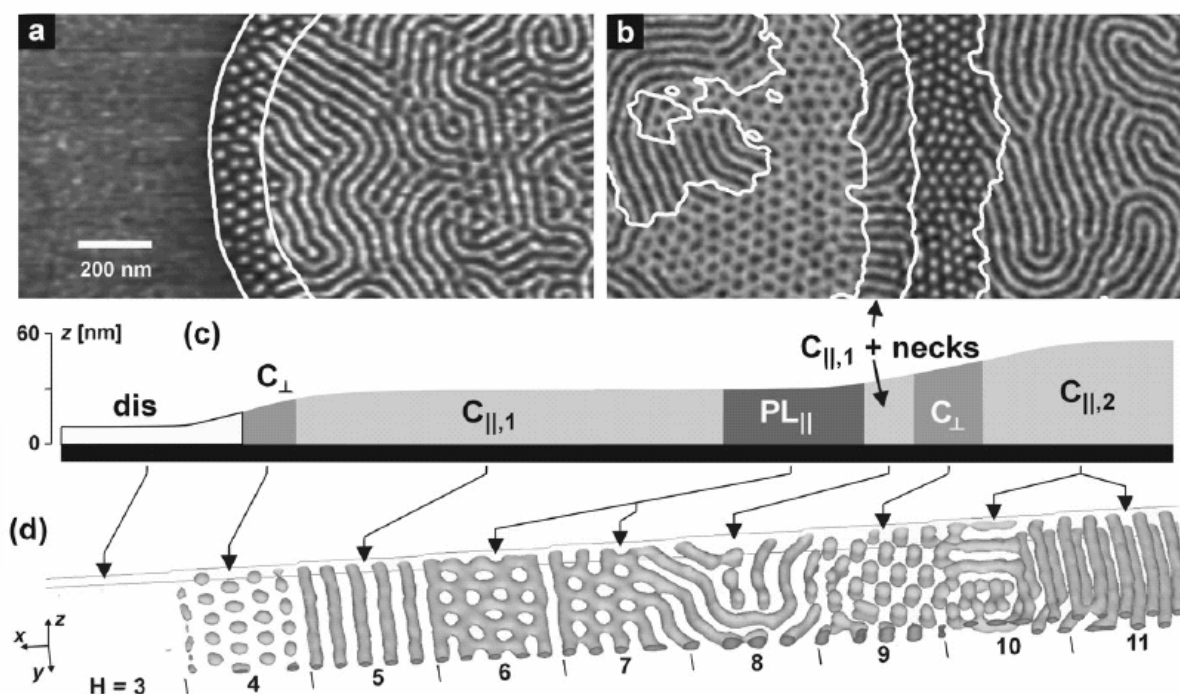


Figure 3. Tapping Mode SFM phase images of thin poly(styrene)-block-poly(butadiene)-block-poly(styrene) (SBS) block copolymer films on silicon substrates after annealing in chloroform vapor. The surface is everywhere covered with an ~ 10 nm thick layer of poly(butadiene). Bright (dark) corresponds to poly(styrene) (poly(butadiene)) microdomains below this top poly(butadiene) layer. Contour lines calculated from the corresponding height images are superimposed. (c): Schematic height profile of the phase images shown in (a) and (b). (d): Simulation of an $A_3B_{12}A_3$ block copolymer film in one large simulation box with film thickness increasing from left to right. (from Reference [29]. Copyright 2002, American Physical Society).

While the equilibrium phase behavior in thin films of AB and ABA block copolymers can be regarded as largely understood, the more complex ABC triblock terpolymers have not yet been investigated in much detail. Elbs *et al.* and Fukunaga *et al.* have presented experiments on the thin

film phase behavior of poly(styrene)-*block*-poly(2-vinylpyridine)-*block*-poly(*tert*-butyl methacrylate) (PS-*b*-P2VP-*b*-PtBMA) triblock terpolymers.^{32,33,34,35,36,37} For the case of a PS-*b*-P2VP-*b*-PtBMA triblock terpolymer with volume fractions $\phi_{\text{PS}} : \phi_{\text{P2VP}} : \phi_{\text{PtBMA}}$ scaling as 1 : 1.4 : 3 a rich variety of thin film structures was found.³³

In this thesis a systematic investigation of the thin film phase behavior of PS-*b*-P2VP-*b*-PtBMA triblock terpolymers within a composition range of $\phi_{\text{PS}} : \phi_{\text{P2VP}} : \phi_{\text{PtBMA}} = 1 : 2 : x$, with x ranging from 3.05 to 4, is performed.

1.3. Polymer-analogous reactions to amphiphilic block copolymers

Numerous groups have focused on the solution behavior of amphiphilic block copolymers, which contain at least one polyelectrolyte block.^{38,39,40,41,42,43,44} Usually, precursor polymers are synthesized, e.g. with anionic polymerization, which are subsequently chemically modified via polymer-analogous reactions to polyacids or polybases. Giebeler *et al.* have recently performed the modification of poly(styrene)-*block*-poly(2-vinylpyridine)-*block*-poly(*tert*-butyl methacrylate) to poly(styrene)-*block*-poly(2-vinylpyridine-hydrochloride)-*block*-poly(methacrylic acid) in bulk.⁴⁵ They were interested in the amphiphilic behavior after the hydrolysis of the PtBMA block. The bulk morphologies formed by the unhydrolyzed polymers via self-assembly could not be obtained with the modified polymers, as micelle formation was energetically favored.⁴⁶

Because of the large differences in solubility, amphiphilic block copolymer molecules self-associate in most cases into micelles that consist of a core formed by an insoluble hydrophobic block and a shell of water-soluble blocks.^{47,48} A review about block copolymer micelles has been recently published by Hamley.⁴⁹

The advantage of modifying thin films, instead of bulk material, is that less material is to be hydrolyzed and that the structure is not altered upon the polymer-analogous reaction. For example, Liu *et al.* prepared thin films with nanochannels from a blend of triblock terpolymers consisting of poly(isoprene) (PI), poly(2-cinnamoyl ethyl methacrylate) (PCEMA), and poly(*tert*-butyl acrylate) (PtBA) mixed with small amounts of poly(*tert*-butyl acrylate) (HPtBA).⁵⁰ Via extracting the homopolymer from the structured films and hydrolysing the poly(*tert*-butyl acrylate) block to a poly(acrylic acid) block, they obtained membranes that appeared to be permeable for gas, but not for liquids. Figure 4 shows a reaction scheme of their approach.

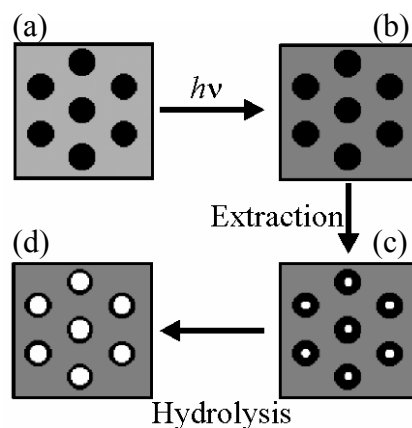
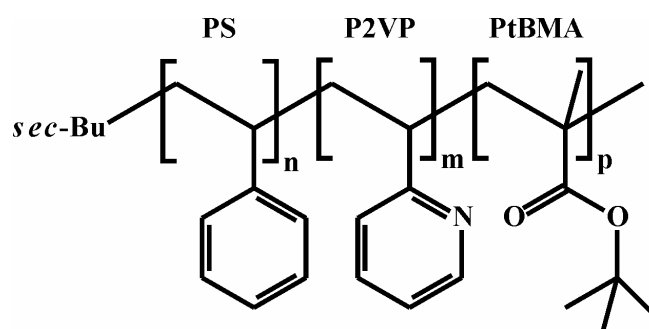


Figure 4. Strategy of the preparation of nanoporous membranes of poly(isoprene)-block-poly(2-cinnamoyl ethyl methacrylate)-block-poly(*tert*-butyl acrylate) triblock terpolymers mixed with homo(poly(*tert*-butyl acrylate)). (a): PtBA/HPtBA microdomains (black) form in a matrix of PI and PCEMA (grey rectangle). (b): Via UV irradiation the PCEMA block component is crosslinked. (c): Extraction of the HPtBA domains yields membranes with nanochannels (white dots). (d) Larger nanochannels are produced by extracting HPtBA and hydrolysing the PtBA block. (taken from Reference [50], Copyright 1999, Wiley-VCH).

1.4. Synthesis and bulk phase behavior of investigated polymers

In this thesis thin films of a triblock terpolymer consisting of poly(styrene) (PS), poly(2-vinylpyridine) (P2VP) and poly(*tert*-butyl methacrylate) (PtBMA) are studied.



Scheme 1. Structure of poly(styrene)-block-poly(2-vinylpyridine)-block-poly(*tert*-butyl methacrylate) triblock terpolymers.

Within the scope of my diploma thesis I have synthesized a series of monodisperse PS-*b*-P2VP-*b*-PtBMA triblock terpolymers with constant block length ratio of the first two blocks and increasing amount of the last block via living anionic polymerisation.⁵¹

The corresponding publication about the bulk phase behavior⁵² is presented in this thesis as supplementary information (Appendix 6.1). The bulk morphologies have been characterized with transmission electron microscopy and small angle X-ray scattering. Figure 5 shows a ternary phase

diagram of the synthesized polymers together with sketches of the anticipated structures. The colors of these sketches were chosen such as to match the grey values in transmission electron micrographs after staining: The black phase corresponds to PS, the grey phase to P2VP, and the white phase to PtBMA. The systematic variation of the length of one block with respect to the other two blocks reveals the following picture: The polymer with the highest amount of PtBMA forms a core-shell cylinder structure with PS cores which are embedded in shells of P2VP and surrounded by a matrix of the majority component PtBMA. Upon decreasing the length of PtBMA, we identify a coexistence region of core-shell gyroids, core-shell cylinders, and a perforated lamella structure. A symmetric composition, i.e., with all three blocks having the same length, shows a lamella morphology. Further decrease of PtBMA leads to an inverted core-shell gyroid structure with PtBMA forming the core and PS the matrix phase, via a cylinder-in-lamellae morphology (undulated lamellae) to a gyroid morphology comparable to two-component block copolymers, where PS and PtBMA mix and only two different microphases can be distinguished. The morphologies may be considered as core-shell analogues of the corresponding diblock copolymer morphologies.

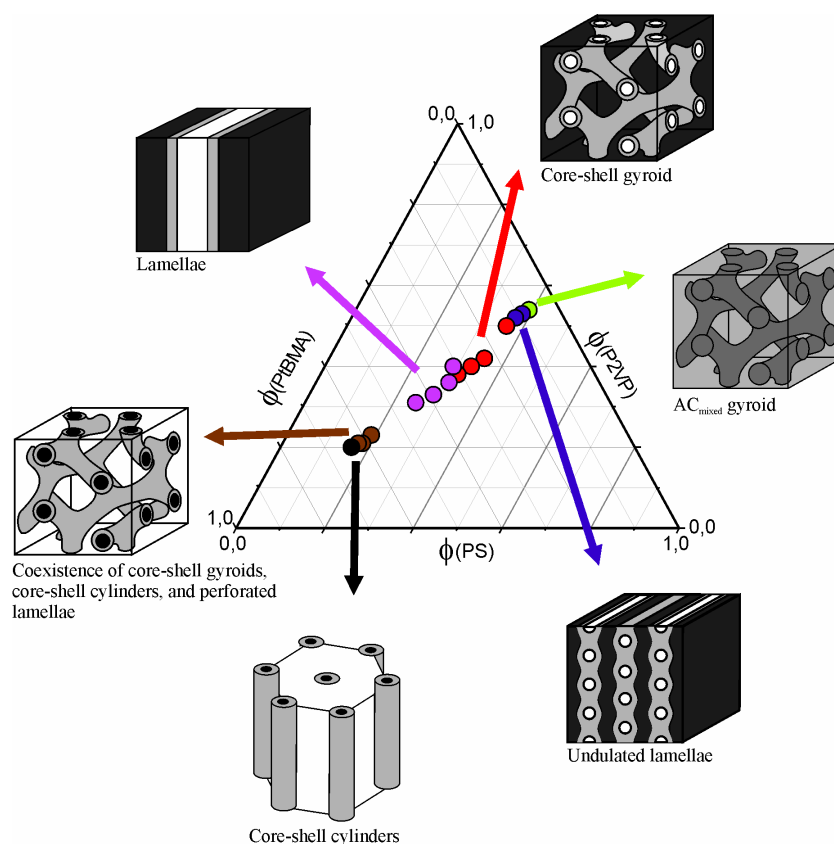


Figure 5. Ternary phase diagram of PS-*b*-P2VP-*b*-PtBMA triblock terpolymers.^{51,52} Color code corresponds to staining with RuO₄. PS: black; P2VP: grey; PtBMA: white.

1.5. Objectives of this thesis

One of the scopes of my thesis was to systematically explore the thin film phase behavior of PS-*b*-P2VP-*b*-PtBMA triblock terpolymers within a defined composition range. The results were compared with the respective bulk microdomain structures and with the thin film phase behavior of less complex model systems. Furthermore, polymer-analogous reactions were performed on a particular thin film structure to study the versatility of this structure for possible applications.

1.6. References

- (1) Bates, F. S.; Fredrickson, G. H. *Annu. Rev. Phys. Chem.* **1990**, 41, 525.
- (2) Thomas, E. L.; Lescanec, R. L. *Philos. Trans. R. Soc. London Ser. A* **1994**, 348, 149.
- (3) Stadler, R.; Auschra, C.; Beckmann, J.; Krappe, U.; Voigt-Martin, I.; Leibler, L. *Macromolecules* **1995**, 28, 3080.
- (4) Abetz, V. Block Copolymers, Ternary Triblocks In: *Encyclopedia of Polymer Science and Technology*; Kroschwitz, J. I., Ed.; 3rd ed.; Wiley: New York, 2003; Vol. 1, pp. 482.
- (5) Mogi, Y.; Kotsuji, H.; Kaneko, Y.; Mori, K.; Matsushita, Y.; Noda, I. *Macromolecules* **1992**, 25, 5408.
- (6) Mogi, Y.; Mori, K.; Kotsuji, H.; Matsushita, Y.; Noda, I.; Han, C. C. *Macromolecules* **1993**, 26, 5169.
- (7) Mogi, Y.; Nomura, M.; Kotsuji, H.; Ohnishi, K.; Matsushita, Y.; Noda, I. *Macromolecules* **1994**, 27, 6755
- (8) Gido, S. P.; Schwark, D. W.; Thomas, E. L. *Macromolecules* **1993**, 26, 2636.
- (9) Hückstädt, H.; Göpfert, A.; Abetz, V. *Polymer* **2000**, 41, 9089.
- (10) Breiner, U.; Krappe, U.; Stadler, R. *Macromol. Rapid. Commun.* **1996**, 17, 567.
- (11) Breiner, U.; Krappe, U.; Thomas, E. L.; Stadler, R. *Macromolecules* **1998**, 31, 135.
- (12) Krappe, U.; Stadler, R.; Voigt-Martin, I. *Macromolecules* **1995**, 28, 4458.
- (13) Breiner, U.; Krappe, U.; Abetz, V.; Stadler, R. *Macromol. Chem. Phys.* **1997**, 198, 1051.
- (14) Breiner, U.; Krappe, U.; Jakob, T.; Abetz, V.; Stadler, R. *Polym. Bull.* **1998**, 40, 219.
- (15) Brinkmann, S.; Stadler, R.; Thomas, E. L. *Macromolecules* **1998**, 21, 6566.
- (16) Abetz, V.; Goldacker, T. *Macromol. Rapid. Commun.* **2000**, 21, 16.
- (17) Krausch, G. *Mat. Sci. Eng. Rep.* **1995**, 14, 1.
- (18) Fasolka M. J.; Mayes, A. M. *Ann. Rev. Mat. Res.* **2001**, 31, 323.
- (19) Anastasiadis, S. H.; Russell, T. P.; Satija, S. K.; Majkrzak, C. F. *Phys. Rev. Lett.* **1989**, 62, 1852.
- (20) Walton, D. G.; Kellogg, G. J.; Mayes, A. M.; Lambooy, P.; Russell, T. P. *Macromolecules* **1994**, 27, 6225.
- (21) Kellogg, G. J.; Walton, D. J.; Mayes, A. M.; Lambooy, P.; Russell, T. P.; Gallagher, P. D.; Satija, S. K. *Phys. Rev. Lett.* **1996**, 76, 2503.
- (22) Mansky, P.; Chaikin, P.; Thomas, E. L.; *J. Mater. Sci.* **1995**, 30, 1987.
- (23) Park, M.; Harrison, C.; Chaikin, P. M.; Register, R. A.; Adamson, D. H. *Science* **1997**, 276, 1401.
- (24) Park, C., Yoon, J., Thomas, E. L. *Polymer* **2003**, 44, 6725.

- (25) Cheng, J. Y.; Ross, C. A.; Chan, V. Z.-H.; Thomas, E. L.; Lammertink, G. H.; Vansco, G. J. *Adv. Mater.* **2001**, 13, 1174.
- (26) Jeoung, E.; Galow, T. H.; Schotter, J.; Bal, A.; Ursache, M.; Tuominen, M.; Stafford, C. M.; Russell, T. P.; Rotello, V. M. *Langmuir* **2001**, 17, 6396.
- (27) Kim, H.-C.; Jia, X.; Stafford, C. M.; Kim, D. H.; McCarthy, T. J.; Tuominen, M.; Hawker, C. J.; Russel, T. P. *Adv. Mater.* **2001**, 13, 795.
- (28) Knoll, A.; Horvat, A.; Lyakhova, K. S.; Krausch, G.; Sevink, G. J. A.; Zvelindovsky, A. V.; Magerle, R. *Phys. Rev. Lett.* **2002**, 89, 035501-1.
- (29) Knoll, A.; Magerle, R.; Krausch, G. *J. Chem. Phys.* **2004**, 120, 1105.
- (30) Horvat, A.; Lyakhova, K. S.; Sevink, G. J. A.; Zvelindovsky, A. V.; Magerle, R. *J. Chem. Phys.* **2004**, 120, 1117.
- (31) Lyakhova, K. S.; Sevink, G. J. A.; Zvelindovsky, A. V.; Horvat, A.; Magerle, R. *J. Chem. Phys.* **2004**, 120, 1127.
- (32) Elbs, H.; Fukunaga, K.; Stadler, R.; Sauer, G.; Magerle, R.; Krausch, G. *Macromolecules* **1999**, 32, 1204.
- (33) Elbs, H.; Abetz, V.; Hadziioannou, G.; Drummer, C.; Krausch, G. *Macromolecules* **2001**, 34, 7917.
- (34) Elbs, H.; Drummer, C.; Abetz, V.; Krausch, G. *Macromolecules* **2002**, 35, 5570.
- (35) Fukunaga, K.; Elbs, H.; Magerle, R.; Krausch, G. *Macromolecules* **2000**, 33, 947.
- (36) Fukunaga, K.; Hashimoto, T.; Elbs, H.; Krausch, G. *Macromolecules* **2002**, 35, 4406.
- (37) Fukunaga, K.; Hashimoto, T.; Elbs, H.; Krausch, G. *Macromolecules* **2003**, 36, 2852.
- (38) Kamachi, M.; Kurihara, M.; Stille, J. K. *Macromolecules* **1972**, 5, 161.
- (39) Ramireddy, C.; Tuzar, Z.; Prochazka, K.; Webber, S. E.; Munk, P. *Macromolecules* **1992**, 25, 2541.
- (40) Patrickios, C. S.; Hertler, W. R.; Abbott, N. L.; Hatton, T. A. *Macromolecules* **1994**, 27, 930.
- (41) Bronstein, L. M.; Sidorov, S. N.; Valetsky, P. M. *Langmuir* **1999**, 15, 6256.
- (42) Gohy, J.-F.; Antoun, S.; Jérôme, R. *Macromolecules* **2001**, 34, 7435.
- (43) Qin, S.-H.; Qiu, K.-Y. *J. Polym. Sci., Part A: Polym. Chem.* **2001**, 39, 1450.
- (44) Bieringer, R.; Abetz, V.; Müller, A. H. E. *Eur. Phys. J. E* **2001**, 5, 5.
- (45) Giebeler, E.; Stadler, R. *Macromol. Chem. Phys.* **1997**, 198, 3815.
- (46) Giebeler, E. PhD thesis, Mainz, **1996**.
- (47) Förster, S.; Schmidt, M.; *Adv. Polym. Sci.* **1995**, 120, 53.

- (48) Kassapidou, K.; Jesse, W.; Kuil, M. E.; Lapp, A.; Egelhaaf, S.; van der Maarel, J. R. C. *Macromolecules* **1997**, 30, 2671.
- (49) Hamley, I. W. *The Physics of Block Copolymers*; Oxford University Press: Oxford, 1998.
- (50) Liu, G.; Ding, J.; Stewart, S. *Angew. Chem. Int. Ed.* **1999**, 38, 835.
- (51) Ludwigs, S. Diploma thesis, Bayreuth, **2002**.
- (52) Ludwigs, S.; Böker, A.; Abetz, V.; Müller, A. H. E.; Krausch, G. *Polymer* **2003**, 44, 6815.

2. Overview of thesis – Results

This thesis includes four publications which are presented in Chapters 3.1 to 3.4.

First, the thin film phase behavior of poly(styrene)-*block*-poly(2-vinylpyridine)-*block*-poly(*tert*-butyl methacrylate) (SVT) triblock terpolymers was systematically investigated with combinatorial gradient techniques. (Chapter 3.1)

The assignment of thin film surface structures to distinct microdomain structures was corroborated by simulations based on a dynamic density functional theory. The results of the simulations were directly compared to the experimental results (Chapter 3.2)

On the basis of these fundamental investigations highly ordered nanostructured thin films could be prepared via self-assembly. Several polymer-analogous reactions were performed on this nanostructure which open the way towards possible applications. (Chapter 3.3)

The modification to an amphiphilic nanostructure appeared to be very interesting, as the conformation of the polymer could be changed via the pH-value of the surrounding medium. (Chapter 3.4)

In the following, summaries of the main results together with descriptions of the experimental methods are presented.

2.1. Experiments on thin film phase behavior

2.1.1. Methods

Thickness gradients were prepared on silicon wafers with a flow-coating apparatus, which had been established at the National Institute of Science and Technology (NIST) in USA.¹

The substrate, usually a pure silicon wafer, is fixed on a motorized translation stage which allows a constant acceleration in x-direction. A drop of polymer solution is spread over the substrate under a blade mounted at an angle of 5° relative to the substrate (Fig. 1). When the stage is drawn in x-direction, the solution is spread on the substrate, and the solvent dries within seconds of spreading. A polymer film is finally left on the substrate with a gradient in film thickness.

By adjusting the acceleration rate and the concentration of the polymer solution, gradients with different ranges in film thickness can be prepared, for example from 20 to 120 nm in one single experiment. Figure 2 shows a photograph of a silicon wafer with different thickness gradients, the thickness increasing from right to left.

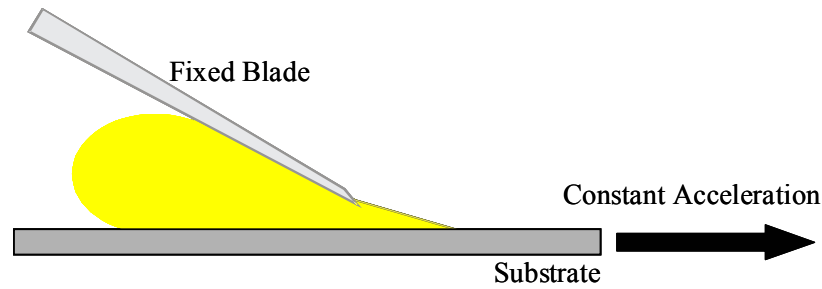


Figure 1. Principle of flow-coating gradient technique.

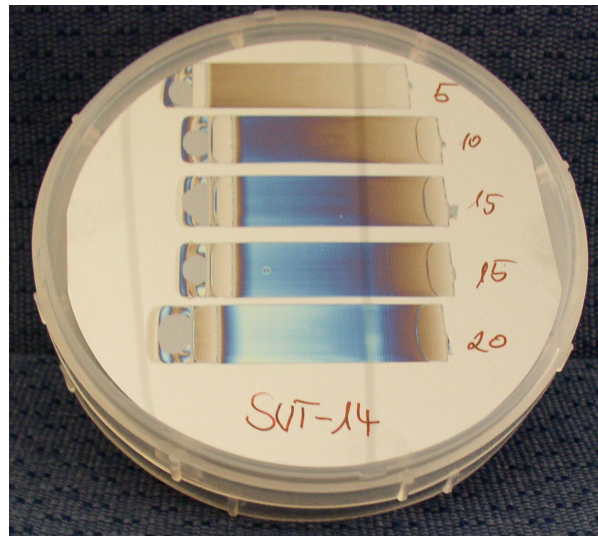


Figure 2. Thin films with gradients in film thickness on a silicon substrate. The thickness increases from right to left. The numbers indicate different acceleration rates.

- **Substrate surface energy gradients**

Substrates with different surface energies were prepared with a combinatorial gradient technique. Chemically grafted monolayers of trialkylsilanes are deposited on silicon wafers in the vapor phase, and the resulting self-assembled monolayers (SAM) are exposed to UV irradiation with stepwise increasing exposure time. An increasing amount of oxidated species is formed across the sample.^{2,3,4} The change in surface energy is evaluated by contact angle measurements of water and diiodomethane. Figure 3(a) shows the water contact angle measured across a wafer from the hydrophobic towards the hydrophilic substrate region. The surface energy can be estimated by using the Good and Girifalco geometric mean approximation.^{5,6,7}

Finally, a combinatorial library can be created with orthogonal gradients in film thickness and surface energy, Figure 3(b).⁸

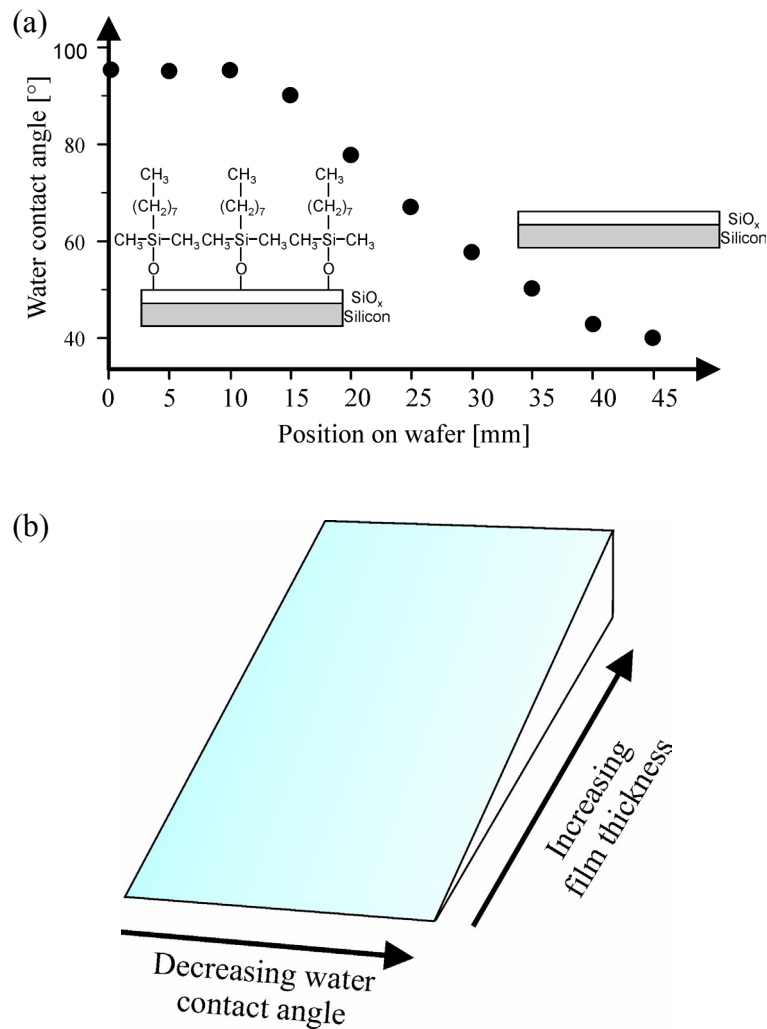


Figure 3. (a): Substrate surface energy gradient. Water contact angles measured at different sample positions. The insets show the surface composition at the two extreme cases (hydrophobic, left, and hydrophilic, right). (b): Sketch of a combinatorial library with orthogonal gradients in film thickness and substrate surface energy.

- **Annealing in solvent vapor**

In order to induce mobility and facilitate equilibration of the microdomain structures, the films were subsequently exposed to a controlled atmosphere of chloroform vapor. This procedure is analogous to temperature annealing with the advantage that it can be used for high-molecular weight and temperature-sensitive polymers. The experimental setup is shown in Figure 4.⁹ Two flows of nitrogen, one of them saturated with chloroform, are mixed just before entering the sample chamber. The sample can be watched with an optical microscope to follow terrace formation. After annealing, the sample is quickly dried with pure air to quench the microdomain structure.

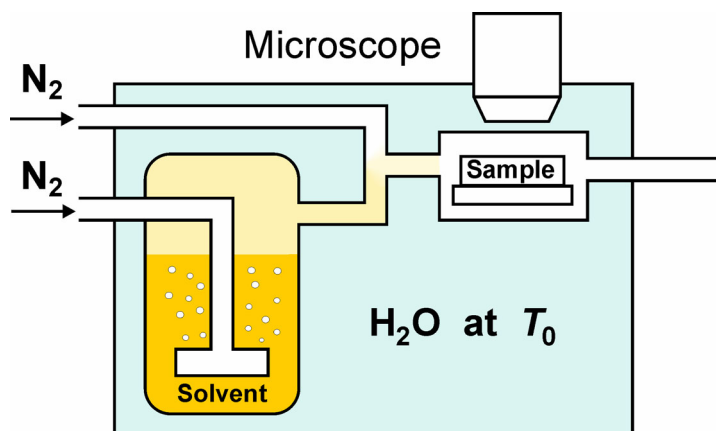


Figure 4. Sketch of the experimental set-up for swelling in solvent vapor. (from Reference [9], Copyright 2004, American Institute of Physics).

• Imaging techniques

The thin film surface structures were studied with optical microscopy, scanning force microscopy (SFM) and scanning electron microscopy (SEM). No staining was performed for SEM measurements. While SFM is a non-destructive technique for surface investigations, it is well-known that electron beam damage during SEM imaging can lead to considerable volume shrinkage of polymethacrylate phases.¹⁰ Using the in-lens detector of the SEM at a quite low accelerating voltage of 0.8 kV enables the detection of a material contrast between the different components of the block copolymers. Scratches with a needle were made on the samples to enable step height measurements with SFM and to mark and find characteristic sample spots with all techniques.

2.1.2. Results

During vapor annealing the original smooth gradient in film thickness exhibits terraces of well-defined thickness, which are characterized by uniform interference colors in optical microscopy. This finding suggests that the local thickness adjusts to local minima of the free energy of the system which are related to energetically preferred microdomain structures in the film. Figure 5(a) shows the film thickness with increasing terrace height of a thin film of PS-*b*-P2VP-*b*-PtBMA with volume fractions $\phi_{\text{PS}} : \phi_{\text{P2VP}} : \phi_{\text{PtBMA}} = 1 : 1.2 : 4$ after exposure to chloroform vapor ($p_{\text{CHCl}_3} = 0.9 p_{\text{sat}}$, $t = 120$ h). In bulk, this polymer forms core-shell cylinders. The height profiles between neighboring terraces, measured with SFM, are merged laterally. As the SFM images show only low contrast in topography due to a thin layer of PtBMA at the air/film surface, the characterization of the surface structures has been mainly performed from scanning electron micrographs (Fig. 5(b)). Upon exposure to the electron beam in SEM, this first layer of PtBMA is removed.

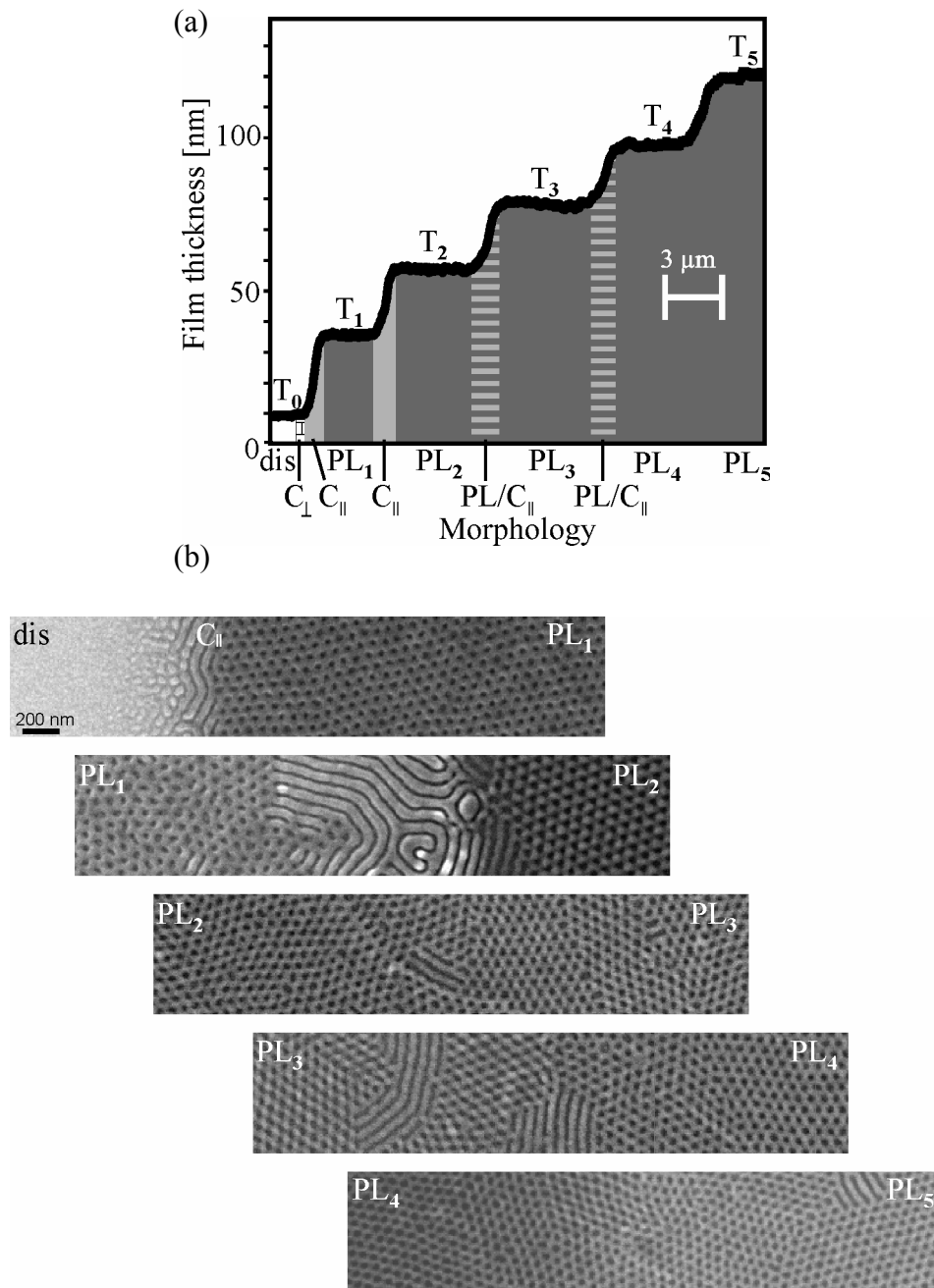


Figure 5. Thin film phase behavior of a thin film of $S_{16}V_{21}T_{63}^{140}$ ($p_{CHCl_3} = 0.9$, $p_{sub} = t = 120$ h). (a): Height profiles between neighboring terraces (measured with SFM) which are merged laterally. The transitions from T_0 to T_1 , from T_1 to T_2 , from T_2 to T_3 , from T_3 to T_4 , and from T_4 to T_5 are shown. (b) Corresponding SEM images of the same sample regions. The terrace structures can be assigned to perforated lamellae (PL).

The first terrace of perforated lamellae can be visualized as P2VP/PS/P2VP lamellae which are perforated by channels of PtBMA interconnecting between two outer layers of PtBMA, one being at the air/film interface, the other resulting from a wetting layer which is formed next to the substrate. Figure 6 shows the simulation result of such a structure: the white phase corresponds to PS, the red phase to P2VP, and the blue phase to the majority component PtBMA.

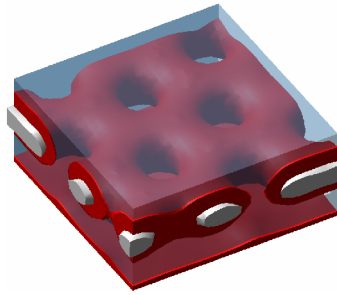


Figure 6. Sketch of the perforated lamella phase. Result of a MesoDyn simulation.¹¹

To test the stability of the structure to variations of the interaction between the film and the substrate, gradients in substrate surface energy have been prepared orthogonal to the gradients in film thickness. Summarizing, it was found that the terraces, exhibiting the PL phase, are formed irrespective of the chemical nature of the substrate. This effect may be explained by the wetting layer which is formed beneath all surface structures.

The results on the core-shell cylinder forming system apply for the whole composition range of $\phi_{PS} : \phi_{P2VP} : \phi_{PtBMA} = 1 : 1.2 : x$, with x ranging from 3.05 to 4, as thin films of triblock terpolymers, which exhibit a coexistence of core-shell gyroids, core-shell cylinders and perforated lamellae in bulk, exhibit the same surface structures with increasing film thickness. Also the microdomain distances and the film thicknesses are comparable.

The influence of the solvent used for annealing on the structure formation is also discussed. While showing the same structure in bulk and solution, in thin films a morphological phase transition is induced: Treatment with chloroform (CHCl_3) shows the above described phases, and exposure to tetrahydrofuran (THF) vapor leads to cylinders oriented parallel (C_{\parallel}) to the film plane in the whole thickness range. Figure 7 shows the transition from the substrate to the first terrace (T_1) of cylinders. This phenomenon may be explained by a slight selectivity of CHCl_3 for P2VP, while THF appears to be non-selective for all blocks.

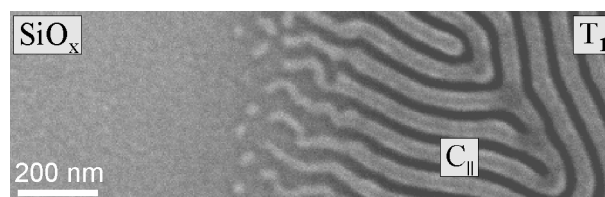


Figure 7. Thin film of $S_{16}V_{21}T_{63}^{140}$ after exposure to THF vapor ($p_{\text{THF}} = 0.95p_{\text{sat}}$, $t = 120$ h. (b): SEM micrograph of the transition from the silicon substrate to T_1 .

In thin films, ABC triblock terpolymers display a similar phase behavior as found in the cylinder-

forming ABA system studied by Knoll *et al.*^{9,12,13,14} Core-shell structures are analogous to the two-component system. In addition, ABC triblock terpolymers can exhibit a much larger variety of surface structures due to the delicate interplay between the large number of block-block and block-surface interactions. Only slight variations in the sample preparation have for example induced four different cylindrical structures on one sample: core-shell cylinders, spheres-in-cylinders, cylinders-at-cylinders, and helices-around-cylinders.

2.2. Comparison of mesoscale simulations with experiments

2.2.1. Method

The experimental results are supported by simulations based on dynamic density functional theory.^{15,16,17} A dynamic version of the self-consistent field simulation technique was used to model a melt of SVT triblock terpolymers as $A_3B_4C_{12}$ Gaussian chains with different beads A (= PS), B (= P2VP) and C (= PtBMA). The volume fraction considered in the parameterization of the simulation chain is well within the composition range $\phi_{PS} : \phi_{P2VP} : \phi_{PtBMA} = 1 : 1.2 : x$, with x ranging from 3.05 to 4. In the simulations it cannot be distinguished between small variations in the volume fractions which have shown to lead to different microdomain phases in bulk. For the component-component interaction potentials Gaussian kernels are used characterized by ϵ_{AB} , ϵ_{AC} , and ϵ_{BC} . Polymer films on silicon substrates are mimicked as polymer melts confined between two parallel hard walls, one wall representing the substrate M_0 and the other the free surface M_1 . The component-wall interaction parameters are ϵ_{AM_0} , ϵ_{BM_0} , ϵ_{CM_0} , ϵ_{AM_1} , ϵ_{BM_1} , and ϵ_{CM_1} . The spatiotemporal evolution of component densities $\rho_i(r, t)$, is obtained using the complete free energy functional $F[\{\rho_i\}]$ and the chemical potentials $\mu_i = \delta F[\{\rho_i\}]/\delta \rho_i$. The Langevin diffusion equation is solved numerically starting from homogeneous densities. The interaction parameters between the different components, and the interaction parameters between the components and the walls, were tuned such that they match the experimental situation. The film thickness H was systematically varied.

2.2.2. Results

Based on the experimental results, the interaction parameters between the components, and the interaction parameters between the components and the interfaces could be determined. With this parameterization, a detailed match was found between the experimental results and the simulations based on SCF theory, both in bulk and in thin films. In the simulations, the bulk structure is identified as a core-shell gyroid structure (Fig. 8), which is quite stable with respect to rather large variations in the interaction parameters between the different components. Upon shearing, a

perforated lamella and a cylinder phase are found next to the gyroid phase boundaries. This observation is in line with the experiments, where a core-shell gyroid structure is found to coexist with core-shell cylinders and a perforated lamella like structure for $\phi_{PS} : \phi_{P2VP} : \phi_{PIBMA} = 1 : 1.2 : 3.05$ to 3.65 .

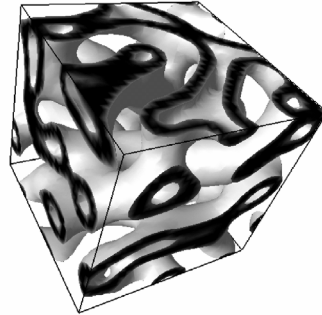


Figure 8. Simulation result for a melt of $A_3B_4C_{12}$ Gaussian chains in a $32 \times 32 \times 32$ large simulation box. The component-component interaction parameters are $\epsilon = (7.0, 8.0, 6.0)$. The isodensity surface of the B-component is shown.

Figure 9 and 10 show also matching coincidence between the surface structures found in the simulations of $A_3B_4C_{12}$ Gaussian chains confined in a thin film and those observed in the experiments performed on a SVT triblock terpolymer with volume fractions scaling as $\phi_{PS} : \phi_{P2VP} : \phi_{PIBMA} = 1 : 1.2 : 3.65$. The surface structures are displayed as function of the film thickness H .

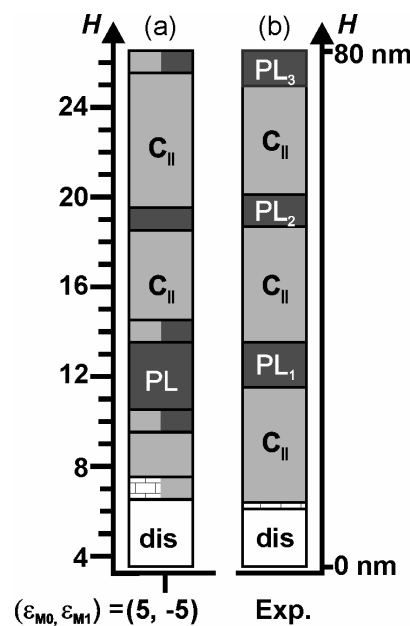


Figure 9. Surface structures in thin films as function of the film thickness. Color code: white: dis; light grey: $C_{||}$; dark grey: PL; tiled: C_{\perp} . (b): Experimental phase diagram for $S_{17}V_{22}T_{61}$ ¹³².

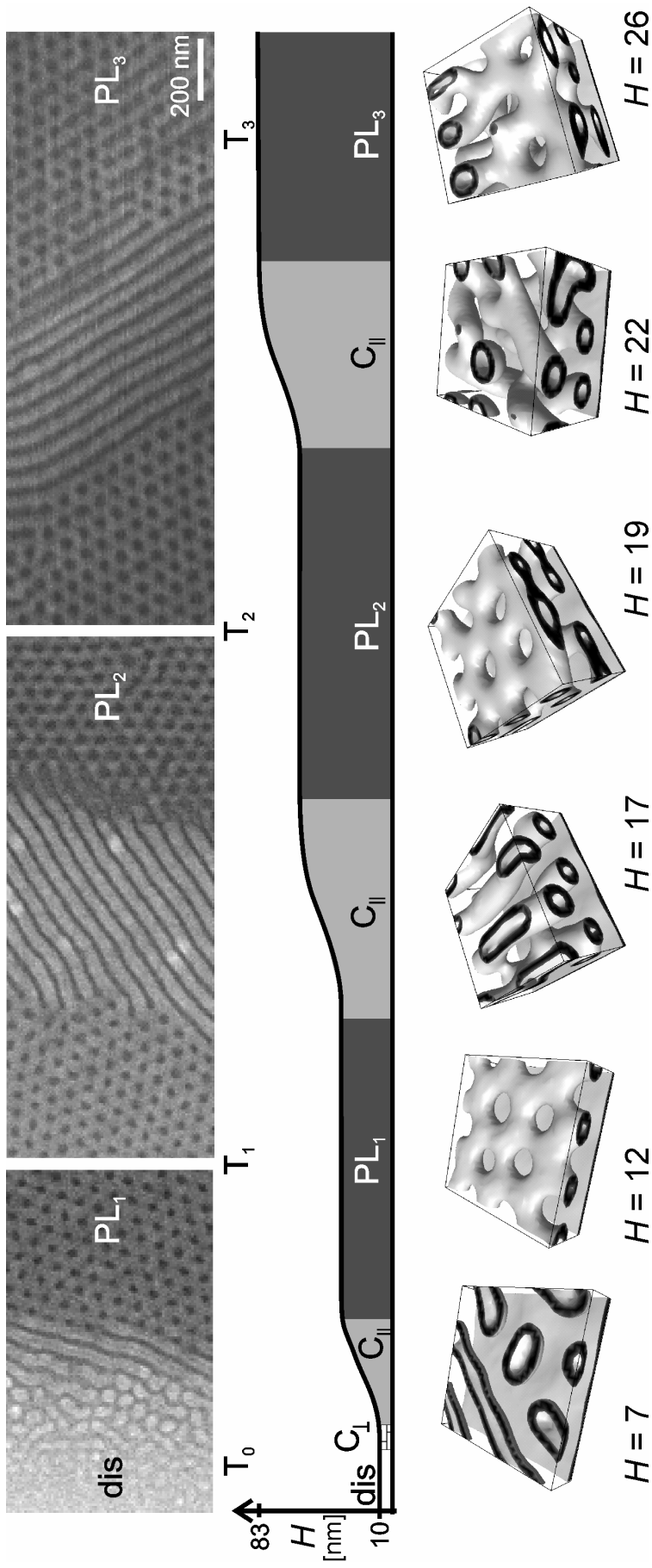


Figure 10. Comparison of experiments with simulation results. (a): Scanning electron micrographs of a thin film of poly(styrene)-block-poly(2-vinylpyridine)-block-poly(tert-butyl methacrylate) triblock terpolymers (S_{17}, V_{32}, A_{61}) on a silicon substrate after annealing in chloroform vapor. (b): Schematic height profile of the micrographs shown in (a). (c): Matching computer simulations of an $A_3B_3C_{12}$ block terpolymer film. The isodensity surfaces of the B-density are shown for different film thicknesses H .

Like in thin films of two-component systems the film thickness is modulating the stability region of the different phases via additivity of surface fields and commensurability effects.^{12,13,14} The phase behavior is much more complex in thin films of ABC triblock terpolymers due to the larger number of degrees of freedom.

One of the major results of this study is that slight changes in the interaction parameters between the components and/or between the components and the surfaces lead to significant changes in the phase diagram and to shifts of phase boundaries. As an example, Figure 11 shows surface structures as function of the film thickness for different interaction parameters between the components. Although in the bulk, a core-shell gyroid structure is observed for a variety of different interaction parameters, the presence of confining walls induces a zoo of surface structures. This is also in accordance to the experimental observations, where slight changes in solvent vapor lead to different cylindrical structures.

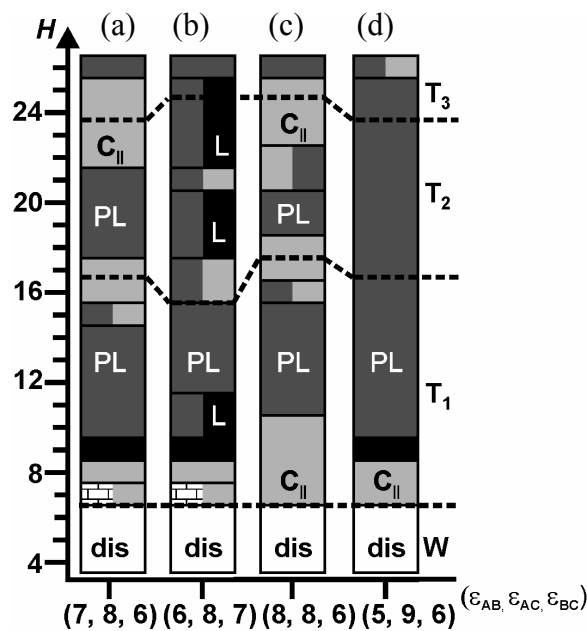


Figure 11. Influence of interaction parameters on surface structures in thin films as function of the film thickness. Color code: white: dis; light grey: C_{||}; dark grey: PL; black: L; tiled: C_⊥.

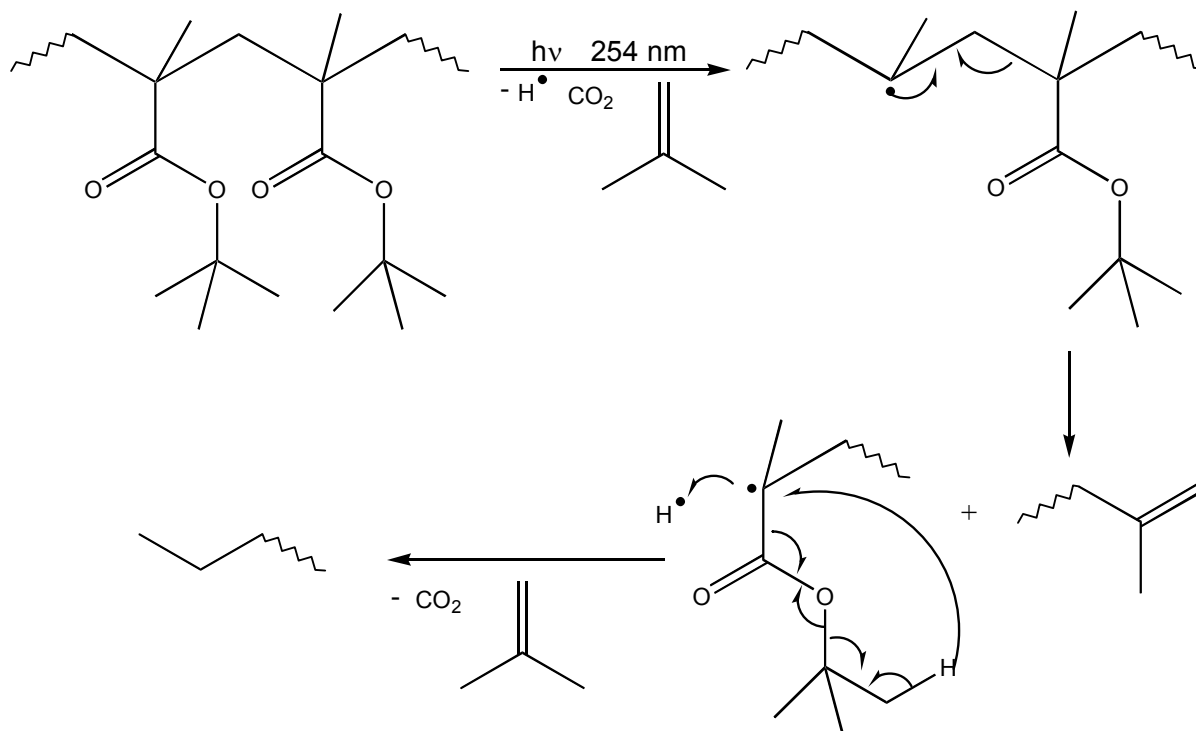
2.3. From functional nanostructures towards possible applications

2.3.1. Methods

- **Selective removal of poly(*tert*-butyl methacrylate) via UV exposure**

Thin films on silicon substrates showing a perforated lamella structure were exposed to UV-light ($\lambda = 256$ nm) for 5 minutes. The samples were subsequently thoroughly rinsed with n-hexane for 2

minutes. During the irradiation, PtBMA is depolymerized via photolysis, as depicted in Scheme 1.



Scheme 1. Mechanism of the depolymerisation of poly(tert-butyl methacrylate).¹⁸

- **Preparation of free-standing films for TEM investigations**

Thin films (~ 40 nm thick) were prepared on polished NaCl-substrates and exposed to solvent vapor as described above. Then, the NaCl-substrates were dissolved in water and the free standing block copolymer films were picked up onto small copper grids. For transmission electron microscopy the films were stained with RuO₄ causing PS and P2VP to appear as dark phases and PtBMA as white phase in the micrographs.

2.3.2. Results

Some routes towards possible applications were shown, focusing on one particular microdomain structure¹¹: Via solvent annealing in chloroform vapor a highly ordered single layer (T₁) of perforated lamellae (PL) could be produced. The large scale SEM image displayed in Figure 12 shows that this structure is formed with a very small number of defects over an area of about 12×4 μm². No particular measures for improving the order, like topographic patterning of the substrate¹⁹ or alignment with a suitable solvent treatment²⁰ are needed.

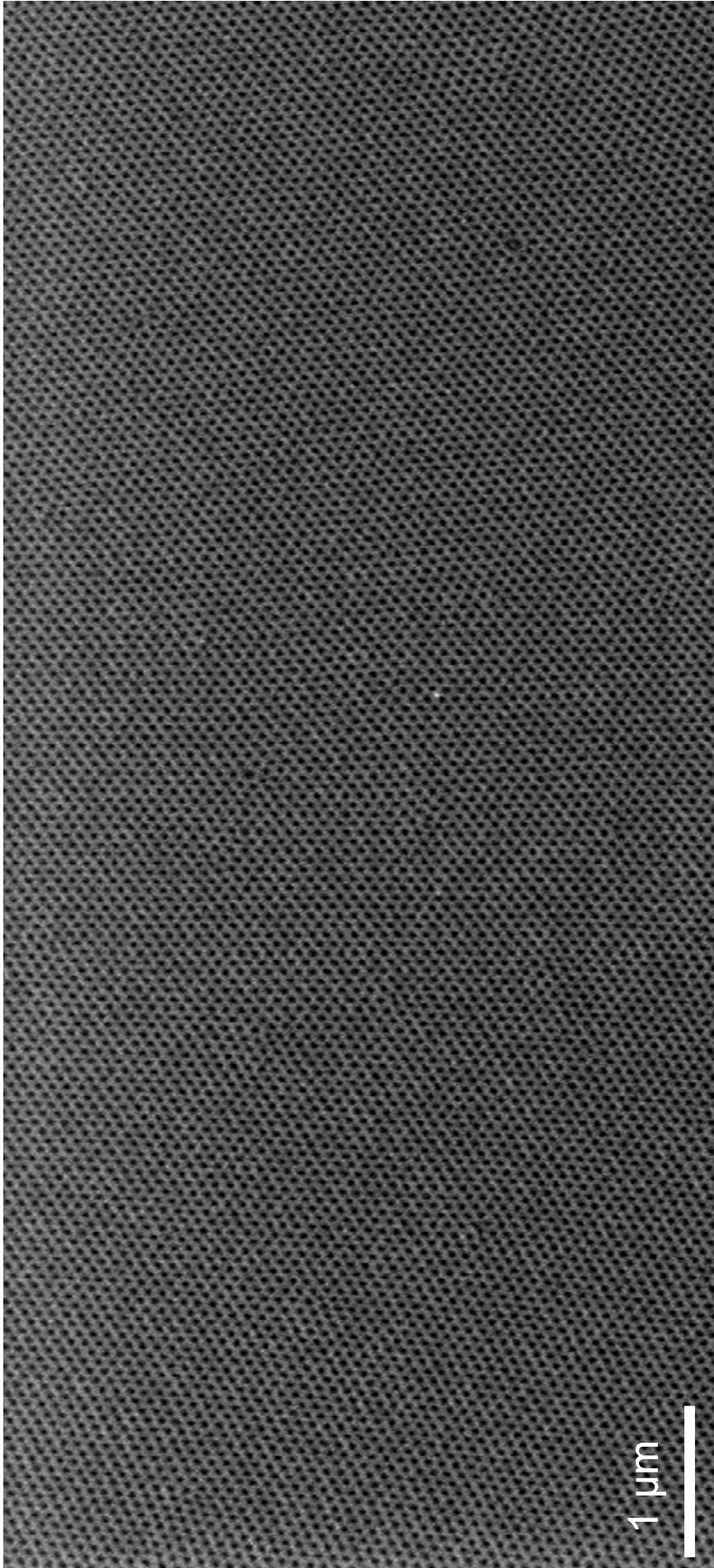


Figure 12. Highly ordered perforated lamella structure in a thin film of poly(styrene)-block-poly(2-vinylpyridine)-block-poly(tert-butyl methacrylate) triblock terpolymers. FE-SEM image of a ~37 nm thick film after solvent vapor treatment; the partial pressure p_{CHCl_3} was reduced from 0.94 p_{sat} to below 0.3 p_{sat} within 100 h.¹¹

Selective removal of the PtBMA phase makes the PL phase potentially useful for lithographic applications similar to the case of perpendicularly oriented poly(methyl methacrylate) (PMMA) cylinders in poly(styrene)-*block*-poly(methyl methacrylate) block copolymer thin films, where PMMA can also be selectively removed via UV-light. Figure 13 shows an SFM image before (a) and after (b) removal of PtBMA. The original rather smooth surface topography exhibits a highly ordered hexagonal arrangement of holes. If etching is performed through the whole layer of PL to the substrate, a mask is left which can be used for etching, material deposition, etc.^{21,22}

Till now, only spherical and cylindrical mesostructures have been used for nanolithographic applications. In the latter case, the cylinders tend to orient parallel to the boundary surfaces and quite some effort has been taken to overcome this tendency and stabilize a perpendicular orientation, which is desired for many applications.^{23,24}

The advantage of the perforated lamella phase is that after removal of PtBMA the surface of the remaining skeleton is still covered by a layer of P2VP, which can be chemically modified. In particular, quaternization of P2VP will lead to water soluble channels, thereby circumventing well-known wettability problems, occurring when the holes in the polymer structure are to be filled in a subsequent electrochemical processing step.^{22,25}

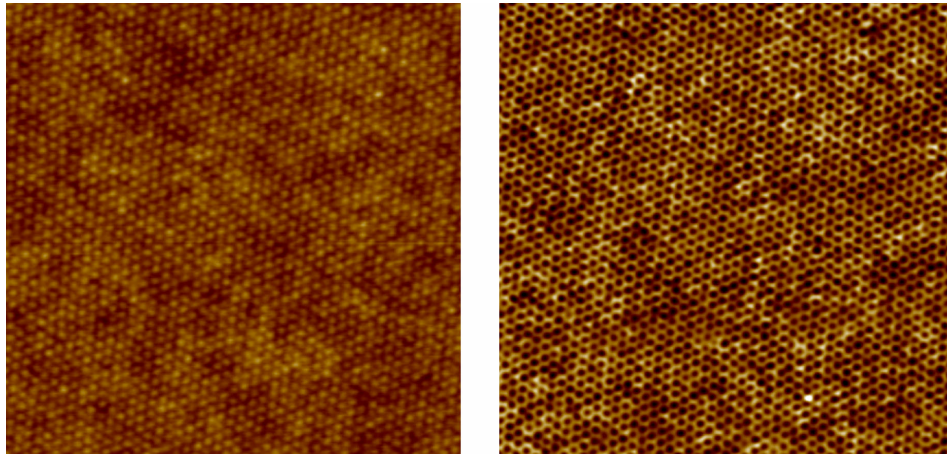


Figure 13. Tapping Mode SFM topography images of the block copolymer film (a) prior to and (b) after exposure to UV radiation ($3 \times 3 \mu\text{m}^2$).

The high density of well-defined nanoscopic holes within one single layer of PL may also be useful for nanomembrane applications. In a first approach free-standing films were prepared from polished NaCl substrates. Figure 14 shows a TEM image taken from such a free-standing film, clearly showing that the quality of the nanostructure is preserved. The removal of PtBMA from such a film has not yet been performed. As the volume of P2VP can be changed by the pH-value as external

stimulus, one may envision opening and closing channels in a switchable nanomembrane.



Figure 14. TEM image of a block copolymer film prepared on a polished NaCl-substrate, floated onto H₂O, and picked up onto a TEM grid (2×2 μm²; preparation: $p_{\text{CHCl}_3} = 0.9$ p_{stab} $t=15$ h), stained with RuO₄. (grey phase: PS & P2VP; white phase: PtBMA).

Another chemical modification is to convert the matrix phase into poly(methacrylic acid) (PMAA) via hydrolysis in HCl. A detailed investigation of the behavior of the hydrolyzed nanostructure in water and as function of the pH is described in the next chapter.

2.4. pH-dependent nanostructures

2.4.1. Methods

Acid-catalyzed hydrolysis of PS-*b*-P2VP-*b*-PtBMA was accomplished by heating prestructured films together with a reservoir of approximately 3 ml of HCl_{conc} for 12-15 h at a temperature of 60°C (Fig. 15). The films were subsequently dried in vacuum. The reaction transforms the PtBMA block to a poly(methacrylic acid) polyelectrolyte block without altering the thin film structure (Scheme 2). The driving force of this reaction is the elimination of gaseous isobutylene. Besides hydrolysing the PtBMA the reaction also yields the hydrochloride of the amine functionality of poly(2-vinylpyridine), as also shown in Scheme 2.

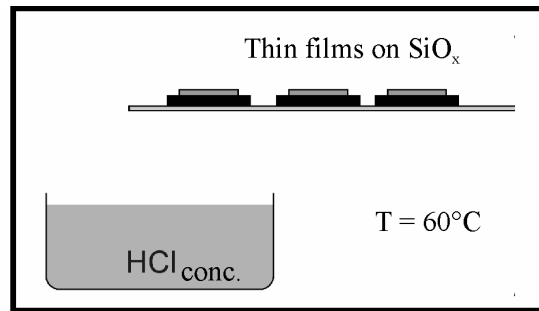
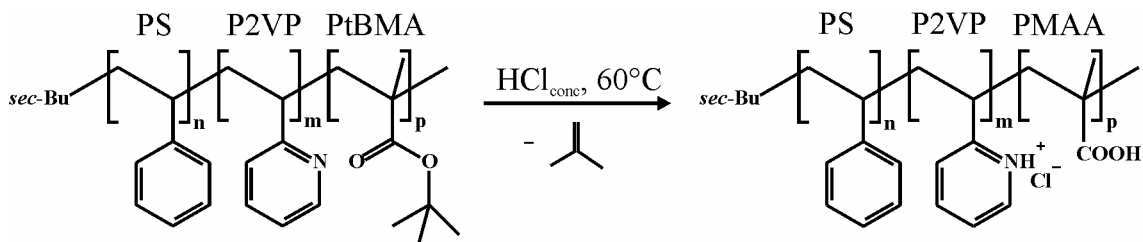


Figure 15. The experimental setup for the hydrolysis of thin films.



Scheme 2. Acid-catalyzed hydrolysis of PS-*b*-P2VP-*b*-PtBMA to PS-*b*-P2VP- H^+ -*b*-PMAA.

• Scanning force microscopy in aqueous environment

Thin films of PS-*b*-P2VP- H^+ -*b*-PMAA on silicon wafers were investigated in the fluid cell of a MultiMode scanning force microscope (from Digital Instruments, Veeco Group) (Fig. 16). Contact-mode tips were used (Veeco NP-S tips consisting of silicon nitride with a spring constant $k = 0,58$ N/m). All experiments were performed in the tapping mode (resonance frequency $\omega \approx 10$ kHz).

For the pH-dependent measurements the water in the chamber was exchanged with buffer systems. To avoid effects due to different counterions and ionic strengths²⁶ sodium-phosphate buffers ($H_3PO_4 / NaH_2PO_4 / Na_2HPO_4 / Na_3PO_4$) were used which allow tuning the pH in the range from 2 to 10. For film thickness measurements scratches with a needle were made onto the samples after hydrolysis.

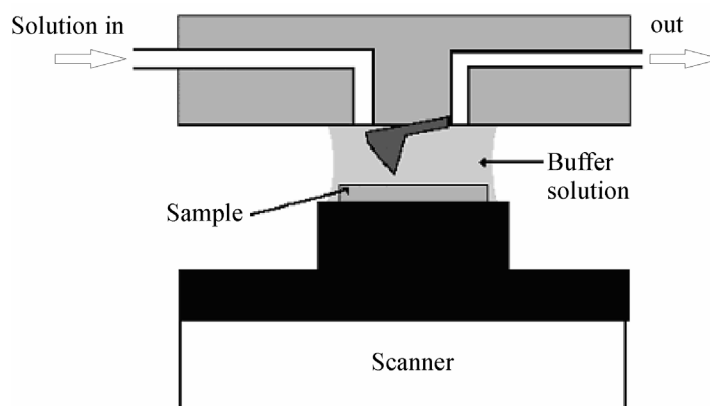


Figure 16. Scanning force microscopy (SFM) in buffer solutions.

2.4.2. Results

A pH-responsive nanostructure is obtained by polymer-analogous reactions performed on a highly ordered perforated lamella structure. When the triblock terpolymer is hydrolyzed in HCl, a perforated lamella is left with a hydrophilic matrix of poly(methacrylic acid). Figures 17(a) and (b) show SFM images (in the dry state) of a terpolymer film before and after acid-catalyzed hydrolysis. The unhydrolyzed film shows a rather smooth surface topology with a hexagonal pattern of bright dots, which are assigned to a perforated lamella (PL). The height difference between protrusions and valleys amounts to 2 nm. After hydrolysis a hexagonal arrangement of protrusions forms with the height difference between protrusions and valleys amounting to ~ 15 nm. Since PMAA is rather hygroscopic, the film swells even at ambient conditions. Figure 17(c) and (d) represent the corresponding sketches of the microdomain structure before and after hydrolysis. The protrusions of the acid component form on top of the perforations where more PMAA material is present.

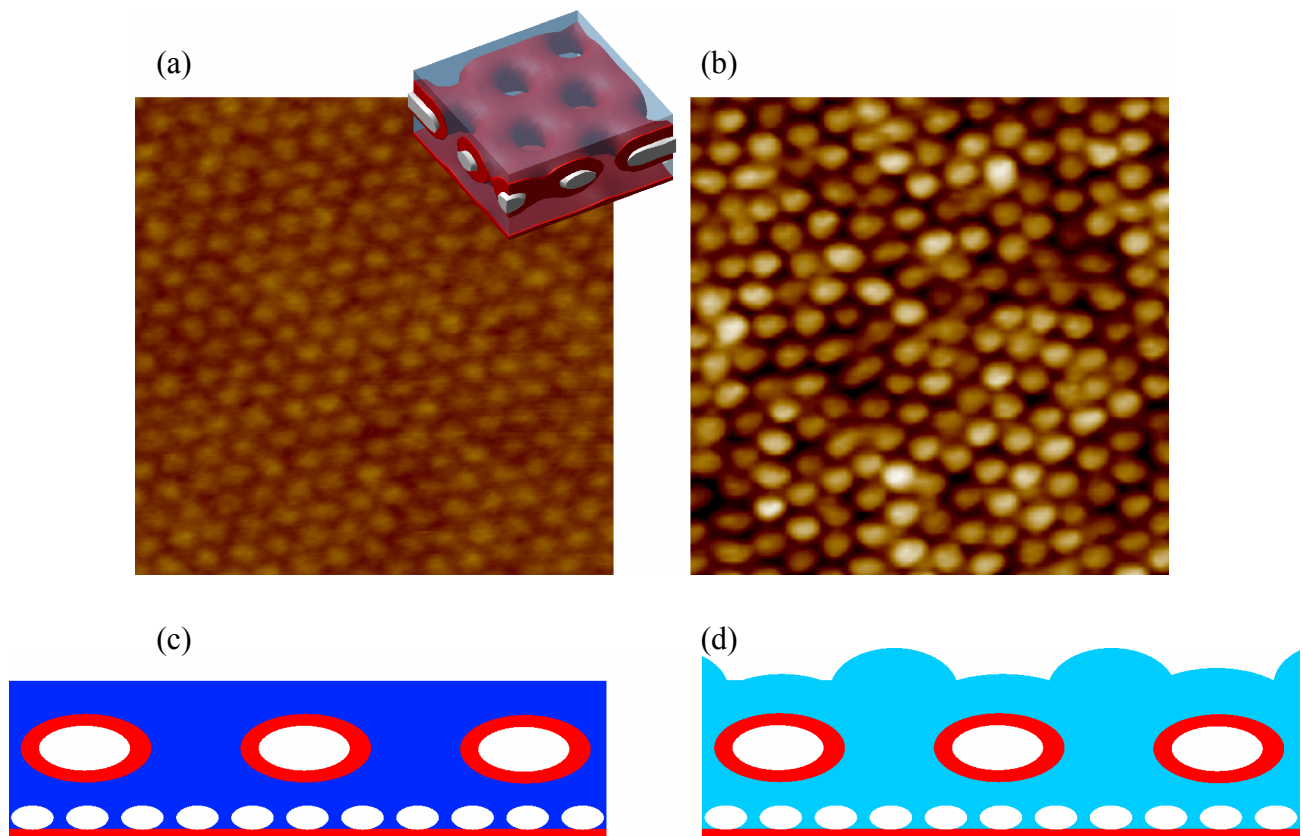


Figure 17. SFM images of the perforated lamella structure (PL) before (a) and after hydrolysis (b). The inset in (a) is a MesoDyn simulation¹¹ of the first terrace of PL, the phases can be assigned to PS (white phase), P2VP (red phase) and PtBMA (blue phase). (c) and (d): Schematic cross-sections of a PL phase before and after hydrolysis. The image size of the SFM images is $1 \times 1 \mu\text{m}^2$. The height scale for (a) and (b) is $\Delta z = 0-10$ nm.

As the pH of the solution is changed, the structure undergoes well defined changes, which are followed in-situ via SFM. As neither the film thickness nor the morphology undergo a transition at

low pH-values ($\text{pH} < 6$) the role of P2VP seems to be negligible for the present investigations. At $\text{pH} \sim 6$ a strong increase of the original film thickness is observed. In the same pH region the structure undergoes a well-defined change: Holes appear at the positions where the protrusions of the perforated lamellae have been, (Fig. 18 (a) and (b)). The hexagonal arrangement of the pattern is not affected, for a better visualization of the effect a typical defect is marked with a box.

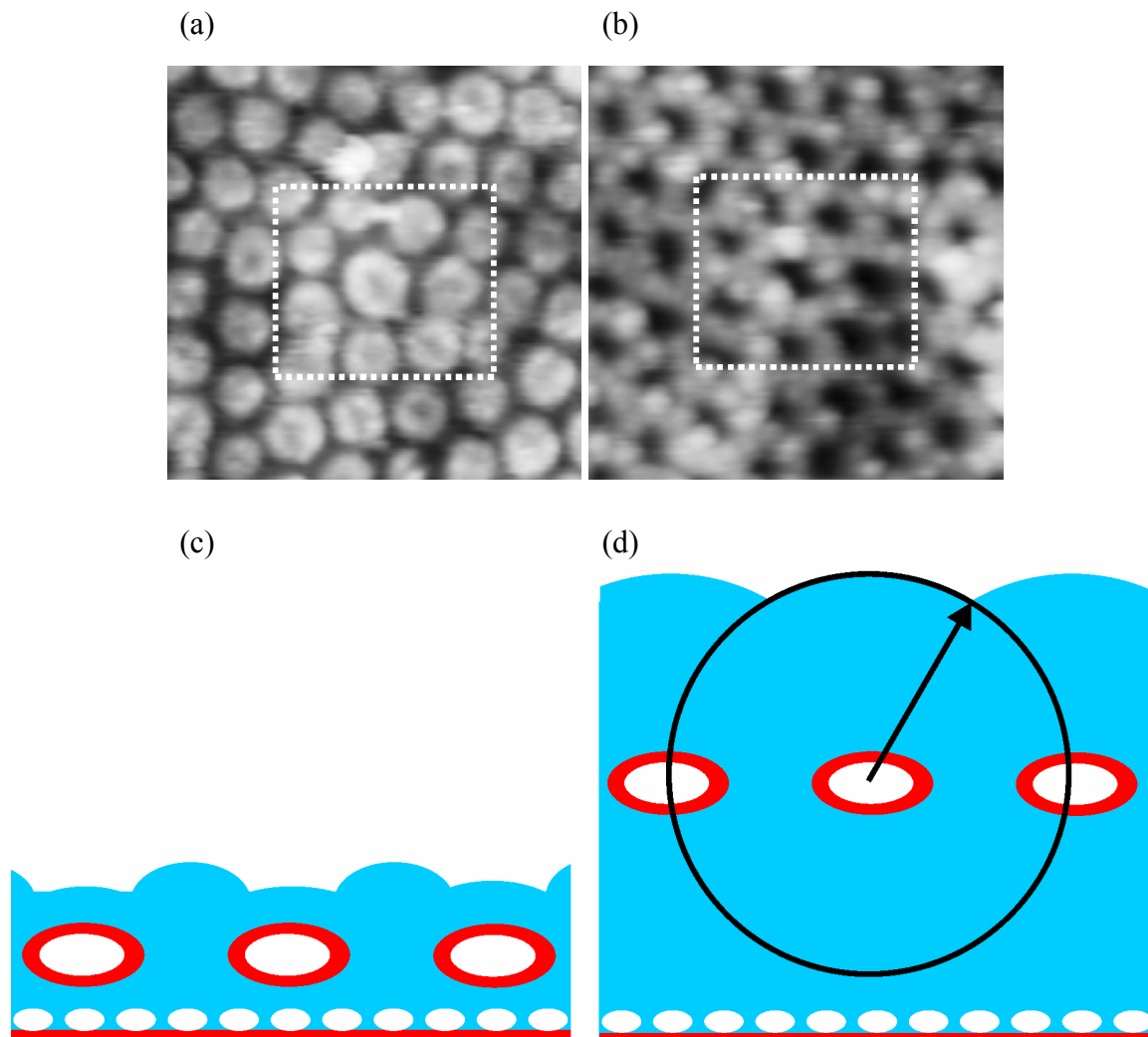


Figure 18. SFM images of one layer of perforated lamellae at $\text{pH} < 6$ (a) and $\text{pH} > 6$ (b). The image size is $500 \times 500 \text{ nm}^2$. The height scale is $\Delta z = 0\text{-}30 \text{ nm}$ for (a), and $\Delta z = 0\text{-}80 \text{ nm}$ for (b). The white box marks the same sample position. (c) and (d): Sketches of the PL phase at $\text{pH} < 6$ and $\text{pH} > 6$, respectively.

The strong increase in the film thickness is explained by a conformational change of the majority component PMAA: while the PMAA chains are Gaussian chain like and confined as matrix phase of the perforated lamella at $\text{pH} < 6$, the chains conformations increase with increasing pH-value of the solution. The chains begin to swell and reach an expanded state at pH-values around 8. As they are chemically linked to P2VP which is immobile at these pH-values, they can only swell to a

certain degree. This is indicated by the circle in Figure 18(d). The first two blocks PS and P2VP act as skeleton of the PL phase which withstands the mechanical forces exerted on the strongly swollen PMAA. In contrast to the PL phase, core-shell cylinders oriented parallel to the interfaces cannot withstand these forces and are solubilised at high pH-values.

2.5. Individual contributions to joint publications

The results presented in this thesis were obtained in collaboration with others, and published as indicated below. In the following, my own contributions to the different publications are specified.

Chapter 3.1

This work is submitted to *Macromolecules* under the title ‘**Combinatorial mapping of the phase behavior of ABC triblock terpolymers in thin films: experiments**’ by S. Ludwigs*, K. Schmidt, C. Stafford, M. Fasolka, A. Karim, E. Amis, R. Magerle, and G. Krausch*.

I performed all the experiments presented in this work. The publication was written by me.

K. Schmidt was involved in measuring small-angle X-ray scattering on CHCl₃ solutions within the scope of her Diplomarbeit.

C. Stafford, M. Fasolka, A. Karim and E. Amis from the National Institute of Science and Technology (NIST) in Gaithersburg, USA provided the facilities to produce both film thickness gradients and substrate surface energy gradients. They taught me how to use their equipment, when I visited NIST in March 2003.

I have profited from scientific discussions with R. Magerle and G. Krausch.

Chapter 3.2

This work is submitted to *Macromolecules* under the title “**Phase behavior of ABC triblock terpolymers in thin films: mesoscale simulations**” by S. Ludwigs*, A. V. Zvelindovsky, G. J. A. Sevink, G. Krausch, and R. Magerle*.

I have run all the simulations and evaluated them. The publication was written by me, whereas R. Magerle, A. V. Zvelindovsky¹, G. J. A. Sevink¹, and G. Krausch contributed to the discussion.

(¹ from Leiden University, NL)

I have used an adapted non-commercial version of the MesoDyn Code.^{15,16,17}

Chapter 3.3

This work is published in *Nature Materials* **2003**, 2, p. 744, under the title ‘**Self-assembly of functional nanostructures of ABC triblock terpolymers**’ S. Ludwigs, A. Böker, A. Voronov, N. Rehse, R. Magerle, and G. Krausch*.

I have performed all the experiments presented in this work. I have discussed the results with G. Krausch. The manuscript was written together with G. Krausch.

Together with A. Böker I have synthesized the polymers in my Diplomarbeit.

I used the UV-depolymerisation technique which had been established by A. Voronov.

N. Rehse and R. Magerle have introduced me in working with the MesoDyn Code.

Chapter 3.4

This work is to be submitted to *Macromolecules* under the title ‘**pH-dependent nanostructures in thin films**’ by S. Ludwigs*, K. Schmidt, and G. Krausch.

I have performed the chemical modification of a thin film microdomain structure to an amphiphilic, pH-responsive structure. I established the measurement of the morphology in the aqueous phase with scanning force microscopy and started to investigate the pH-dependence of the morphology. Kristin Schmidt studied this behavior in more detail under my supervision within the scope of her Diplomarbeit. The publication was written by me.

** marks the corresponding authors of the papers*

2.6. References

- (1) Meredith, J. C.; Smith, A. P.; Karim, A.; Amis, E. J. *Macromolecules* **2000**, 33, 9747.
- (2) Roberson, S. V.; Sehgal, A.; Fahey, A.; Karim, A. *Appl. Surf. Sci.* **2002**, 200, 150.
- (3) Peters, R. D.; Yang, X. M.; Kim, T. K.; Sohn, B. H.; Nealey, P. F. *Langmuir* **2000**, 16, 4625.
- (4) Kim, T. K.; Yang, X. M.; Peters, R. D.; Sohn, B. H.; Nealey, P. F. *J. Phys. Chem. B* **2000**, 104, 7403.
- (5) Girifalco, L. A.; Good, R. J. *J. Chem. Phys.* **1957**, 61, 904.
- (6) Girifalco, L. A.; Good, R. J. *J. Chem. Phys.* **1960**, 64, 561.
- (7) Genzer, J.; Kramer, E. J. *Phys. Rev. Lett.* **1997**, 78, 4946.
- (8) Smith, A. P.; Sehgal, A.; Douglas, J. F.; Karim, A.; Amis, E. J. *Macromol. Rapid Commun.* **2003**, 24, 131.
- (9) Knoll, A.; Magerle, R.; Krausch, G. *J. Chem. Phys.* **2004**, 120, 1105.
- (10) Sawyer L. C.; Grubb, D. T. *Polymer Microscopy*, 2nd ed.; Chapman & Hall: London, 1996.
- (11) Ludwigs, S.; Böker, A.; Voronov, A.; Rehse, N.; Magerle, R.; Krausch, G. *Nature Materials* **2003**, 2, 744.
- (12) Knoll, A.; Horvat, A.; Lyakhova, K. S.; Krausch, G.; Sevink, G. J. A.; Zvelindovsky, A. V.; Magerle, R. *Phys. Rev. Lett.* **2002**, 89, 035501-1.
- (13) Horvat, A.; Lyakhova, K. S.; Sevink, G. J. A.; Zvelindovsky, A. V.; Magerle, R. *J. Chem. Phys.* **2004**, 120, 1117.
- (14) Lyakhova, K. S.; Sevink, G. J. A.; Zvelindovsky, A. V.; Horvat, A.; Magerle, R. *J. Chem. Phys.* **2004**, 120, 1127.
- (15) Fraaije, J. G. E. M. *J. Chem. Phys.* **1993**, 99, 9202.
- (16) Fraaije, J. G. E. M.; van Vlimmeren, B. A. C.; Maurits, N. M.; Postma, M.; Evers, O. A.; Hoffmann, C.; Altevogt, P.; Goldbeck-Wood, G. *J. Chem. Phys.* **1997**, 106, 4260.
- (17) Sevink, G. J. A.; Zvelindovsky, A. V.; van Vlimmeren, B. A. C.; Maurits, N. M.; Fraaije, J. G. E. M. *J. Chem. Phys.* **1999**, 35, 16.
- (18) Grassie, N.; Scott, G. *Polymer Degradation and Stabilisation*, Cambridge University Press: Cambridge, 1988.
- (19) Segalman, R. A.; Yokoyama, H.; Kramer, E. J. *Adv. Mater.* **2001**, 13, 1152.
- (20) Kim, G.; Libera, M. *Macromolecules* **1998**, 31, 2569.
- (21) Park, M.; Harrison, C.; Chaikin, P. M.; Register, R. A.; Adamson, D. H. *Science* **1997**, 276, 1401.
- (22) Thurn-Albrecht, T.; Schotter, J.; Kastle, G. A.; Emley, N.; Shibauchi, T.; Krusin-Elbaum, L.; Guarini, K.; Black, C. T.; Tuominen, M. T.; Russell, T. P. *Science* **2000**, 290, 2126.

- (23) Mansky, P.; Russell, T. P.; Hawker, C. J.; Pitsikalis, M.; Mays, J. *Science* **1997**, 275, 1458.
- (24) Thurn-Albrecht, T.; DeRouchey, J.; Russell, T. P.; Mays, J.; Pitsikalis, M.; Morkved, T.; Jaeger, H. *Macromolecules* **2000**, 33, 3250.
- (25) Jeoung, E.; Galow, T. H.; Schotter, J.; Bal, M.; Ursache, A.; Tuominen, M. T.; Stafford, C. M.; Russell, T. P.; Rotello, V. M. *Langmuir* **2001**, 17, 6369.
- (26) Jeon, C. H.; Makhaeva, E. E.; Khokhlov, A. R. *Macromol. Chem. Phys.* **1998**, 199, 2665.

3. Publications

3.1. Combinatorial mapping of the phase behavior of ABC triblock terpolymers in thin films: experiments

Sabine Ludwigs^{1*}, K. Schmidt¹, C. Stafford³, M. Fasolka³, A. Karim³, E. Amis³, Robert Magerle¹, and Georg Krausch^{1,2*}

¹*Physikalische Chemie II and ²Bayreuther Zentrum für Kolloide und Grenzflächen (BZKG) Universität Bayreuth, D-95440 Bayreuth, Germany*

³*Polymers Division, National Institute of Standards and Technology (NIST), Gaithersburg, MD 20899, USA*

*Corresponding authors: sabine.ludwigs@uni-bayreuth.de and georg.krausch@uni-bayreuth.de,
Tel: +49-921-552751, Fax: +49-921-552059.*

Submitted to *Macromolecules*

Abstract

We report on the thin film phase behavior of poly(styrene)-*block*-poly(2-vinylpyridine)-*block*-poly(*tert*-butyl methacrylate) triblock terpolymers with volume fractions $\phi_{\text{PS}} : \phi_{\text{P2VP}} : \phi_{\text{PtBMA}}$ scaling as 1 : 1.2 : x , with x ranging from 3.05 to 4. On controlled annealing in the vapor of a non-selective solvent the films form terraces of well-defined thickness with a highly ordered hexagonally perforated lamella structure. Using a gradient combinatorial technique we are able to systematically map the dependence of the morphology on the film thickness. By imposing an additional gradient in substrate surface energy orthogonal to the gradually increasing film thickness we demonstrate that the perforated lamella is a stable phase, regardless of the chemical nature of the substrate, which makes the structure and methodology robust for application in nanotechnology.

Introduction

In recent years block copolymers have attracted increasing interest as a promising means to create nanopatterned surfaces, since they self-assemble into highly-ordered structures with characteristic domain spacings between 5 and 50 nm. Recent developments in controlled synthesis^{1,2,3,4} together with theoretical models^{4,5,6,7,8,9,10,11,12,13,14,15} allow to precisely control the morphology and the length scale of the microdomains. Especially triblock terpolymers form a large variety of well-ordered microdomain structures of molecular dimension.² Introduction of functional components and subsequent chemical modification may lead to properties tailored for specific applications.

While block copolymer melts and block copolymer solutions usually show a rather random distribution of microdomain orientations in the bulk, additional driving forces for the structure formation exist near surfaces and in thin films. Typically the polymeric component with the lowest surface energy preferentially accumulates at the surface and the component with the lowest interfacial energy is attracted to the supporting substrate. The presence of such external surfaces and the confinement of the material to a film thickness comparable to the bulk domain spacing can result in large scale alignment of the microdomains and stabilization of novel domain structures.^{14,15,16,17,18,19,20,21}

The majority of studies on block copolymer nanolithography^{22,23,24} has focused on thin films of diblock copolymers, which exhibit spheres or cylinders of the minority component. When the surfaces preferentially attract the majority block, the cylinders align parallel to the substrate.^{25,26,27,28} Quite some effort has been taken to stabilize cylinders oriented perpendicular to the interfaces which is often desired for further processing.^{29,30,31,32,33,34,35}

In a previous Letter we presented a core-shell cylinder forming triblock terpolymer [poly(styrene)-*block*-poly(2-vinylpyridine)-*block*-poly(*tert*-butyl methacrylate)] (PS-*b*-P2VP-*b*-PtBMA) showing a highly ordered perforated lamella structure in thin films.³⁶ This particular thin film structure is a potential candidate for future applications, it can e.g. serve as a lithographic mask or a nanoporous membrane after selective removal of one of the components and it can also be chemically converted into an amphiphilic structure without losing its order. Both, experiments and simulations on cylinder-forming poly(styrene)-*b*-poly(butadiene)-*b*-poly(styrene) block copolymers have shown that the perforated lamella phase can be stabilized by surface interactions in thin films.^{13,14,18}

The film thickness has been shown to be a relevant parameter for the structure formation of block copolymers in thin films. Knoll *et al.* have recently presented experiments and matching computer simulations of thin films of an A-B-A triblock copolymer which model in detail the experimentally observed phase behavior.^{14,15,16,37} With increasing film thickness, both experiments and simulations showed the same sequence of thin film phases: a disordered phase for the smallest thickness, very

short upright A-cylinders, A-cylinders oriented parallel to the film plane, a perforated A-lamella, parallel oriented A-cylinders, perpendicular oriented A-cylinders, and finally two layers of parallel oriented A-cylinders. The phase transitions occurred at well-defined film thickness with cylinders oriented parallel to the interfaces being formed predominantly on the terraces.

In the present paper we compare the structure formation of the above-mentioned core-shell cylinder forming PS-*b*-P2VP-*b*-PtBMA triblock terpolymer in solution and in thin films. In the latter case the samples are annealed in controlled solvent vapor atmosphere with the structure formation process taking place in concentrated solutions. In this study we employ gradient combinatorial techniques which enable a systematic analysis of the film phase behavior in a single specimen. In addition to rapidly providing a comprehensive map of the phase behavior, such techniques reduce the problems of reproducibility since processing parameters are held constant. For instance here we keep solution concentration and solvent exposure constant and vary film thickness and substrate interaction. Our aim is to understand and eventually control the rather complex phase behavior of triblock terpolymers.

Experimental section

Molecular characteristics

Using sequential living anionic polymerization we synthesized a series of monodisperse triblock terpolymers consisting of poly(styrene) (PS), poly(2-vinylpyridine) (P2VP), and poly(*tert*-butyl methacrylate) (PtBMA) with increasing molecular weight of the PtBMA block. Details about synthesis and bulk characterization have been described previously.³⁸ Table 1 summarizes the molecular parameters of the polymers investigated in the present contribution. Depending on the volume fraction of PtBMA the materials in bulk form core-shell cylinders ($\phi_{\text{PS}} : \phi_{\text{P2VP}} : \phi_{\text{PtBMA}} = 1 : 1.2 : 4$) and a coexistence of core-shell gyroids, core-shell cylinders, and what we assume to be a perforated lamella structure ($\phi_{\text{PS}} : \phi_{\text{P2VP}} : \phi_{\text{PtBMA}} = 1 : 1.2 : 3.05$ to 3.63). In the following we denote the polymers as $S_xV_yT_z^{M_w}$ with the subscripts representing the weight fractions of the respective blocks (parts of hundred), and the superscript M_w indicating the total weight-averaged molecular weight in kg/mol. We will focus our investigations on the polymer with the highest amount of PtBMA, $S_{16}V_{21}T_{63}^{140}$, which forms in the bulk a well-defined core-shell cylinder structure with poly(styrene) forming the core surrounded by a shell of poly(2-vinylpyridine) within a matrix of poly(*tert*-butyl methacrylate).

Solutions of $S_{16}V_{21}T_{63}^{140}$ both in chloroform (CHCl_3) and in tetrahydrofuran (THF) with different mass fractions w_p were investigated with small angle X-ray scattering (SAXS). Synchrotron SAXS

measurements were performed at the ID2 beamline at the European Synchrotron Radiation Facility (ESRF, Grenoble, France). All solutions were directly prepared in capillaries with about 2 mm diameter. The typical photon flux obtained at the ID2 sample position is $8 \cdot 10^{12}$ photons/sec, the energy bandwidth is $\Delta E/E = 2 \cdot 10^{-4}$. All experiments were obtained at 12.5 keV corresponding to an X-ray wavelength of 0.1 nm. The scattering intensities were detected via a CCD camera. The detector system is housed in a 10 m evacuated flight tube. The scattering patterns were corrected for the beam stop and the background prior to evaluations. The calculations of the scattering intensities were obtained with the Fit2D evaluation program.

Table 1. Block terpolymer molecular characteristics

Polymer ^a	M_w [kg/mol]	M_w/M_n ^b (GPC)	$\phi_{PS} : \phi_{P2VP} : \phi_{PtBMA}$ ^b	d_{SAXS} [nm] ^b	Morphology ^c
S ₁₉ V ₂₅ T ₅₆ ¹²⁰	120	1.03	1 : 1.2 : 3.05	(71±3) nm	G/PL/C
S ₁₇ V ₂₂ T ₆₁ ¹³²	132	1.03	1 : 1.2 : 3.65	(74±3) nm	G/PL/C
S ₁₆ V ₂₁ T ₆₃ ¹⁴⁰	140	1.03	1 : 1.2 : 4	(72±3) nm	C

^aS_{%PS}V_{%P2VP}T_{%PtBMA}^{M_w} with the subscripts representing the weight fractions of the respective blocks (parts in hundred), while M_w is the total weight-averaged molecular weight in kg/mol;

^bKey: M_w/M_n , polydispersity determined with GPC; $\phi_{PS} : \phi_{P2VP} : \phi_{PtBMA}$, volume fraction; d_{SAXS} , bulk domain spacing determined with SAXS measurements.

^cKey: G, core-shell-gyroids; PL, perforated lamellae; C, core-shell cylinders.

Thin film sample preparation

Thin films were cast onto polished silicon substrates from chloroform solutions. The polymer solutions were placed between a glass blade located about 100 μm above a silicon substrate at a relative angle of 5°. The substrate was moved relative to the blade at constant acceleration resulting in linear gradients in film thickness. Solutions with 1 – 2 wt.% polymer resulted in a gradually increasing film thickness from (30 to 120) nm. The thickness variation was detected with an automated Filmetrics F20 UV-visible interferometer. For detailed information about preparation of gradients in film thickness, see reference ³⁹. The as-prepared samples were subsequently annealed in a well-controlled atmosphere of chloroform or tetrahydrofuran vapor for several days to induce mobility and facilitate equilibration. Details of the experimental set-up are described in reference ¹⁶. As the molecular weight of the investigated polymer is quite high (140 kg/mol) relatively high vapor pressures ($p_{\text{CHCl}_3} = 0.9 p_0$, $p_{\text{THF}} = 0.95 p_0$, with p_0 being the vapor pressure of saturated chloroform and THF, respectively) were needed to ensure a reproducible microstructure formation process in thin films.

After swelling in solvent vapor for a certain time interval the microdomains were frozen in via

quenching with pure air. This results in a shrinking of the swollen film thickness. The samples were then investigated with light microscopy, scanning force microscopy (SFM) (Dimension 3100 Metrology SFM from Digital Instruments operated in Tapping Mode) and field-emission scanning electron microscopy (FE-SEM) (LEO 1530). Scratches with a needle were made on the sample to enable imaging of the same spot with all techniques and to facilitate step height measurements with SFM. While SFM is a non-destructive technique for surface investigations, it is well-known that electron beam damage during SEM imaging can lead to considerable volume shrinkage of polymethacrylate phases⁴⁰. Using the in-lens detector of the SEM at a quite low accelerating voltage of 0.8 kV enables the detection of a material contrast between the different components of the block copolymers.

Combinatorial library

On some of our samples, we produced orthogonal gradients in film thickness and surface energy. Chemically grafted self-assembled monolayers (SAM) of trialkylsilanes were prepared by reaction of monofunctional n-octyldimethylchlorosilane (ODS, > 95% mass concentration, Gelest Inc, Tullytown, PA) with silicon wafers in the vapor phase. The SAM is subsequently exposed to UV/ozone radiation with stepwise increasing exposure time. This leads to a chemical modification with a laterally varying density of hydrophilic surface chemical moieties (COOH, COH groups) across the sample.^{41,42,43} Further details about this technique have been described elsewhere.⁴¹ The change in surface energy can be evaluated by static contact angle measurements of water and diiodomethane. Figure 1(a) shows the water contact angle measured every 5 mm across a wafer beginning from the hydrophobic (untreated SAM, 0 mm) towards the hydrophilic substrate region (longest exposure time to UV/ozone source, 45 mm) which exhibits the same water contact angle as pure SiO_x. The surface energy was estimated by using the Good and Girifalco geometric mean approximation.^{41,44,45,46}

Thin films of the block copolymers were subsequently cast onto the substrate with the surface energy gradient from 1-2 wt.% CHCl₃ solutions with a gradient in thickness orthogonal to the energy gradient, Figure 1(b).⁴⁷ This combinatorial library can be divided into a virtual array of individual cells with contact angles ranging from (40 to 95)° across 45 mm and thickness values from (30 to 120) nm across 45 mm.

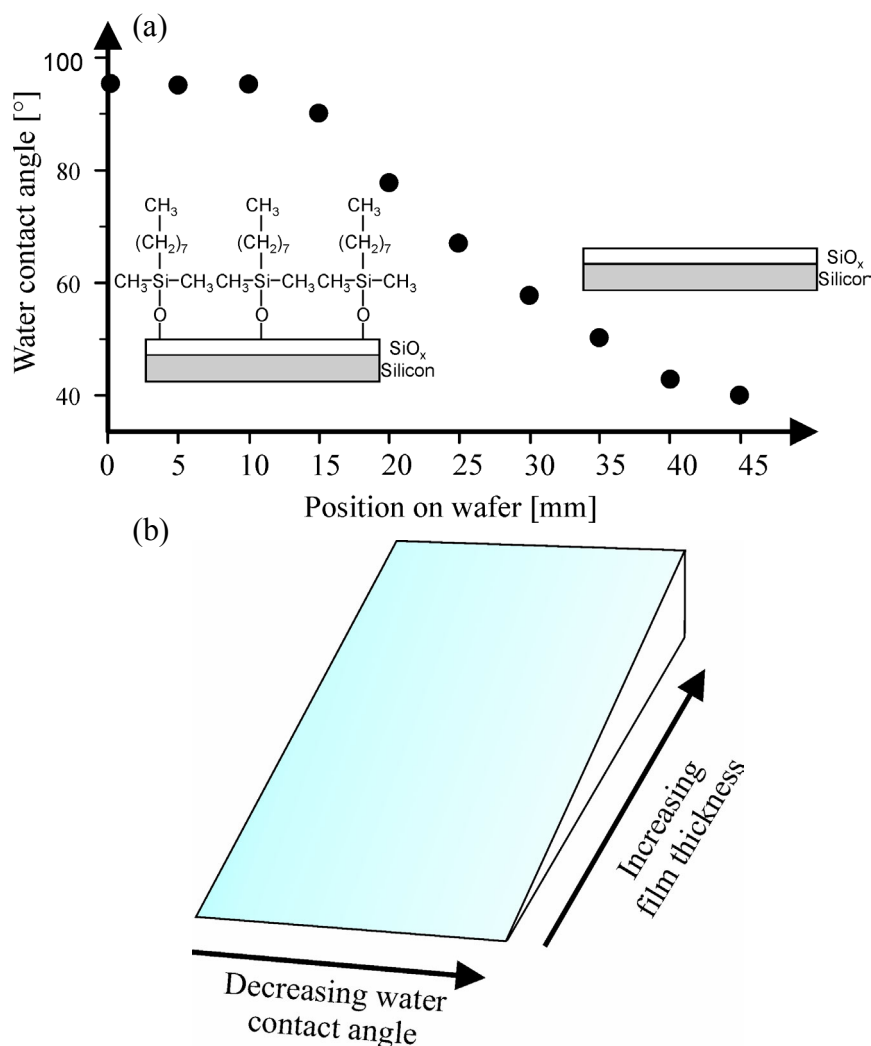


Figure 1. (a): Substrate surface energy gradient. Water contact angles measured at different sample positions. The insets show the surface composition at the two extreme cases (hydrophobic, left, and hydrophilic, right). (b): Sketch of a combinatorial library with orthogonal gradients in film thickness and substrate surface energy.

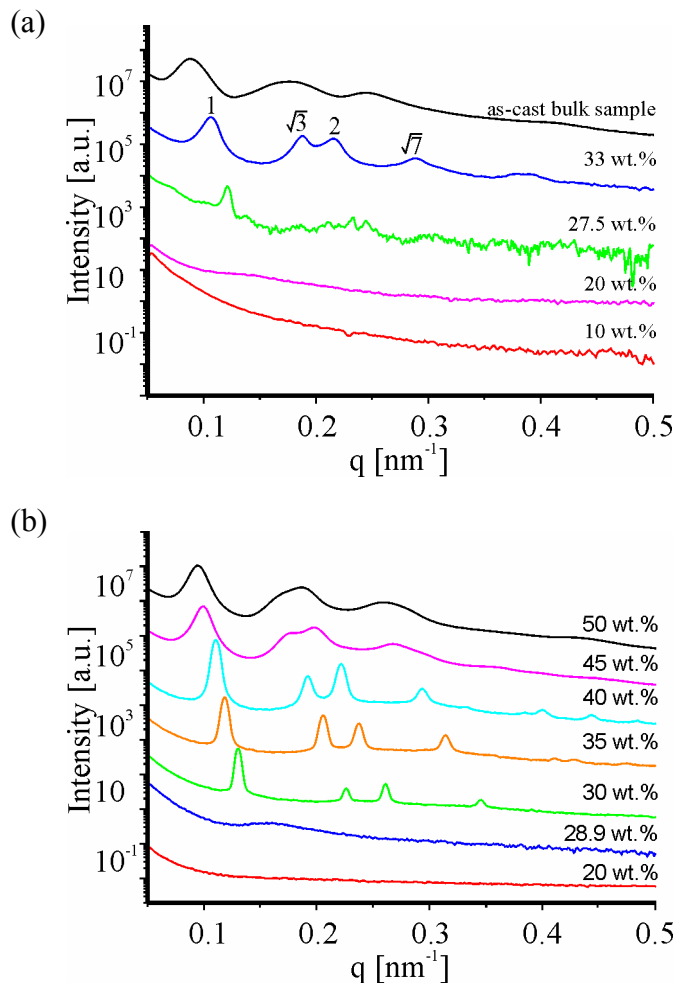
Etching methods

In order to establish the microdomain structure beneath the surface some films were investigated by Nanotomography⁴⁸. For volume imaging ~ 7 nm thick layers of the block copolymer were successively removed by plasma etching and Tapping Mode SFM images were taken after each erosion step at the same spot of the sample. For plasma etching the thin film was placed in a Harrick PDC-32G Plasma Cleaner which was then operated with pure oxygen plasma at 1.5 ± 0.1 mbar and 60W rf for 7s. The etching rates of the block components have been determined to: $v(\text{PS}) = 29.4$ nm/min, $v(\text{P2VP}) = 33.6$ nm/min, $v(\text{PtBMA}) = 63$ nm/min. Alternatively, exposing the thin film to UV-light (UV-B, 150 W, 60 min) and subsequent rinsing with n-hexane was used to selectively remove the methacrylate component.

3.1.1. Results and discussion

Solution behavior of $S_{16}V_{21}T_{63}^{140}$

Figures 2(a) and (b) show SAXS spectra of solutions of $S_{16}V_{21}T_{63}^{140}$ in CHCl_3 and THF, respectively, with polymer weight fractions w_p between 10 and 50 wt.%. Above a certain concentration the SAXS spectra show Bragg peaks with relative positions of $1 : \sqrt{3} : 2 : \sqrt{7}$ characteristic of hexagonally ordered cylinders. This finding is consistent with the hexagonal structure found for dry bulk samples cast from solution.³⁸ From the SAXS spectra the order-disorder transition for THF solutions $w_{p,\text{ODT,THF}}$ can be located between 28.9 wt.% and 30 wt.%. With additional birefringence experiments (not shown here) we determined the order-disorder transition for CHCl_3 solutions to $w_{p,\text{ODT,CHCl}_3} = (26 \pm 0.5)$ wt.%. Figure 2(c) shows the domain spacing as function of the polymer weight fraction. With increasing polymer weight fraction the domain spacing increases with a maximum value found for the melt spacing after solvent evaporation ($w_p = 100\%$).



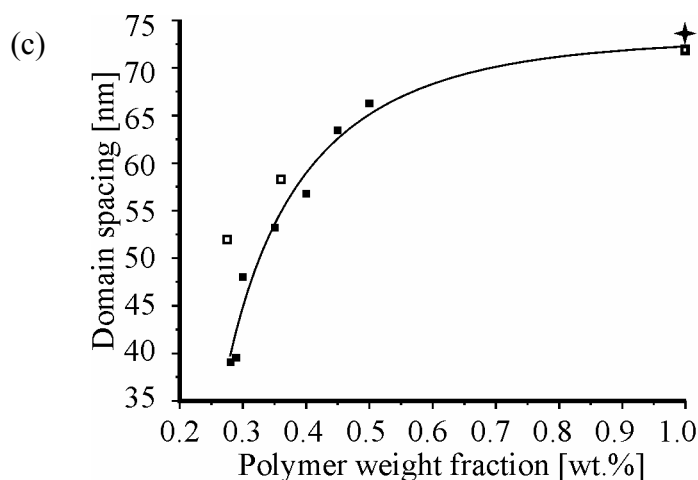
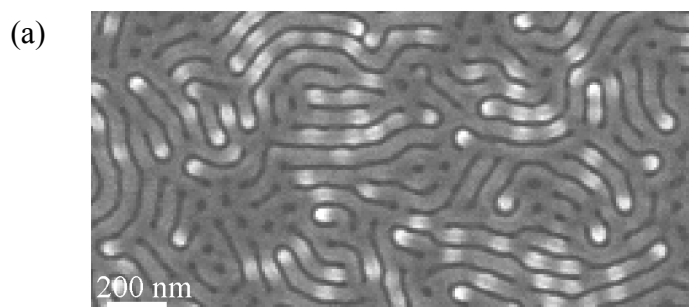


Figure 2. SAXS spectra of $S_{16}V_{21}T_{63}^{140}$ in $CHCl_3$ (a) and THF (b) solutions; (c) shows the domain spacing as function of the polymer weight fraction, open symbols correspond to $CHCl_3$ solutions, closed symbols represent THF solutions, the star marks the domain spacing of a $CHCl_3$ -cast bulk sample. The line is a guide to the eye.

Structure formation process in thin films

Rather high vapor pressures of the solvent are needed for a reproducible structure formation in thin films. The degree of swelling during solvent vapor exposure can be determined with a spectroscopic ellipsometer.^{49,50} At vapor pressures of $p_{CHCl_3} = 0.9 p_0$ the films swell to 2.5 times their dry thickness resulting in polymer concentrations of $w_p = 32.5$ wt.%. This concentration is well above the determined order-disorder transition. The viscosity at this concentration is very high because of the high molecular weight of the polymer (140 kg/mol). Accurate control of the vapor pressure and sufficiently long annealing times are indispensable for reproducible formation of ordered microdomain structures. As an example, Figures 3(a) and (b) show ~ 40 nm thick films after insufficient annealing. In both cases the structures show little long-range order and appear to be unstable against further evolution in presence of solvent vapor. The annealing times required to form equilibrium microdomain structures increase with increasing film thickness: For thin film gradients with thicknesses between (30 and 120) nm annealing times of about 120 h are required to obtain stable structures.



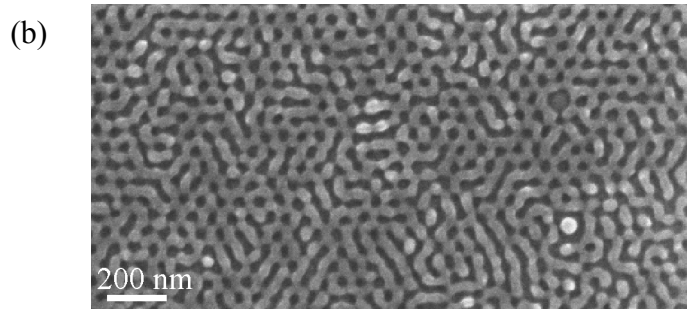


Figure 3. SEM micrographs of a ~ 40 nm thick film of $S_{16}V_{21}T_{63}^{140}$ after annealing in chloroform vapor for 10 (a) and 16 hours (b).

Figure 4(a) shows an optical micrograph of a thin film of $S_{16}V_{21}T_{63}^{140}$ on a silicon substrate prior to annealing. The film thickness increases from about 30 nm (at the top) to about 120 nm (at the bottom) over a lateral distance of about 10 cm. On annealing in CHCl_3 vapor ($p_{\text{CHCl}_3} = 0.9 p_0$, $t = 120$ h), the originally smooth gradient in film thickness develops terraces of uniform thickness characterized by uniform interference colors in the optical micrographs (Figure 4(b)). This finding suggests that the local thickness adjusts to local minima of the free energy of the system which are related to energetically preferred microdomain structures in the film.⁵¹ In the following the terraces are denoted as T_0 , T_1 , T_2 , T_3 , T_4 and T_5 in the succession of increasing film thickness. The terraces show the same progression from holes to islands to smooth surface as function of film thickness as found in other block copolymer systems.^{14,51}

The terraced surface structures were investigated with scanning force microscopy and subsequent scanning electron microscopy at the same spot of the sample: Scratches with a needle were made to mark a particular sample region and to enable height measurements with SFM. Figure 5(a) shows as example a SFM height image of the slope between the neighboring terraces T_1 and T_2 next to a scratch down to the pure silicon substrate, together with a cross section corresponding to the height difference between T_1 and T_2 . The local film thickness d was determined with the step height feature of the Nanoscope III 5.13r10sr1. software and amounts to $d_{T_1} \approx 35$ nm for the first terrace, $d_{T_2} \approx 59$ nm for the second terrace, and $\Delta d(T_1, T_2) \approx 24$ nm for the thickness difference between the two terraces. Figure 5(b) shows the height image of T_1 with a higher magnification. The topography is still very smooth, the difference between peaks and valleys amounts to 2 nm. Figure 5(c) finally exhibits the corresponding SEM image of the same region (compare the identically located boxes in Figures 5(a), (b) and (c)) which shows clearly resolved stripe-like and dot like patterns. In principle we should be able to correlate the topography of Figure 5(c) with Figures 5(a) and (b). This is complicated because of a PtBMA cover layer on top which is in fact etched in the SEM (this effect will be discussed later). The left part of the SEM image (T_2) appears darker than the right part (T_1).

At the SEM operating conditions chosen here (acceleration voltage ~ 0.8 kV) we find quite consistently that the secondary electron yield from thicker regions of the films is smaller than from thinner regions resulting in the observed “color” differences in the SEM images. At these low electron energies the thickness of the insulating polymer layer seems to have a profound effect on the secondary electron yield. This effect is diminished in higher thickness transition layers.

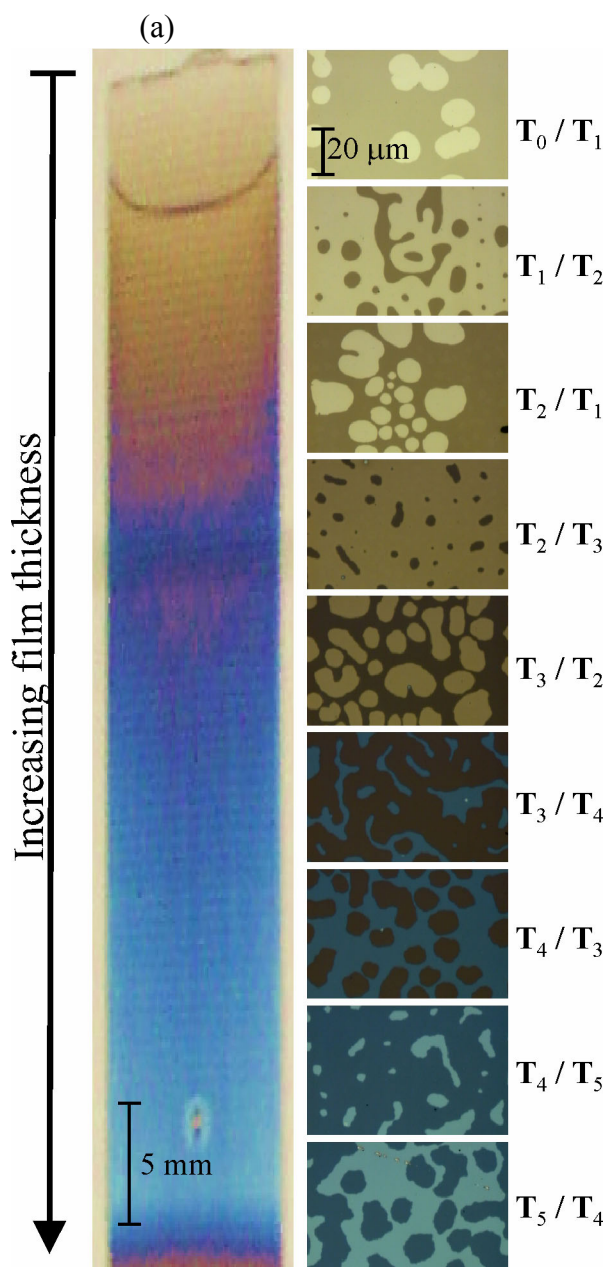


Figure 4. Optical micrographs of the film thickness gradient before (a) and after annealing in solvent vapor (b). The terraces are labeled from T_0 to T_5 with increasing film thickness.

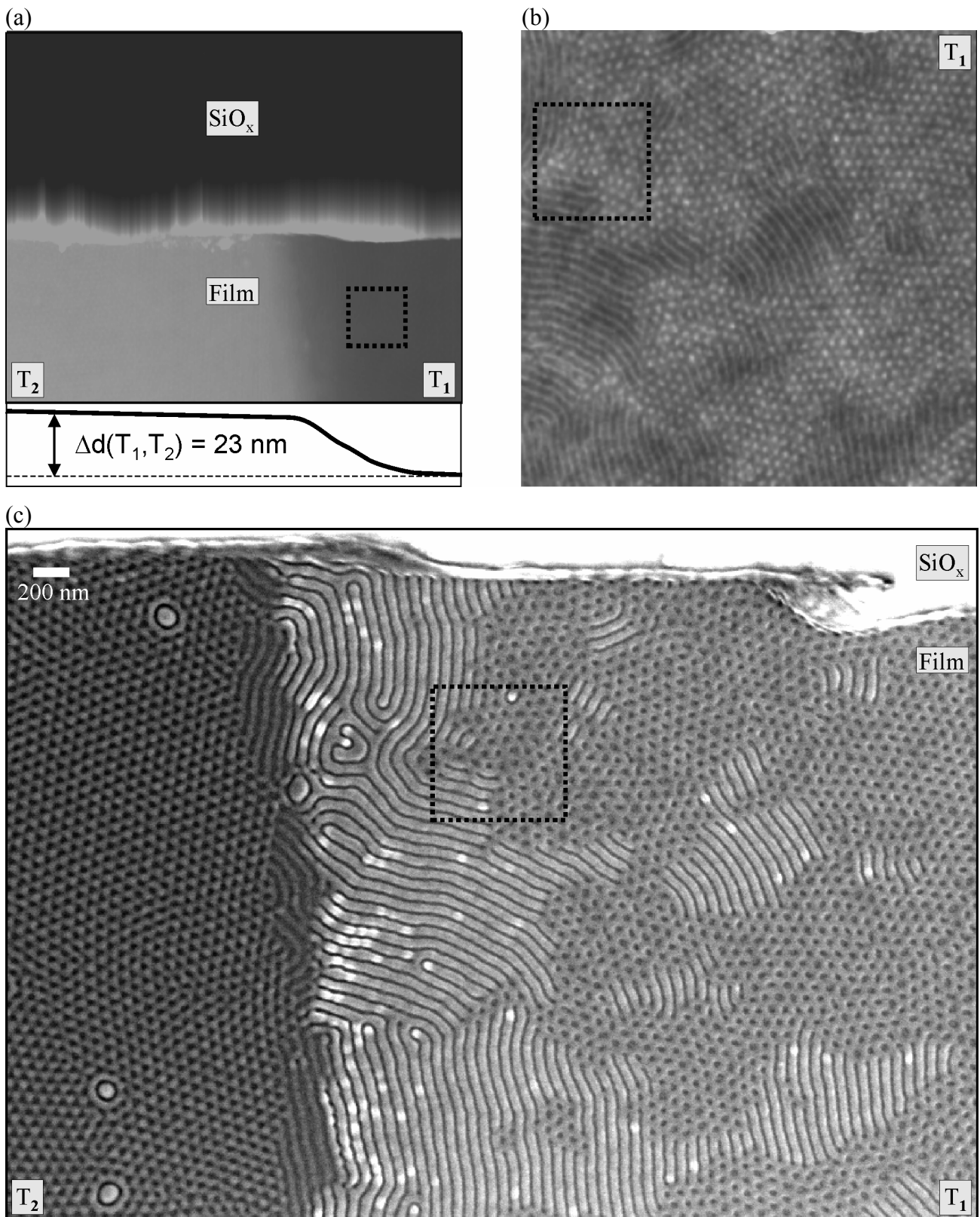
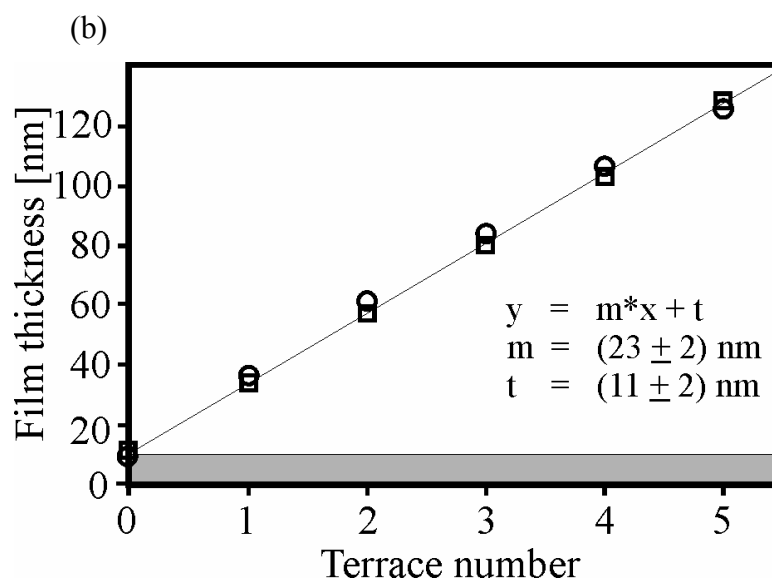
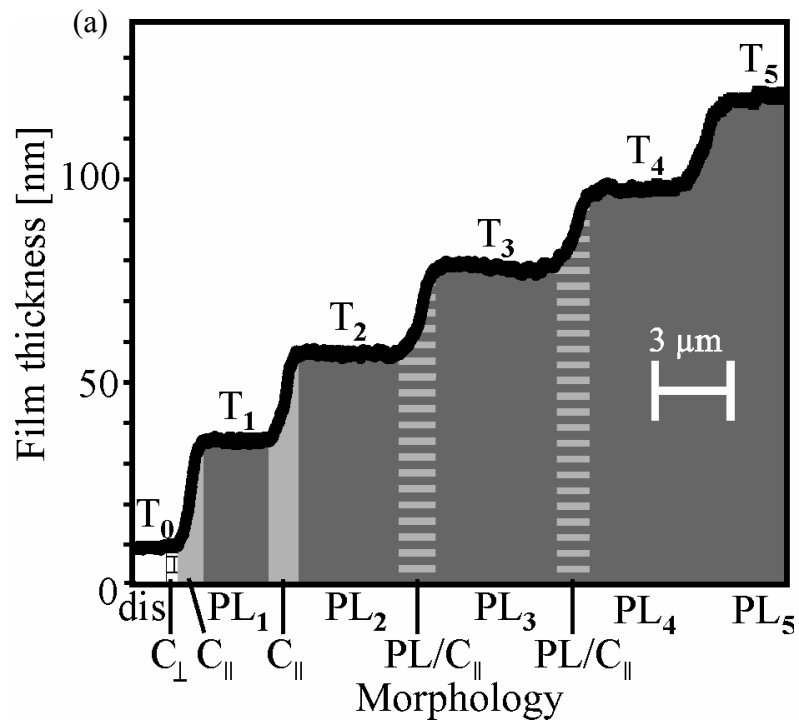


Figure 5. Images of a thin film of $S_{16}V_{21}T_{63}^{140}$ after exposure to $p_{\text{CHCl}_3} = 0.9 p_0$ for 120 h (with p_0 being the vapor pressure of saturated chloroform) taken with different techniques. (a) SFM topography image of a transition between T_1 and T_2 next to a scratch (image size: $6 \times 6 \mu\text{m}^2$) together with the corresponding height profile, (b) higher magnification SFM topography image of T_1 (image size: $3 \times 3 \mu\text{m}^2$), (c) SEM image of the same sample region; the black boxes indicate the same sample positions.

Thin film phase behavior of $S_{16}V_{21}T_{63}^{140}$, annealed in $CHCl_3$ vapor

In this section we systematically investigate the morphology as function of the film thickness for a thin film of $S_{16}V_{21}T_{63}^{140}$ prepared on a hydrophilic substrate (SiO_x) after annealing in $CHCl_3$ vapor ($p_{CHCl_3} = 0.9 p_0, t = 120$ h). In a second experiment we systematically vary the substrate nature from hydrophilic to hydrophobic to test the stability of the structure to variations of substrate conditions, surface energy being an important substrate parameter.



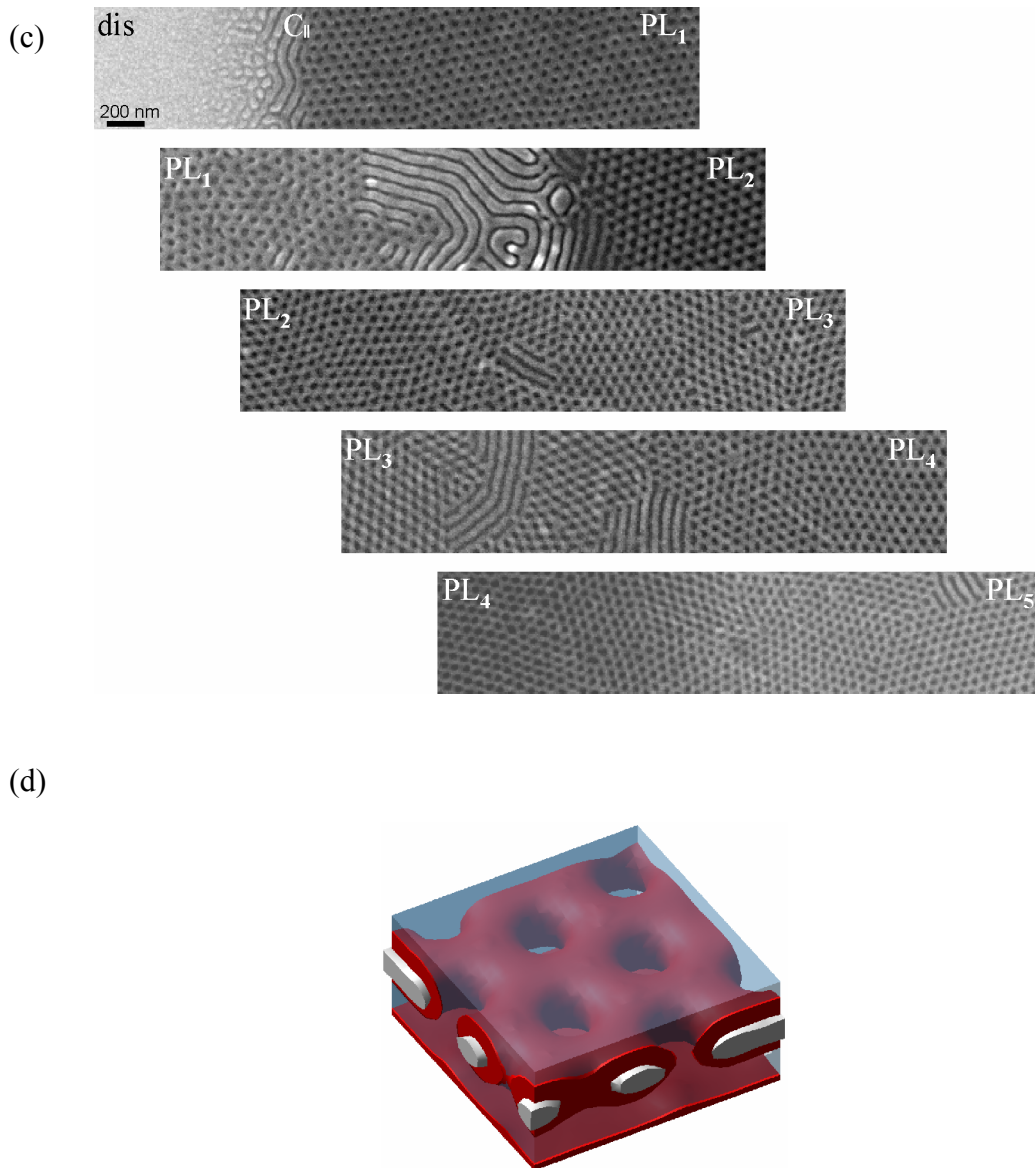


Figure 6. Thin film phase behavior of a thin film of $S_{16}V_{21}T_{63}^{140}$ ($p_{CHCl_3} = 0.9 p_o$, $t = 120$ h). (a): Height profiles between neighboring terraces (measured with SFM) which are merged laterally. The transitions from T_0 to T_1 , from T_1 to T_2 , from T_2 to T_3 , from T_3 to T_4 , and from T_4 to T_5 are shown. (b): Film thickness as function of the terrace number, the circles represent terraces formed on hydrophilic substrates (SiO_x), the boxes represent terraces formed on hydrophobic substrates (SAM); the height of the symbols includes the error bar. (c): Corresponding SEM images of the same sample regions. The terrace structures can be assigned to perforated lamellae (PL). (d): Mesodyn simulation of the first terrace of perforated lamellae, the phases can be assigned to PS (white phase), P2VP (red phase) and PtBMA (blue phase).³⁶

In Fig. 6(a) we have summarized the development of the film thickness with increasing step height from terrace T_0 to T_5 for a thin film prepared on SiO_x . The thickness values are determined from SFM height images of neighboring terraces, and subsequently merged. The film thickness as

function of the terrace number is displayed in Fig. 6(b). The open circles in 6(b) correspond to terraces observed on SiO_x . The heights increase linearly with the number of layers in the film. The first terrace exhibits a film thickness of $d_{T0} \approx (11 \pm 2)$ nm. The offset corroborates the existence of a wetting layer with a thickness of $d_{T0} \approx (11 \pm 2)$ underneath the terraces T_1 to T_5 . The height differences between the remaining terraces were found to have a constant value of $\Delta d \approx (23 \pm 2)$ nm. We emphasize that there is no significant difference in film thickness no matter whether the terraces appear as holes, islands, or smooth surface. The thickness of individual terraces shows a scatter of some 2 nm. This rather small scatter may be explained by our combinatorial approach: The morphology as function of the film thickness is investigated in a single experiment.

The scanning electron micrographs (Fig. 6(c)) exhibit the following sequence of structures: The regions with the lowest film thickness (T_0) show a disordered structure (dis), followed by a liquid-like distribution of dots (bright dots) which may be assigned to perpendicularly oriented PS/P2VP-cylinders in a PtBMA matrix (C_{\perp}). The stripe-like pattern can be identified as cylinders aligned parallel to the plane of the film (C_{\parallel}). The terraces show a hexagonal arrangement of dark dots, which are identified as a perforated lamella (PL). For detailed discussion of the PL phase see below. The slopes between adjacent terraces exhibit C_{\parallel} between T_1 and T_2 and a coexistence of C_{\parallel} and PL between T_2 and T_3 and between T_3 and T_4 . At larger film thickness, the perforated lamella phase is observed throughout the entire thickness range as surface structure (see, e.g., between T_4 and T_5).

Scanning force microscopy height images of the PL phase exhibit a rather smooth surface topography which can be explained by a thin layer of the matrix phase poly(*tert*-butyl methacrylate) at the air/film interface. PtBMA is the component with the lowest surface energy and preferentially accumulates at the air surface: $\gamma_{\text{PS}} = 41 \text{ mN/m}^{52}$, $\gamma_{\text{P2VP}} = 40 \text{ mN/m}^{53}$, $\gamma_{\text{PtBMA}} = 30.5 \text{ mN/m}^{52}$. The scanning electron micrographs reveal a clearly resolved hexagonal arrangement of dark dots, because the topmost layer of the methacrylic ester is removed upon exposure to the electron beam. Similarly, upon exposure of the film to UV light the top 7 nm of the thin film are removed and a hexagonal array of holes develops beneath the originally rather flat surface, which can also be imaged with SFM. Figure 7 shows SFM images prior to (a) and after exposure to UV irradiation (b). Etching in an oxygen plasma can be used for volume imaging of one layer of PL: After three etching steps (Fig. 7(c) after 15 sec, (d) after 75 sec, (e) after 135 sec) and removal of an approximately ~ 30 nm thick layer ($d_{T1} \approx 35 \pm 2$) nm a hexagonal array of holes is still visible in the scanning force microscopy height image. This finding is attributed to the somewhat higher etching rate of PtBMA, which causes the PS and P2VP rich domains to protrude over the PtBMA rich areas after etching. Further etching did not change the structure and the film thickness. The wetting layer beneath the PL phase cannot be resolved in this manner. This may be explained by a chemical

cross-linking process of the polymers, as especially poly(styrene) and poly(2-vinylpyridine) tend to crosslink in the presence of radicals. This makes it also impossible to investigate thicker terraces of PL.

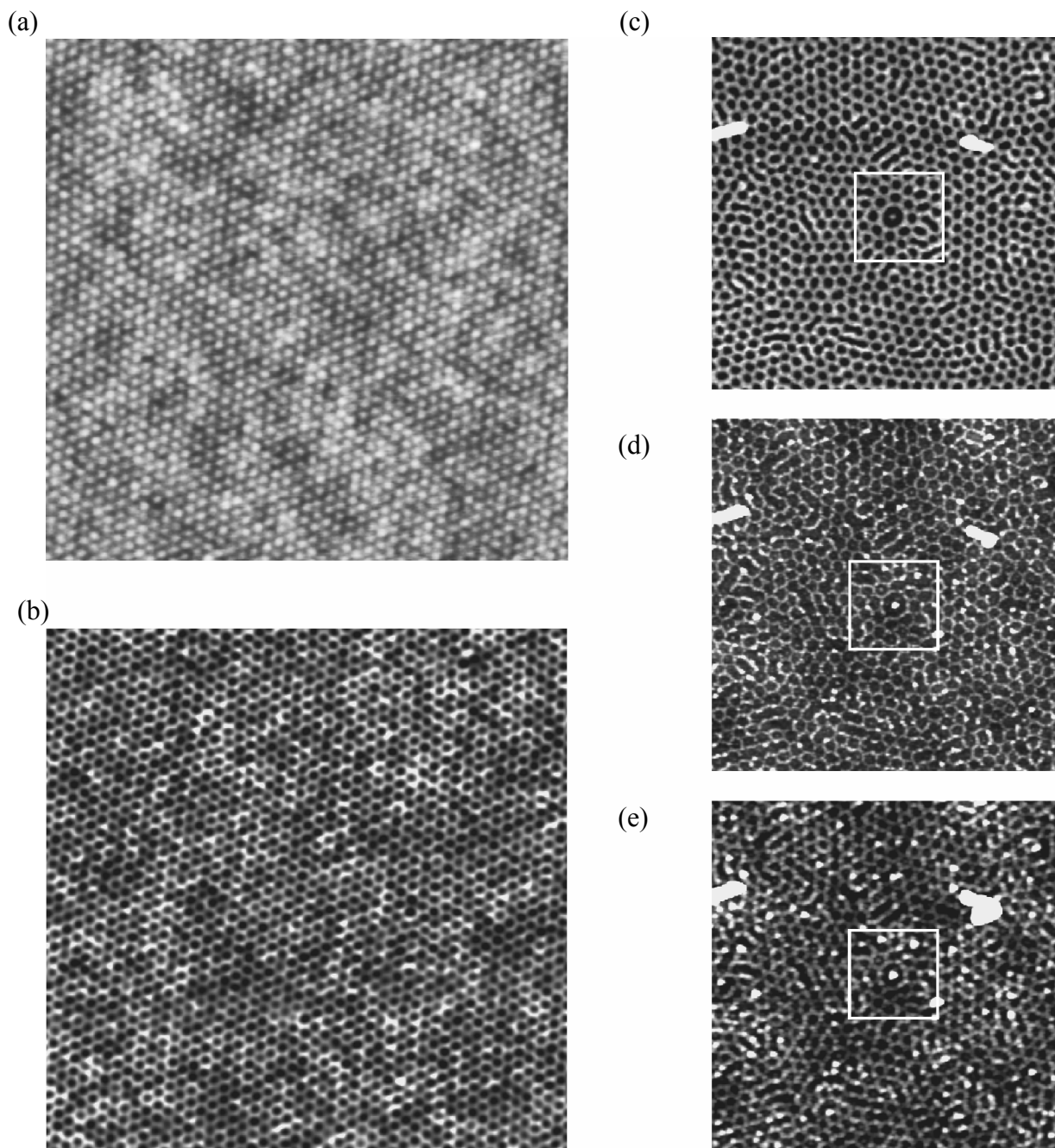


Figure 7. SFM images of a perforated lamella structure. Before (a) and after (b) exposure to UV light for 10 minutes. Image size: $3 \times 3 \mu\text{m}^2$, height scale: $\Delta z = 0\text{-}10 \text{ nm}$. (c) to (e): Layer-by-layer imaging: SFM images after 15 sec (c), 75 sec (d), and 135 sec (e) etching in oxygen plasma. Image size: $2 \times 2 \mu\text{m}^2$, height scale: $\Delta z = 0\text{-}10 \text{ nm}$.

The PL phase can be visualized as a P2VP/PS/P2VP sheet perforated by PtBMA channels, which connect between two outer PtBMA layers. The experimental results are supported by recent

calculations based on the dynamic functional theory (DDFT) using the MesoDyn code.³⁶ Figure 6(d) shows a sketch of the first terrace of PL. The PtBMA majority phase has the lowest surface energy and therefore is attracted to the free surface of the film. We assume that due to the particular stoichiometry of the block copolymer ($\phi_{\text{PtBMA}} = 61$ vol.%) the wetting layer next to the substrate is terminated by a PtBMA-rich surface which can also attract PtBMA. In consequence the perforated lamella phase is stabilized between two interfaces both attracting the majority component of the polymer. In the experiments, in the case of the polar SiO_x substrate, the wetting layer ($d_{T_0} \approx 10$ nm) is attributed to a thin, laterally homogeneous layer of polymer chains physisorbed from solution via the most polar block poly(2-vinylpyridine) block⁵⁴. Fukunaga *et al.* have shown that polystyrene-*b*-poly(2-vinylpyridine)-*b*-poly(*tert*-butyl methacrylate) is pinned with P2VP onto SiO_x substrates with PtBMA forming a uniform layer on top.^{55,56}

Effect of substrate surface energy

We also prepared a combinatorial library of $\text{S}_{16}\text{V}_{21}\text{T}_{63}$ ¹⁴⁰ with orthogonal gradients in film thickness (30 to 120 nm) and water contact angle (95° to 40°). Using the same annealing conditions as above ($p = 0.9 p_0$, 120 h) the smoothly varying film thickness is again turned into six terraces ($T_0 - T_5$) of well defined thickness orthogonal to different substrate surface energies with water contact angles ranging from 95° to 40°. Fig. 6(b) includes the thickness values obtained for thin films prepared at the hydrophobic extreme value, i.e. untreated self-assembled monolayers (SAM, water contact angle: 95°). The heights increase linearly with the number of layers in the film. As the values identically track values observed on the hydrophilic SiO_x substrate, we conclude that the substrate surface energy does not affect the film thickness of the individual terraces. This is also observed for the full range of intermediate surface energies across the surface energy gradient substrate, i.e., surface energy does not influence the surface patterns. The offset d_{T_0} corroborates the existence of a wetting layer. On a hydrophobic substrate we assume that PS is attracted by the substrate and PtBMA forms a layer on top, as poly(styrene) is the least polar block. As the surface structures and the film heights are the same on hydrophilic and hydrophobic substrates we assume a half-lamella layer terminating with poly(*tert*-butyl methacrylate). Removing the thin film from the substrate and investigating the bottom of the film could probably help to resolve the structure of the thinnest layer. The graded specimen presents a range of surface energies for which PS, P2VP, or both are present at the substrate. The majority component PtBMA ($\phi_{\text{PtBMA}} = 61$ vol.%) always forms the uniform top layer of this wetting layer. We assume that the influence of the substrate is screened by this wetting layer. This is supported by computer simulations of Lyakhova *et al.*³⁷ and Ludwigs *et al.*⁵⁷

In summary, we have found four characteristic patterns at the film surface irrespective of the substrate nature: A rather featureless pattern, which we identify as disordered phase (dis), upright standing cylinders (C_{\perp}), cylinders oriented parallel to the surfaces (C_{\parallel}) and perforated lamellae (PL) at the terraces. Considering the terrace heights and the thickness of the wetting layer beneath all terraces ($d_{T0} \approx 11$ nm) we anticipate that layers of PL with a natural domain size of $\Delta d \approx (23 \pm 2)$ nm are stacked on top of each other, however, there is no direct experimental evidence for this. The slopes between the first terraces are formed of C_{\parallel} , with increasing film thickness we also find PL between the terraces. This phenomenon is explained with confinement effects which play a non-negligible role in one or two microdomain thick layers, while they are much smaller in thicker films.

Similar surface structures have been recently found in cylinder-forming SBS block copolymers.^{14,15,16,37} With increasing film thickness both experiments and simulations showed a disordered phase for the smallest thickness, very short upright cylinders C_{\perp} , parallel cylinders C_{\parallel} , and perforated lamellae PL. The phase transitions occurred at well-defined film thicknesses with C_{\parallel} being formed on the terraces. Our results can be compared to this behavior only to some extent. While the phase behavior of SBS is dominated by the bulk structure (C_{\parallel} and C_{\perp}), we find the PL as dominating surface structure of a core-shell cylinder forming system. In analogy to the SBS system we can assign the dot-like structure (bright dots) to very short cylinders oriented perpendicular to the surfaces (C_{\perp}), though a clear hexagonal arrangement is not observed in the SEM images.

Comparison with thin film phase behavior of $S_{17}V_{22}T_{61}^{132}$ and $S_{19}V_{25}T_{56}^{120}$:

In the previous section we have focused on the thin film phase behavior of $S_{16}V_{21}T_{63}^{140}$ which shows a core-shell cylinder structure in bulk. Decreasing the volume fraction of PtBMA towards a symmetric composition we identify a composition region in the phase diagram which exhibits a coexistence of core-shell gyroids, core-shell cylinders, and perforated lamellae. The polymers and their molecular parameters are listed in Table 1. The investigation of thin films of these polymers prepared in the manner described above exhibits the same sequence of surface structures with gradually increasing film thickness as the core-shell cylinder phase. Again the PL phase dominates the phase behavior in thin films. Figure 8(a) shows the terrace transitions from T_0 to T_2 for $S_{17}V_{22}T_{61}^{132}$ after exposure to $p_{\text{CHCl}_3} = 0.9 p_0$ for 120 h. The film thickness in dependence of the terrace number is shown in Fig. 8(b). The terraces measured for $S_{19}V_{25}T_{56}^{120}$ (circles) and for $S_{17}V_{22}T_{61}^{132}$ exhibit similar thickness values which amount to $\Delta d(T_1, T_2) \approx (23 \pm 2)$ nm, the wetting layer amounts to $d_{T0} \approx (14 \pm 2)$ nm. The thickness values do not differ significantly from the data observed for the core-shell cylinder system, $S_{16}V_{21}T_{63}^{140}$. This is not surprising as the SAXS data

also show similar values for the bulk domain spacing, see Table 1.

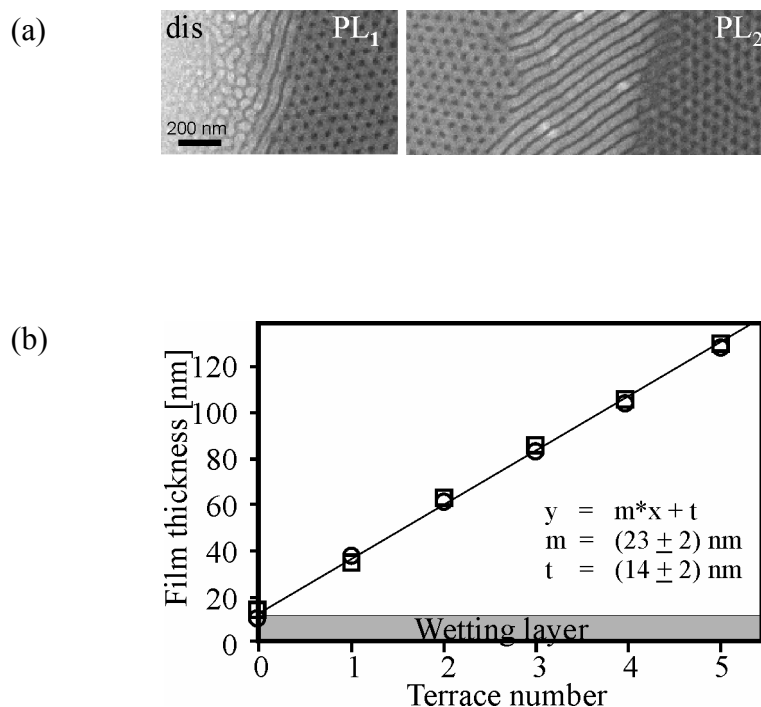


Figure 8. Thin films of $S_{17}V_{22}T_{61}^{132}$ and $S_{19}V_{25}T_{56}^{120}$ after exposure to $CHCl_3$ vapor ($p_{CHCl_3} = 0.9p_0$, $t = 100$ h). (a): SEM images of the transition between $T_0 - T_1$ and $T_1 - T_2$ of a thin film of $S_{17}V_{22}T_{61}^{132}$. (b): Film thickness as function of the terrace number; circles represent thickness values observed for $S_{17}V_{22}T_{61}^{132}$ and squares represent values observed for $S_{19}V_{25}T_{56}^{120}$. The height of the symbols includes the error bar.

Comparison with thin film phase behavior of $S_{16}V_{21}T_{63}^{140}$, annealed in THF vapor

We have further investigated thin film specimens of $S_{16}V_{21}T_{63}^{140}$ on silicon wafers after annealing in THF vapor ($p_{THF} = 0.95 p_0$, 120 h), Fig. 9(a) shows the film thickness as function of the terrace number. The higher terraces amount to integer multiples of the first terrace - T_1 - with a value of $d_{T1} \approx (36 \pm 3)$ nm. The terraces exhibit stripe patterns which are assigned to cylinders oriented parallel to the substrate. From scanning electron micrographs we assume a core-shell morphology with a PS core (dark grey) and P2VP shell (light grey) in a matrix of PtBMA (dark). In the thinnest regions of the sample we find two different sample areas: in some parts of the sample the first terrace T_1 is formed next to areas where no polymer film is left (pure SiO_x) (Fig. 9(b)), and in other parts terraces with a thickness of $d_{T1/2} \approx 20$ nm can be detected (Fig. 9(c)). The latter corresponds to $T_{1/2}$ and exhibits cylinders oriented parallel to the substrate ($C_{||}$) as well as a small amount of hexagonally ordered bright dots which can be assigned to perpendicularly oriented cylinders (C_{\perp}).

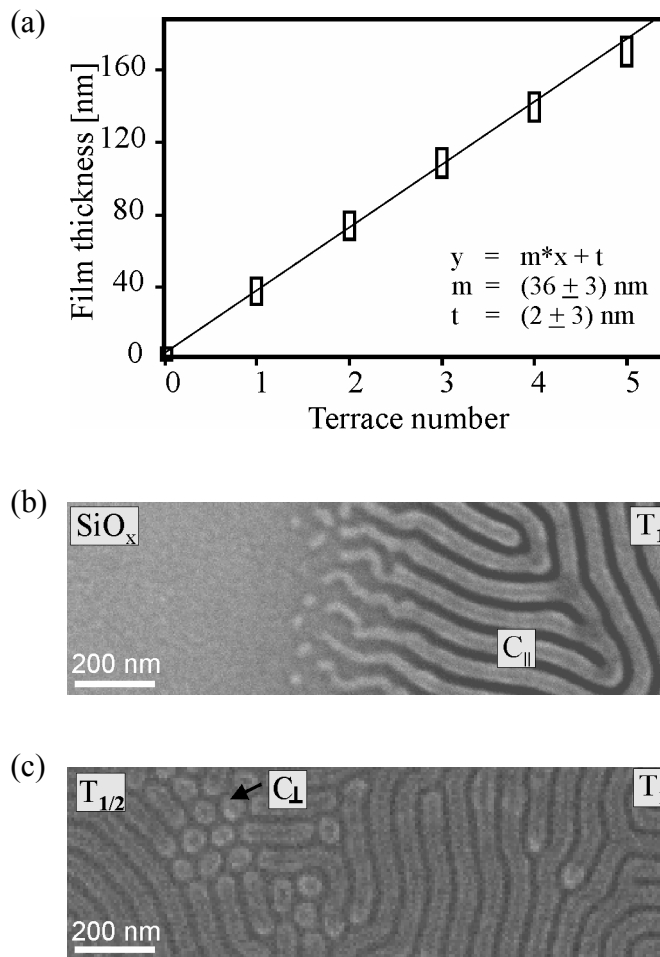


Figure 9. Thin film of $S_{16}V_{21}T_{63}^{140}$ after exposure to THF vapor ($p_{\text{THF}} = 0.95p_0$, 120 h). (a): Film thickness as function of the terrace number. The height of the symbols includes the error bar. (b) and (c): SEM micrographs of the transition from the silicon substrate to T_1 (b) and the transition between $T_{1/2}$ and T_1 (c).

In contrast to samples prepared in CHCl_3 vapor no transition from a core-shell cylinder structure in bulk to perforated lamellae in thin films is found after preparation in THF vapor. All terraces and transitions show cylinders. The surface field apparently causes the cylinders to orient parallel to the substrate. The cylinders seem to adjust themselves to a thickness corresponding to the instantaneous thickness during the swelling process.

Recently Elbs *et al.* have used spectroscopic ellipsometry to determine the swelling behavior of thin films of the homopolymers PS, P2VP and PtBMA in controlled atmosphere of chloroform and THF.^{49,50} From the degree of swelling as function of the solvent vapor pressure they could estimate Flory-Huggins interaction parameters between polymers and solvents. They found that the rather polar solvent chloroform swells P2VP more and the nonpolar polymer PS less. THF turned out to be almost non-selective, hardly any difference in the degree of swelling between the three homopolymers could be detected. Therefore they expected the thin phase diagrams of the triblock

terpolymers to be slightly different in the different solvents. Briefly, their thin film investigations show the following results⁵⁸: samples annealed in THF vapor exhibited the tendency of forming cylinders oriented parallel to the surface – which is in accordance to our present results. Exposure to chloroform vapor led to structures with a smaller mean curvature which they assumed to be gyroid-like and which show perforated lamellae with our experimental route. Their sample preparation was based on swelling thin films of $S_{17}V_{26}T_{57}^{110}$ in solvent vapor and slowly extracting the solvent by decreasing the solvent vapor pressure. During solvent evaporation the concentration of the polymer solutions increases in concentration and at high concentrations the relaxation time of the polymer solution can eventually reach the time scale of the preparation process and the respective morphology will be frozen. In the present contribution we have used an improved method of sample preparation. We anneal our samples well above the order-disorder transition in the ordered (microphase-separated) state in a controlled atmosphere of solvent vapor at a defined vapor pressure which results in swelling of the films to about 2.5 times of their original dry thickness. The structure formation process takes place in these high concentrated solutions. Via quenching the films by evaporation of the high vapor pressure solvent in pure air, the films shrink in z-direction and the respective microdomain structures are frozen in. In contrast to Elbs *et al.* we work with controlled solvent vapor pressures and fast extraction rates which were shown not to influence the microdomain structures.¹⁶

Despite the influence of preparation Elbs *et al.* have observed similar tendencies of structure formation in chloroform and tetrahydrofurane. Regarding the bulk and solution data the difference in selectivity obviously does not affect microdomain formation: a cylindrical phase is formed in both solvents. In thin films the additional interfaces and the confinement of the material to the bulk domain spacing stabilize surface reconstructions, mostly perforated lamellae after annealing in a slightly selective solvent, like chloroform. The thin film phase behavior of films annealed in THF is dominated by the bulk structure.

Additional complex thin film structures

In addition to our systematic findings about the relationship between the morphology and the film thickness we finally give an impression of the complexity of the phase behavior of ABC triblock terpolymers in thin films. We have already underlined the importance of a well-defined sample preparation in the previous sections. Figure 10 shows surface structures found on one single film of $S_{17}V_{22}T_{61}^{132}$ after exposing it to $CHCl_3$ vapor for 50h. The sample was prepared in an experimental setup, where the vapor pressure could slightly vary because of changes in the temperature of the environment ($p_{CHCl_3} \sim 0,9p_0$). We were unable to reproduce this particular sample preparation. In

Figure 10(a) a SEM image of the first terrace of a modified perforated lamella phase next to cylinders oriented parallel to the surfaces is displayed. As the PL phase looks quite strange in electron microscopy, we have performed scanning force microscopy on a similar sample position. Figure 10(b) shows a SFM image after removing a layer of ~ 7 nm thickness in oxygen plasma. Around dark holes which are assigned to PtBMA perforations six grey protrusions are formed. The skeleton of the perforated lamella phase seems to be modified. We assume that the PS block does not form a continuous core, but rather breaks up into isolated PS microdomains embedded within P2VP. This is analogous to the cylinders found in the right part of Fig. 10(a) and Fig. 10(c). They can be assigned to a sphere-in-cylinder structure with isolated PS microdomains (dark grey in the image) embedded within P2VP cylinders surrounded by a continuous matrix of the majority component PtBMA. Other cylindrical structures found on the same sample are displayed in Figure 10(d), (e) and (f): a familiar core-shell cylindrical structure (PS-core, P2VP-shell, PtBMA matrix), (d); a cylinder(P2VP)-at-cylinder (PS) morphology; and a helix (P2VP)-around-cylinder (PS) morphology.

The sketches have been taken from Elbs *et al.* who have first seen these structures in thin films of $S_{17}V_{26}T_{57}^{110}$ prepared in THF vapor.⁵⁸ The corresponding bulk structures had been first published by Stadler and coworkers.^{59,60}

We assume that the coexistence of these different cylinder morphologies results from fluctuations in the polymer concentration during the annealing process in solvent vapor. We have already mentioned that the solvent annealing is a crucial point for the structure formation. Even smallest differences may induce transitions between neighbouring structures. The core-shell structure arises for example from the sphere-in-cylinder morphology by merging the isolated PS spheres into a continuous PS cylinder. While the overall cylinder structure does not change, the microphase separation between the first blocks is apparently very sensitive to concentration fluctuations.

We emphasize through these examples the rich variety of surface structures possible in thin films of ABC triblock terpolymers. We expect these structures can reproducibly be formed under well-controlled conditions; either under equilibrium conditions (steady state, e.g. constant solvent vapor) conditions, or perhaps only under controlled processing conditions (e.g., solvent vapor ramps or controlled evaporation rates). Combinatorial methods are aptly suited for either routes of future studies.

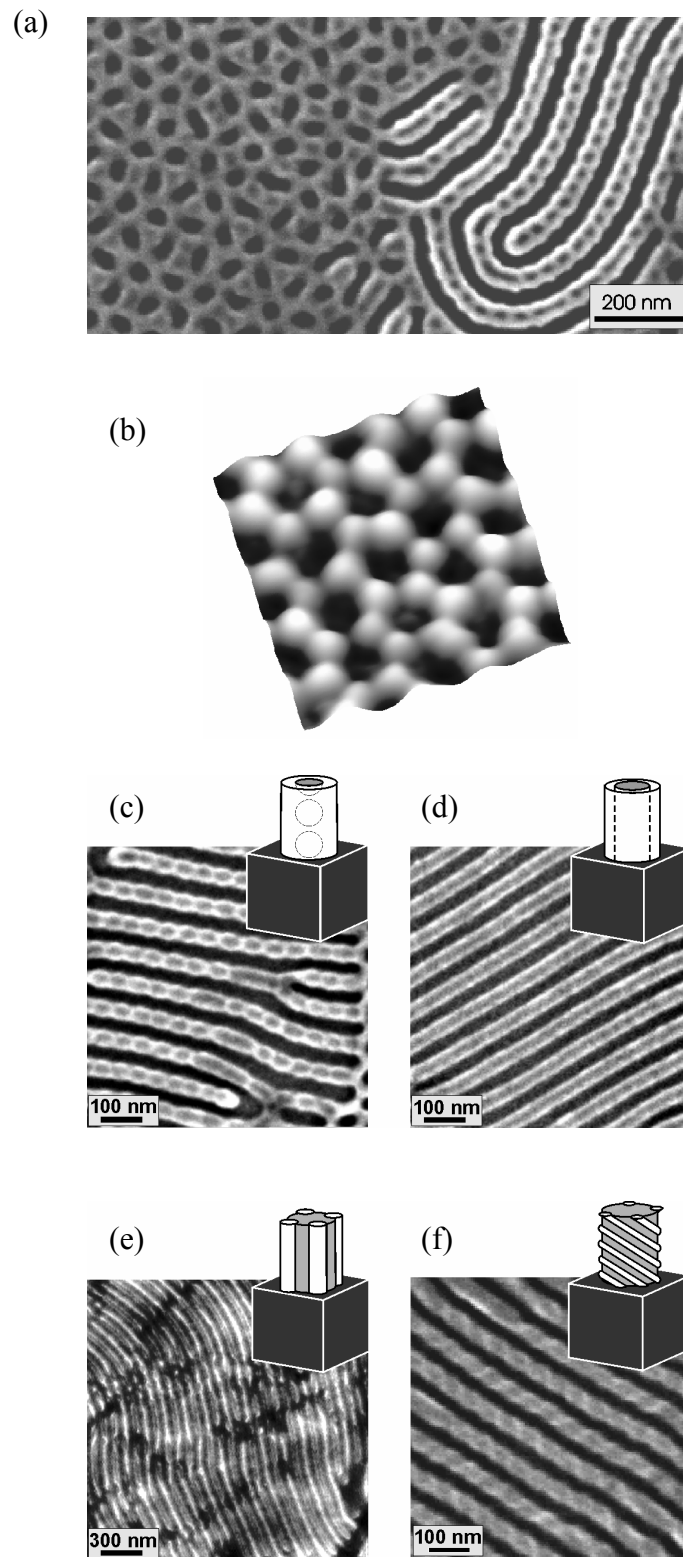


Figure 10. Surface structures found on one thin film of $S_{17}V_{22}T_{61}^{132}$ after preparation in $CHCl_3$ vapor ($p_{CHCl_3} \sim 0.9p_0$, 50 h). (a): SEM image of the transition between perforated lamellae (T_1) and a sphere-in-cylinder morphology; (b): SFM image of T_1 after removing a layer of ~ 7 nm in oxygen plasma (300×300 nm², the height difference between the protrusions and holes amounts to around 4 nm). (c)-(f): SEM images of different cylinder morphologies: sphere-in-cylinder morphology (c), core-shell-cylinders (d), cylinders-at-cylinders (e) and helix-around cylinder morphology (f). The sketches are adapted from Ref. (58). Color code: light grey corresponds to PS, grey to P2VP, dark grey to PtBMA.

3.1.2. Conclusion

We apply a gradient combinatorial approach to the investigation of thin film structures of ABC triblock terpolymers consisting of poly(styrene), poly(2-vinylpyridine), and poly(*tert*-butyl methacrylate) in the stoichiometric range of $\phi_{\text{PS}} : \phi_{\text{P2VP}} : \phi_{\text{PtBMA}} = 1 : 1.2 : 3.05$ to 4. With gradients in films thickness we find a systematic dependence between the morphology and the film thickness. Terraces of well-defined film thickness exhibiting a perforated lamella structure are formed after annealing in a well-controlled atmosphere of nearly saturated CHCl_3 vapor. Due to the chemical nature of the block components and the particular stoichiometry of the polymer a wetting layer with a PtBMA-rich top layer is formed next to the substrate. Irrespective of the nature of the substrate the perforated lamella phase develops, as the influence of the substrate is screened by the wetting layer. The nature of the solvent used for annealing is shown to have a significant influence on the structure formation. While the same structure is observed in bulk and solution, the confinement of the material to a certain film thickness induces a morphological phase transition: Using the same preparation procedure as with CHCl_3 , the use of THF leads to terraces exhibiting cylinders oriented parallel to the surfaces. No perforated lamella phase is formed at any film thickness. This phenomenon may be explained by a slight selectivity of CHCl_3 for P2VP, while THF appears to be non-selective for all blocks.

We finally emphasize the importance of a well-controlled atmosphere of solvent vapor for the annealing process. As the structure formation process takes place in highly concentrated polymer solutions even slight changes in concentration may induce phase transitions between neighboring morphologies. Thin films of triblock terpolymers can exhibit a wealth of structures due to the delicate interplay between the large number of block–block and block-surface interactions. This complex phase behavior in thin films can be corroborated by computer simulations which are presented in the accompanying paper.⁵⁷

Acknowledgements

We thank C. Abetz for SEM measurements, M. Hund for help with etching experiments, C. Thunig for help with ODT measurements and A. Knoll for fruitful discussions. We acknowledge support from the Deutsche Forschungsgemeinschaft (SFB 481) and the VolkswagenStiftung.

References

- (1) Bates, F. S.; Fredrickson, G.H. *Annu. Rev. Phys. Chem.* **1990**, 41, 525
- (2) Bates, F. S.; Fredrickson, G. H. *Physics Today* **1999**, 52, 32.
- (3) Hamley, J.W. *The Physics of Block Copolymers*, Oxford University Press, Oxford, **1998**.
- (4) Stadler, R.; Auschra, C.; Beckmann, J.; Krappe, U.; Voigt-Martin, I.; Leibler, L. *Macromolecules* **1995**, 28, 3080.
- (5) Leibler, L. *Macromolecules* **1980**, 13, 1602.
- (6) Matsen, M. W.; Bates, F. S. *Macromolecules* **1996**, 29, 1091.
- (7) Matsen, M. W.; Bates, F. S. *J. Chem. Phys.* **1997**, 106, 2436.
- (8) Meier, D. J. *Thermoplastic Elastomers*, Carl Hanser Verlag: München, 1987.
- (9) Helfand, E.; Wasserman, Z. R. *Macromolecules* 1980, 13, 994.
- (10) Semenov, A. N. *Sov. Phys.* **1985**, JETP 61, 733.
- (11) Nakazawa, H.; Ohta, T. *Macromolecules* **1993**, 26, 5503.
- (12) Phan, S.; Fredrickson, G.H. *Macromolecules* **1998**, 31, 59.
- (13) Huinink, H. P.; van Dijk, M. A.; Brokken-Zijp, J. C. M.; Sevink, G. J. A. *Macromolecules* **2001**, 34, 5325.
- (14) Knoll, A.; Horvat, A.; Lyakhova, K. S.; Krausch, G.; Sevink, G. J. A.; Zvelindovsky, A. V.; Magerle, R. *Phys. Rev. Lett.* **2002**, 89, 035501-1.
- (15) Horvat, A.; Lyakhova, K. S.; Sevink, G. J. A.; Zvelindovsky, A. V.; Magerle, R. *J. Chem. Phys.* **2004**, 120, 1117.
- (16) Knoll, A.; Magerle, R.; Krausch, G. *J. Chem. Phys.* **2004**, 120, 1105.
- (17) Karim, A.; Singh, N.; Sikka, M.; Bates, F. S.; Dozier, W. D.; Felcher, G. P. *J. Chem. Phys.* **1994**, 100, 1620.
- (18) Radzilowski, L. H.; Carvalho, B. L.; Thomas, E. L. *J. Polym. Sci., Part B: Polym. Phys.* **1996**, 34, 3081.
- (19) Konrad, M.; Knoll, A.; Krausch, G.; Magerle, R. *Macromolecules* **2000**, 33, 5518.
- (20) Harrison, C.; Park, M.; Chaikin, P. M.; Register, R. A.; Adamson, D. H.; Yao, N. *Macromolecules* **1998**, 31, 2185.
- (21) Zhang, Q.; Tsui, O. K. C.; Du, B.; Zhang, F.; Tang, T.; He, T. *Macromolecules* **2000**, 33, 9561.
- (22) Mansky, P.; Chaikin, P.; Thomas, E. L.; *J. Mater. Sci.* **1995**, 30, 1987.

- (23) Park, M.; Harrison, C.; Chaikin, P. M.; Register, R. A.; Adamson, D. H. *Science* **1997**, 276, 1401.
- (24) Park, C.; Yoon, J.; Thomas, E. L. *Polymer* **2003**, 44, 6725.
- (25) van Dijk, M. A.; van den Berg, R. *Macromolecules* **1995**, 28, 6773.
- (26) Magonov, S. N.; Cleveland, J.; Elings, V.; Denley, D.; Whangbo, M.-H. *Surf. Sci.* **1997**, 389, 201.
- (27) Kim, G. ; Libera, M. *Macromolecules* **1998**, 31, 2670.
- (28) Kim, G. ; Libera, M. *Macromolecules* **1998**, 31, 2569.
- (29) Mansky, P.; Harrison, C. K.; Chaikin, P. M.; Register, R. A.; Yao, N. *Appl. Phys. Lett.* **1996**, 68, 2586.
- (30) Mansky, P.; Liu, Y.; Huang, E.; Russell, T. P.; Hawker, C. J. *Science* **1997**, 275, 1458.
- (31) Thurn-Albrecht, T.; DeRouchey, J.; Russell, T. P.; Mays, J.; Pitsikalis, M.; Morkved, T.; Jaeger, H. *Macromolecules* **2000**, 33, 3250.
- (32) Thurn-Albrecht, T.; Schotter, J.; Kastle, G. A.; Emley, N.; Shibauchi, T.; Krusin-Elbaum, L.; Guarini, K.; Black, C. T.; Tuominen, M. T.; Russell, T. P. *Science* **2000**, 290, 2126.
- (33) Park, M.; Harrison, C.; Chaikin, P. M.; Register, R. A.; Adamson, D. H. *Science* **1997**, 276, 1401.
- (34) Jeoung, E.; Galow, T. H.; Schotter, J.; Bal, M.; Ursache, A.; Tuominen, M. T.; Stafford, C. M.; Russell, T. P.; Rotello, V. M. *Langmuir* **2001**, 17, 6369.
- (35) Jeoung, U.; Ryu, D. Y.; Kim, J. K.; Kim, D. H.; Russel, T. P.; Hawker, C. J. *Adv. Mater.* **2003**, 15, 1247.
- (36) Ludwigs, S.; Böker, A.; Voronov, A.; Rehse, N.; Magerle, R.; Krausch, G. *Nature Materials* **2003**, 2, 744.
- (37) Lyakhova, K. S.; Sevink, G. J. A.; Zvelindovsky, A. V.; Horvat, A.; Magerle, R. *J. Chem. Phys.* **2004**, 120, 1127.
- (38) Ludwigs, S.; Böker, A.; Abetz, V.; Müller, A. H. E.; Krausch, G. *Polymer* **2003**, 44, 6815.
- (39) Meredith, J. C.; Smith, A. P.; Karim, A.; Amis, E. J. *Macromolecules* **2000**, 33, 9747.
- (40) Sawyer L. C.; Grubb, D. T. *Polymer Microscopy*, 2nd ed.; Chapman & Hall: London, 1996.
- (41) Roberson, S. V.; Sehgal, A.; Fahey, A.; Karim, A. *Appl. Surf. Sci.* **2002**, 200, 150.
- (42) Peters, R. D.; Yang, X. M.; Kim, T. K.; Sohn, B. H.; Nealey, P. F. *Langmuir* **2000**, 16, 4625.
- (43) Kim, T. K.; Yang, X. M.; Peters, R. D.; Sohn, B. H.; Nealey, P. F. *J. Phys. Chem. B* **2000**, 104, 7403.
- (44) Girifalco, L. A.; Good, R. J. *J. Chem. Phys.* **1957**, 61, 904.

- (45) Girifalco, L. A.; Good, R. J. *J. Chem. Phys.* **1960**, 64, 561.
- (46) Genzer, J.; Kramer, E. J. *Phys. Rev. Lett.* **1997**, 78, 4946.
- (47) Smith, A. P.; Sehgal, A.; Douglas, J. F.; Karim, A.; Amis, E. J. *Macromol. Rapid Commun.* **2003**, 24, 131.
- (48) Magerle, R. *Phys. Rev. Lett.* **2000**, 85, 2749.
- (49) Elbs, H.; Krausch, G. *submitted*.
- (50) Elbs, H. PhD thesis, Bayreuth, 2001.
- (51) Coulon, G.; Russell, T. P.; Deline, V. R.; Green, P. F. *Macromolecules* **1989**, 22, 2581.
- (52) Mark, J. E. *Physical Properties of Polymers Handbook* American Institute of Physics: Woodbury, 1996.
- (53) Ishizu, K.; Yamada, Y.; Fukutomi, T. *Polymer* **1990**, 31, 2047.
- (54) Tassin, J. F.; Siemens, R. L.; Tang, W. T.; Hadziioannou, G.; Smith, B.A. *J. Phys. Chem.* **1989**, 93, 2106.
- (55) Fukunaga, K.; Elbs, H.; Magerle, R.; Krausch, G. *Macromolecules* **2000**, 33, 947.
- (56) Fukunaga, K.; Hashimoto, T.; Elbs, H.; Krausch, G. *Macromolecules* **2003**, 36, 2852.
- (57) Ludwigs, S.; Zvelindovsky, A. V.; Sevink, G. J. A.; Krausch, G.; Magerle, R. *submitted to Macromolecules*.
- (58) Elbs, H.; Drummer, C.; Abetz, V.; Krausch, G. *Macromolecules* **2002**, 35, 5570.
- (59) Stadler, R.; Auschra, C.; Beckmann, J.; Krappe, U.; Voigt-Martin, I.; Leibler, L. *Macromolecules* **1995**, 28, 3080.
- (60) Breiner U.; Krappe U.; Abetz V.; Stadler R. *Macromol. Chem. Phys.* **1997**, 198, 1051.

3.2. Phase behavior of ABC triblock terpolymers in thin films: mesoscale simulations

S. Ludwigs^{a,*}, A. V. Zvelindovsky^b and G. J. A. Sevink^b, G. Krausch^a, and R. Magerle^{a,*}

^a*Physikalische Chemie II, Universität Bayreuth, D-95440 Bayreuth, Germany*

^b*Leiden Institute of Chemistry, Leiden University, P.O. Box 9502, 2300 RA Leiden, The Netherlands*

Corresponding authors: sabine.ludwigs@uni-bayreuth.de and robert.magerle@uni-bayreuth.de

Tel: +49-921-552641, Fax: +49-921-552059.

Submitted to *Macromolecules*

Abstract

Microphase separation and morphology of thin films of ABC triblock terpolymers are studied with a self consistent field theory. Thin films of poly(styrene)-*block*-poly(2-vinylpyridine)-*block*-poly(*tert*-butyl methacrylate) (SVT) triblock terpolymers are modeled as $A_3B_4C_{12}$ Gaussian chains confined in a slit. The bulk morphologies are found to be much more robust with respect to the interaction parameters when compared to the morphologies in the confined situation. By adjusting the interaction parameters between the polymer components and the surfaces we can model the experimentally observed sequence of surface structures as function of the film thickness. At well-defined film thicknesses a highly ordered perforated lamella structure is observed. We systematically explore the influence of film thickness, surface field, and the interaction parameters between the different polymer components on the phase behavior.

Introduction

In recent years it has been shown that ordered block copolymer structures with characteristic sizes in the range of 5 – 50 nm might be a promising material for lithographic masks, membranes and quantum electronic arrays.^{1,2,3} In particular thin film structures are of great interest, as long-range ordering of microdomain structures is facilitated.^{4,5,6} In thin films two factors significantly control the structure formation: The preferential attraction of one type of block to the surface (the surface field) which causes this component to accumulate at the interface, and the commensurability of the natural domain spacing with the film thickness.^{7,8,9}

Most theoretical studies on block copolymers in thin films have focused on two-component systems, either AB diblock or symmetric ABA triblock copolymers, which form lamellae in the bulk (for a review, see Ref. 7,8,9). Compositionally asymmetric, mostly cylinder-forming block copolymers have been studied only recently. Their phase behavior in thin films has been studied with the Ginzburg-Landau equation^{10,11}, cell dynamical simulations¹², Cahn-Hilliard-type coarse-grained models^{13,14}, and Monte Carlo simulations.^{15,16,17} Also various self-consistent field (SCF) studies have been performed for the formation of microphases in thin films of cylinder-forming AB diblock and ABA triblock copolymer melts and solutions.^{18,19,20,21,22} Recently, Knoll *et al.* and Horvat *et al.* have compared experimental results on thin films of poly(styrene)-*block*-poly(butadiene)-*block*-poly(styrene) (SBS) triblock copolymers with SCF-simulations for similar interfaces, where the surface fields are equal at both interfaces.^{23,24,25} They could show a matching sequence of structures with increasing film thickness. Lyakhova *et al.* have additionally investigated the role of dissimilar interfaces on the phase behavior of these block copolymers.²⁶ In experiments, usually supported films are studied that are asymmetric with respect to interactions at the air-film and film-substrate interfaces.

In contrast to two-component systems the phase behavior of ABC triblock terpolymers is much more complex and a much larger number of parameters is needed to describe thin films: the film thickness (H), the volume fractions of the components (ϕ_A , ϕ_B , $\phi_C = 1 - (\phi_A + \phi_B)$), three mutual interaction parameters between the components (ϵ_{AB} , ϵ_{AC} , ϵ_{BC}) and six interaction parameters between the different interfaces and the three components (ϵ_{AM_0} , ϵ_{BM_0} , ϵ_{CM_0} , ϵ_{AM_1} , ϵ_{BM_1} and ϵ_{CM_1} with M_0 and M_1 representing the top surface and the substrate, respectively).

In the field of ABC triblock terpolymer thin films, Pickett and Balazs have used self-consistent field calculations to probe the preferential orientation of lamellae formed by an ABC triblock terpolymer confined between two walls attracting the middle block.²⁷ They found that an orientation of the lamellae perpendicular to the plane of the film orientation is highly favored, indicating that triblock terpolymers possess distinct advantages over diblocks in technological applications. Monte Carlo

simulations by Feng and Ruckenstein for ABC melts in thin films show that the microdomain morphology can be very complicated, and is affected both by the composition and by the interactions.²⁸ Finally, Chen and Fredrickson have applied self-consistent field theory and strong segregation limit studies (SSL) to investigate confined films of linear ABC triblock terpolymer melts²⁹ for the particular case where A and C blocks are equal in size, the interaction parameters are identical, and both walls having identical chemical properties. Their findings confirm that surface fields and film thicknesses can be employed to manipulate the microdomain structure, shape, and orientation.

In the present contribution we model a specific system of compositionally asymmetric triblock terpolymers consisting of poly(styrene) (PS), poly(2-vinylpyridine) (P2VP) and poly(*tert*-butyl methacrylate) (PtBMA) in a thin film. We relate to a corresponding experimental investigation of the behavior of this material in bulk³⁰ and in thin films.^{31,32}

Using combinatorial gradient techniques Ludwigs *et al.* have systematically explored the dependence of thin film structures of PS-*b*-P2VP-*b*-PtBMA with volume fractions $\phi_{\text{PS}} : \phi_{\text{P2VP}} : \phi_{\text{PtBMA}} = 1 : 1.2 : x$ (with x ranging from 3.05 to 4) on the film thickness and preparation conditions.³² Depending on the volume fraction of PtBMA either core-shell cylinders ($\phi_{\text{PS}} : \phi_{\text{P2VP}} : \phi_{\text{PtBMA}} = 1 : 1.2 : 4$) or a coexistence of core-shell gyroids, core-shell cylinders and a perforated lamella structure ($\phi_{\text{PS}} : \phi_{\text{P2VP}} : \phi_{\text{PtBMA}} = 1 : 1.2 : 3.05$ to 3.63) are found in the bulk. Table 1 summarizes the molecular parameters of the experimentally investigated polymers.

Table 1. Experimental results: bulk morphologies³⁰

Polymer ^a	$\phi_{\text{PS}} : \phi_{\text{P2VP}} : \phi_{\text{PtBMA}}$ ^b	Bulk morphology ^c
$\text{S}_{18}\text{V}_{24}\text{T}_{58}^{120}$	1 : 1.2 : 3.05	G / PL / C
$\text{S}_{18}\text{V}_{24}\text{T}_{58}^{124}$	1 : 1.2 : 3.33	G / PL / C
$\text{S}_{17}\text{V}_{23}\text{T}_{60}^{129}$	1 : 1.2 : 3.53	G / PL / C
$\text{S}_{17}\text{V}_{22}\text{T}_{61}^{132}$	1 : 1.2 : 3.65	G / PL / C
$\text{S}_{16}\text{V}_{21}\text{T}_{63}^{140}$	1 : 1.2 : 4	C

^a $\text{S}_{\%}\text{PS}\text{V}_{\%}\text{P2VP}\text{T}_{\%}\text{PtBMA}^{M_w}$ with the subscripts representing the weight fractions of the respective blocks (parts in hundred), while M_w is the total weight-averaged molecular weight in kg/mol;

^b $\phi_{\text{PS}} : \phi_{\text{P2VP}} : \phi_{\text{PtBMA}}$, volume fractions;

^cKey: G, core-shell-gyroids; PL, perforated lamellae; C, core-shell cylinders.

For thin film investigations, polymer films with gradients in film thickness were annealed in a controlled chloroform vapor atmosphere, quenched with pure air, and investigated with scanning

electron microscopy and scanning force microscopy.³² The structure formation process takes place in concentrated solutions. While experiencing different morphologies in bulk as a function of the composition, the microdomain structures in thin films are very similar for the whole range of ϕ_{PtBMA} from $\phi_{\text{PS}} : \phi_{\text{P2VP}} : \phi_{\text{PtBMA}} = 1 : 1.2 : 3.05$ to 4.0. Figure 1(a) shows scanning electron micrographs of a thin film of $\text{S}_{17}\text{V}_{22}\text{T}_{61}$ ¹³² annealed in CHCl_3 with a film thickness of ~ 10 to 80 nm. The dark phase can be attributed to the majority component poly(*tert*-butyl methacrylate), which is known to shrink upon exposure to the electron beam. With increasing film thickness the following sequence of structures is found: A featureless pattern, which is identified as disordered phase (dis), bright dots with liquid-like packing, a stripe-like pattern corresponding to parallel oriented core-shell cylinders (C_{\parallel}). The terraces exhibit a hexagonally packed structure of dark dots, which is identified as a perforated lamella phase (PL). At the slopes between the terraces C_{\parallel} is found. For a detailed discussion we refer to the accompanying experimental paper.³²

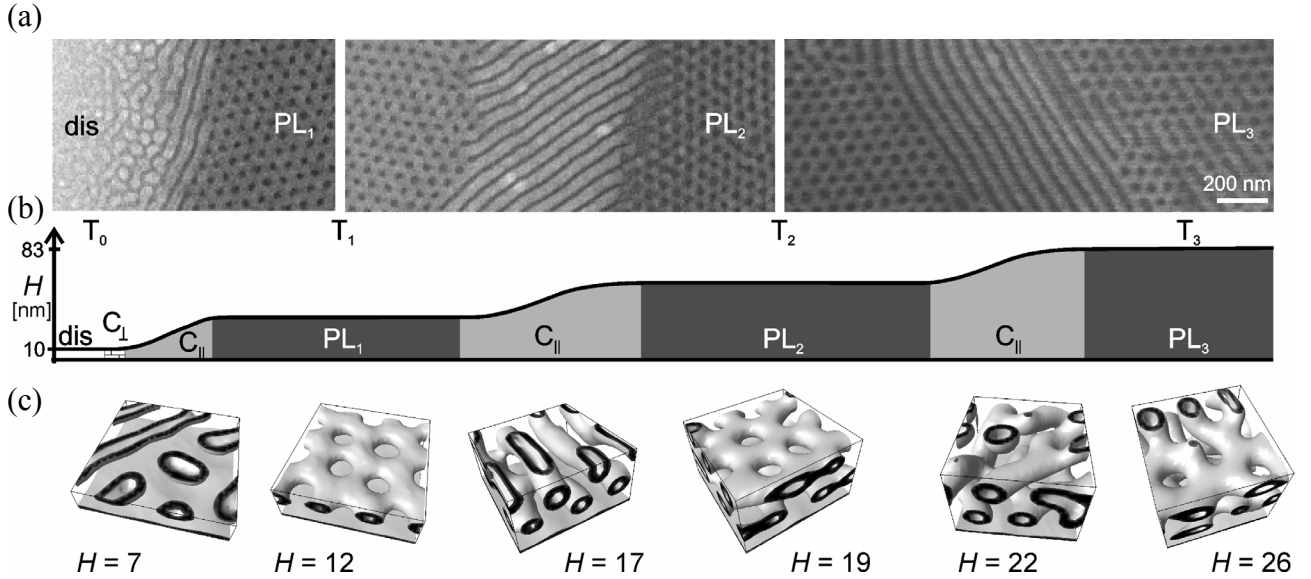


Figure 1. Comparison of experiments with simulation results. (a): Scanning electron micrographs of a thin film of poly(styrene)-b-poly(2-vinylpyridine)-b-poly(*tert*-butyl methacrylate) triblock terpolymer ($\text{S}_{17}\text{V}_{22}\text{T}_{61}$ ¹³²) on a silicon substrate after annealing in chloroform vapour. (b): Schematic height profile of the electron micrographs shown in (a). (c): Simulations of an $\text{A}_3\text{B}_4\text{C}_{12}$ block copolymer film. The isodensity surfaces of the B-density ρ_B are shown for different film thicknesses H . The mutual interaction parameters between the block components are $\boldsymbol{\varepsilon} = (\varepsilon_{AB}, \varepsilon_{AC}, \varepsilon_{BC}) = (7.0, 8.0, 6.0)$. The block-surface interactions are $\varepsilon_{M_0} = (\varepsilon_{AM_0} + \varepsilon_{BM_0})/2 - \varepsilon_{CM_0} = 5.0$ ($M_0 = \text{top surface}$) and $\varepsilon_{M_1} = (\varepsilon_{AM_1} + \varepsilon_{BM_1})/2 - \varepsilon_{CM_1} = -5.0$ ($M_1 = \text{silicon substrate}$).

We model the thin films as a melt of $\text{A}_3\text{B}_4\text{C}_{12}$ flexible chains confined between two walls, one representing the top surface, and the other representing the substrate. The indices correspond to the number of statistical elements (beads) of the same chemical species and they correspond to the

volume fractions of the three components in the polymer. Due to the computational limits of the simulations, we will not distinguish between small variations in the volume fractions, which, in the experiments, have shown to lead to different phases in the bulk. Here, we focus on the energetic interactions between the different components and the interfaces as tunable parameters.

With the input of the experiments of Ludwigs *et al.*³² and several previous studies about SVT triblock terpolymers performed by Elbs *et al.*^{33,34,35} and Fukunaga *et al.*^{36,37,38} we have adjusted the interaction parameters such as to match the experimental phase behavior observed in the experiments of Ludwigs *et al.* We present our simulation results for this set of parameters and compare them with the experimental data which are described in the accompanying article.³² We also explored the behavior of the system in the vicinity of this parameter set.

Method

We apply a dynamic version of the SCF simulation technique^{18,39,40} to model the SVT triblock terpolymers. The block terpolymer is modeled as $A_3B_4C_{12}$ Gaussians chains with different beads A (= poly(styrene)), B (= poly(2-vinylpyridine)) and C (= poly(*tert*-butyl methacrylate)). The relative number of beads coincides with the volume fractions of the different components in the triblock terpolymer. The total number of beads is small enough to ensure computational efficiency. The spatial patterns are found as numerical solutions of diffusion-type equations for component densities. This type of approach ensures spontaneous pattern formation, natural appearance of defects in structures, and metastable states which is common to the situation in the experiments.

Polymer films on silicon substrates are mimicked as a polymer melt confined between two parallel hard walls. The simulations are performed on a cubic grid with $L \times L \times W$ grid points, with $L = 32$ or 64 and W varying from 6 to 28. The walls are presented as planes at $z = 1$ and W , hence the film thickness H equals $W-2$ grid points. For modelling the bulk, periodic boundary conditions apply in all three spatial directions; in the confined case, special boundary conditions apply at the walls.¹⁸

The interactions between the three components and between the components and the walls are characterized by ϵ_{XY} parameters that are directly related to the Flory-Huggins parameters.⁴⁰ The mutual interactions between the different components have been chosen such as to match the bulk structure in the experiments. Strong repulsion between all three components is needed to form core-shell microdomain structures which are dominant in the experimental system.

For thin film investigations we further had to determine the six interaction parameters between the two different walls and the three components: ϵ_{AM_0} , ϵ_{BM_0} , ϵ_{CM_0} , ϵ_{AM_1} , ϵ_{BM_1} , and ϵ_{CM_1} with M_0 representing the top surface and M_1 representing the substrate. We introduce two auxiliary

interaction parameter combinations $\varepsilon_{M_0} = (\varepsilon_{AM_0} + \varepsilon_{BM_0})/2 - \varepsilon_{CM_0}$ and $\varepsilon_{M_1} = (\varepsilon_{AM_1} + \varepsilon_{BM_1})/2 - \varepsilon_{CM_1}$, where the interaction of the A- and B-component with the walls is being averaged. From the experiment we know that the second block B (P2VP) is strongly adsorbed on polar substrates, like SiO_x and that the C-component, which is the majority component, is at the free surface as it has the lowest interfacial energy towards air. Based on this experimentally observed phase behavior we adjusted the surface interactions in the simulations such that the sequence of surface patterns fits the experimental observations.

3.2.1. Results and discussion

Bulk phase behavior

We first compare the simulation results on the phase behavior in bulk with the corresponding experiments. In the experiments, the microdomain structure depends on the composition of the block terpolymer³⁰: PS-*b*-P2VP-*b*-PtBMA polymers with a composition of $\phi_{PS} : \phi_{P2VP} : \phi_{PtBMA} = 1 : 1.2 : 4$ exhibit core-shell cylinders. Decreasing the volume fraction of PtBMA to values between 3.05 to 3.65, leads to a coexistence of core-shell gyroids, core-shell cylinders, and perforated lamellae.

The microphase separation process in bulk was simulated on a cubic grid with $L \times L \times L$ grid points. In most simulations, we have considered $L = 32$. The bulk microphase structure was calculated for different values of the mutual interaction parameters $\boldsymbol{\varepsilon} = (\varepsilon_{AB}, \varepsilon_{AC}, \varepsilon_{BC})$. Starting from homogeneous density distributions, the calculations were run for 10000 time steps; from visual inspection we found that during the last 2000 steps no significant changes occurred.

The isodensity surface of the B-density ρ_B is shown for $\boldsymbol{\varepsilon} = (7.0, 8.0, 6.0)$ in Figure 2(a). The structure is difficult to characterize as it still contains many defects. Because of the large amount of three-arm interconnections the structure resembles a gyroid phase. Investigation of the A- and C-density shows a core-shell gyroid-like phase with the A-component forming the core, surrounded by a shell of the B-component embedded in a matrix of the majority component C. Variations of the box size ($L = 24$ and 16) show similar results. This core-shell gyroid structure is found to be robust in a large parameter range (Table 2).

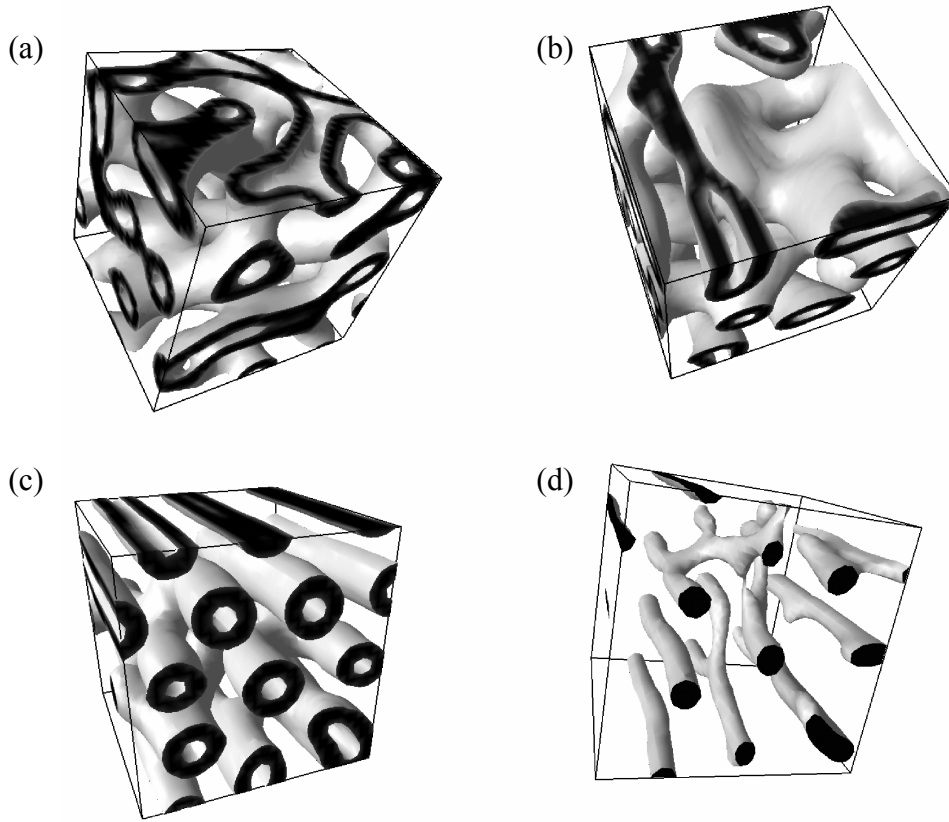


Figure 2. Simulation results for a melt of $A_3B_4C_{12}$ molecules in $32 \times 32 \times 32$ large simulation boxes. The component-component interaction parameters are $\epsilon = (7.0, 8.0, 6.0)$. (a): Isodensity surface of ρ_B after 10000 steps. (b) to (d): Effect of shearing. (b): Isodensity surface of ρ_B after shearing for additional 5000 steps (shear rate: 0.001). (c) ρ_B and (d) ρ_A after shearing (b) for additional 15000 steps (shear rate: 0.002).

Table 2. Simulation results: bulk morphologies for different interaction parameters ϵ .

ϵ_{AB}	ϵ_{AC}	ϵ_{BC}	Morphology ^a	Comments
7.0	8.0	6.0	G	core-shell structure
6.0	8.0	7.0	G	core-shell structure
8.0	8.0	6.0	G	core-shell structure
5.0	9.0	6.0	G	core-shell structure
7.0	9.0	7.0	G	core-shell structure
6.4	5.0	4.5	G	core-shell structure
“	4.0	“	G	A and B mixed
“	3.8	“	G / C	A and B mixed
“	3.0	“	dis	A, B, C mixed
“	2.0	“	dis	A, B, C mixed
“	1.0	“	dis	A, B, C mixed

^a Key: G, gyroid-like; C, cylinders; dis, disordered.

An AB-mixed gyroid structure is found when, starting from a parameter set of $\epsilon = (6.4, 5.0, 4.5)$, the AB interaction parameter between the two endblocks is decreased to $\epsilon = (6.4, 4.0, 4.5)$. A further decrease of this parameter leads to the coexistence of a gyroid-like structure and cylinders $\epsilon = (6.4, 3.8, 4.5)$, and finally to disordered phases where all three components are mixed $\epsilon = (6.4, \leq 3.0, 4.5)$, (Table 2). As the blocks are much smaller than the C-block, the A- and B-component tend to mix if the energetic penalty is too low.

The stability of the connections, important for the determination of the defected microdomain structure as a gyroid or cylinder structure, can be challenged by the application of an external field. Applying a shear field⁴¹ to the core-shell gyroid structure ($\epsilon = (7.0, 8.0, 6.0)$) leads to a partial removal of the interconnections. A perforated lamella like structure is obtained by shearing with a dimensionless shear rate of 0.001 for additional 5000 steps, (Fig. 2(b)), and a cylinder structure by increased shearing with a shear rate of 0.002 for additional 15000 steps, (Fig. 2(c)). As some connections between the cylinders remain after strong shearing for a long period, we conclude that the gyroid structure is most likely to have a slightly lower free energy than the cylinder structure.⁴¹

We conclude that the core-shell gyroid structure, found in a certain composition range in the experiment³⁰, is also found in the simulations. The volume fraction considered in the parameterization of the simulation chain is well within this composition range. Moreover, in the simulations, the bulk core-shell gyroid structure seems to be quite stable with respect to rather large variations in the interaction parameter. Upon shearing a perforated lamella and a cylinder phase are found next to the gyroid phase boundaries: an observation which is in line with the experiments, where a coexistence of gyroids, perforated lamellae, and cylinders is found.³⁰

Thin film phase behavior

We investigate the phase behavior in thin films as function of the film thickness. We consider the previous system exhibiting a core-shell gyroid structure in bulk with $\epsilon = (7.0, 8.0, 6.0)$. Figure 1 shows the experimental results for $S_{17}V_{22}T_{61}$ ¹³² together with simulations. The scanning electron micrographs in Fig. 1(a) represent the first four terraces (T_0, T_1, T_2, T_3) with increasing film thickness from left to right; the corresponding schematic height profile of the film measured relative to the silicon substrate is shown in Fig. 1(b).³² The interaction parameters of the components with the two surfaces are $\epsilon_{M_0} = 5.0$ ($M_0 =$ top surface) and $\epsilon_{M_1} = -5.0$ ($M_1 =$ substrate). With increasing film thickness, both experiments and calculations show the same sequence of surface structures (Fig. 1(c)): The regions with the smallest film thickness (T_0) show a disordered structure (dis), followed by a dot-like structure (which is assigned to C_{\perp} in the experiments), cylinders oriented parallel to the film plane (C_{\parallel}), a perforated lamella structure (PL_1), parallel cylinders (C_{\parallel}), a

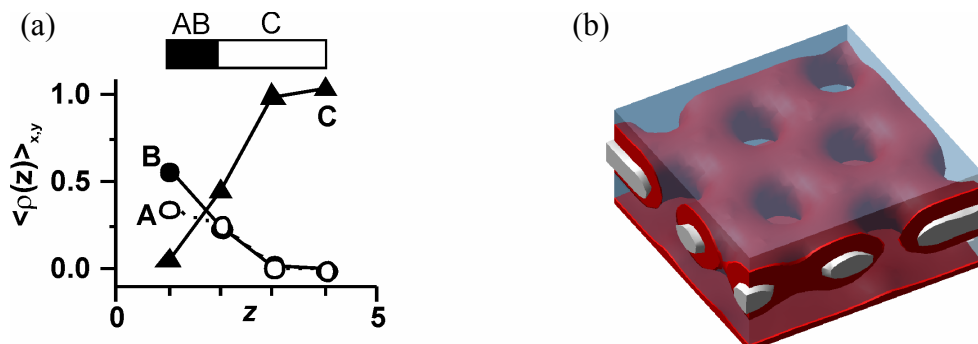
perforated lamella structure (PL₂), parallel cylinders (C_{||}) and again a perforated lamella phase (PL₃). The general observation is that terraces exhibit PL, while the slopes between neighboring terraces exhibit C_{||}.

- *The Wetting layer (W)*

In the experiments, a featureless layer of approximately 10 nm thickness (T₀) is found in the thinnest regions of a SVT film (see Fig. 1(a), left part). From measurements of the film thickness and the step height between terraces it was concluded that a wetting layer of similar thickness is formed next to the substrate in thicker films.³² Elbs *et al.* and Fukunaga *et al.* have shown that SVT block terpolymers are pinned onto SiO_x via the polar P2VP (component B in the simulations), while the majority component PtBMA (component C) forms a uniform layer on top.^{33,36}

In order to elucidate the structure in very thin films (4 grid cells) in the simulations, we have calculated depth profiles of the laterally averaged densities as function of the distance z from the surface (Fig. 3(a)) The A and B-component are accumulated close to the substrate M_1 at $z = 0$. The A-density follows the B-density and a thin AB-mixed wetting layer is formed at the substrate ($z = 0$) terminating in a microphase-separated C-rich layer. The mixing of A and B close to the substrate is attributed to the confinement and the rather small fractions of A and B compared to the majority component C (A₃B₄C₁₂). The AB-mixing is in line with previous observations for AB and ABA block copolymers,^{23,25,26,42} where for very small thickness ($H <$ microdomain spacing) confinement prevents microphase separation and stabilizes a disordered phase.

Regardless of the film thickness both, experiments and simulations, show a wetting layer W next to the substrate terminating with a homogeneous layer of the matrix component C. All thin film microdomain structures are formed on top of this AB-C layer. The wetting layer effectively reduces the film thickness and gives rise for an effective interface with strong C-character for the reduced film causing a screening effect.^{19,26} W screens the substrate from the reduced part of the film and the surface field at the effective interface is effectively the one that would result from a C-coated surface.



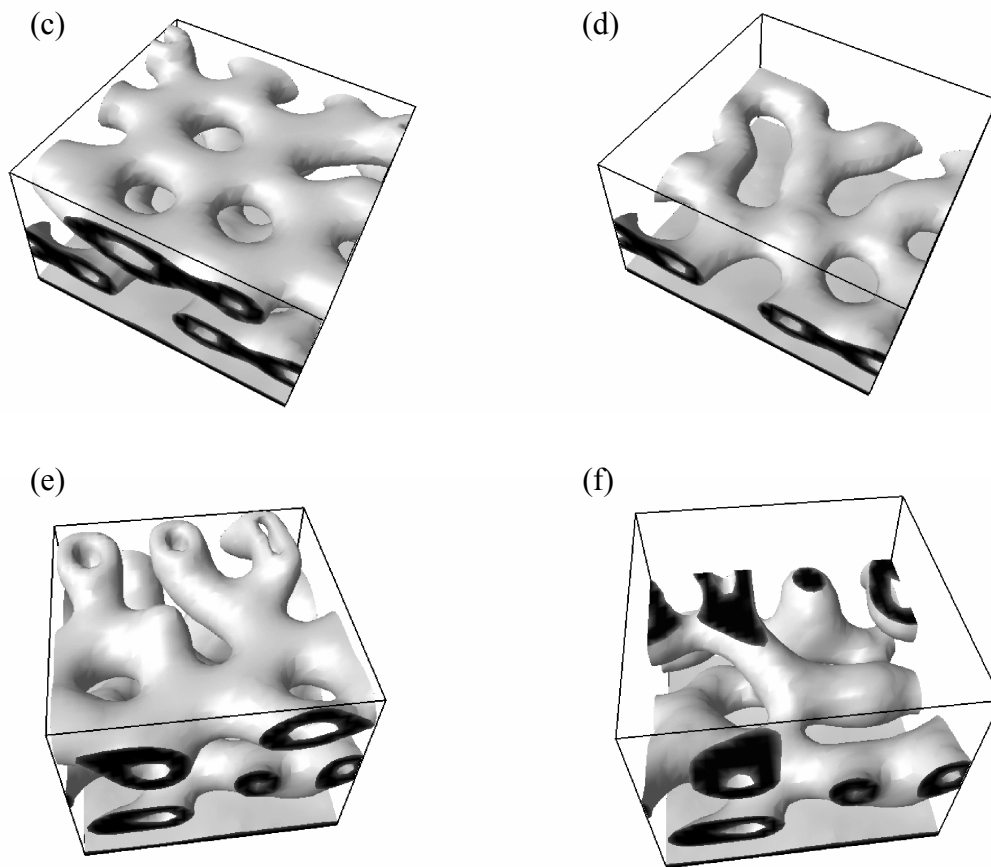


Figure 3. Characteristic surface structures and wetting layer. The interaction parameters are the same as in Fig. 2(c). (a): Wetting layer. Depth profiles of the laterally averaged densities ρ_A , ρ_B , and ρ_C are shown as function of the distance z from the surface for $H = 4$. (b) – (f): Perforated lamella phase. (b): The isodensity surfaces of all three components are shown. The A-component forms the core (white) embedded in a shell of the B-component (red phase) in a matrix of the C-component (blue). (c) and (d): The isodensity surfaces of ρ_B are shown for $H = 19$ before and after removing the top layer of PL, respectively; (e) and (f): same as (c) and (d) for $H = 26$.

- *The PL phase*

At well-defined film thickness a perforated lamella structure is found at the top surface both in experiments and simulations. This structure can be described as a P2VP/PS/P2VP sheet perforated by PtBMA channels, which connect between two outer PtBMA layers. As mentioned above, the morphology is formed on top of a wetting layer; the wetting layer terminates with the C-component. Figure 3(b) visualizes the isodensity surfaces of all three components for the first terrace of PL. The A-, B- and C-components are microphase separated; A and B form a core-shell structure.

In experiments, it was impossible to determine whether the PL structure continues through the depth of the film to the substrate in higher terraces.³² In the simulations, it is easy to look beneath the top surface. The PL phase appears at film thicknesses $H = 12$, 19, and 26 grid points, therefore the thickness of one single layer of PL amounts to $\Delta H = 7$ grid points. The wetting layer at the substrate has a thickness of about 5 grid points. Figure 3(c) to (f) show isodensity surfaces of ρ_B at

$H = 19$ (PL₂) and $H = 26$ (PL₃) before and after removing the top PL layer. At $H = 19$ (corresponding to the second terrace T₂) a defective PL structure forms beneath the top PL layer, while at $H = 26$ a gyroid-like network is found beneath the top PL layer.

Our results for $H = 26$ indicate that the surface field extends into the bulk of the film with a decay length of about one microdomain spacing, similar as found in previous investigations.^{21,25,26} In thicker films the bulk structure (core-shell gyroids) becomes energetically favored in the center of the film, as the confinement effect becomes less important. The PL phase appears as a surface reconstruction of the gyroid phase.

- *The C_{||} structure*

In the experiments, the slopes between neighboring terraces exhibit cylinders oriented parallel to the surface (C_{||}). Figure 4(a) and (d) show scanning electron micrographs on areas that include T₁ and the slopes towards T₀ and T₂, respectively. The majority component PtBMA always appears as dark phase, while the other two components show similar contrast (even with staining), for further details see the accompanying article.³² In the experiments the inner structure of the cylinders cannot be resolved clearly. Core-shell cylinders are either embedded in a PtBMA matrix with a thin layer of PtBMA on top (full cylinders) or all three components are at the free surface which then would be identified as a half-open cylinder. From Fig. 4(a) one may get the impression that there is an inner structure between two dark stripes (PtBMA), but this might also be an artifact of the scanning conditions during imaging with scanning electron microscopy.

Simulations provide a means to interpret the experimentally observed surface structures. Figure 4(b) and (e) show the isodensity surfaces of the B-density at $H = 10$ and $H = 14$ in large simulation boxes ($L = 64$). In order to compare them with the experimental images (a) and (d) we have periodically tiled four two-dimensional slices showing the B-density in the top parts of (b) and (e) in Figure 4(c) and (f), respectively. Stripe patterns (C_{||}) and perforated lamellae are observed to coexist with the stripes connecting to the PL. The three components are microphase separated. In thinner films ($H = 10$) half cylinders are favored with all three components at the top surface, in thicker films ($H = 14$) full cylinders are energetically favored. The thickness of a half cylinder does not coincide with the half value of a full cylinder.

A further detail, where simulations and experiments match extremely well are drop-like defects which are marked with arrows in Fig. 4(d), (e) and (f).

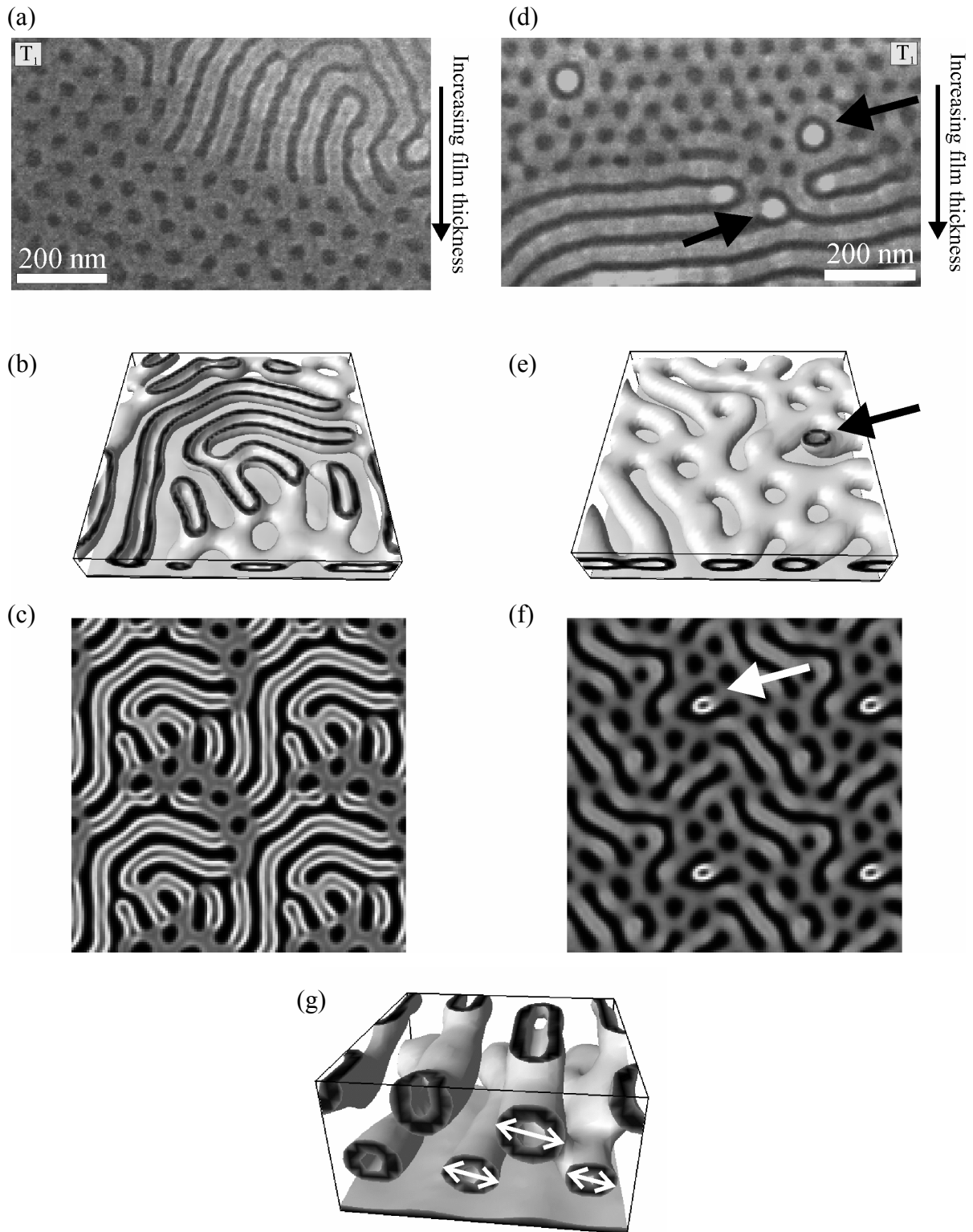


Figure 4. *Cylinders in the slopes between terraces. (a) and (d): Experiments. SEM images of the transition between T_0 and T_1 and between T_1 and T_2 . (b), (c), (e)-(g): Simulation results. The interaction parameters are the same as in Fig. 2(c). The isodensity surfaces of the B -density are shown for a box size of $L \times L \times H = 64 \times 64 \times 10$ in (b) and a box size of $L \times L \times H = 64 \times 64 \times 14$ in (e). (c) and (f): Two-dimensional slices of ρ_B in the vicinity of the surface in (b) and (e), respectively. For visualization purposes we have periodically tiled four images of (b) and (e). (g): Isodensity surface of the B -density for a box size of $L \times L \times H = 32 \times 32 \times 17$.*

Figure 4(g) shows the isodensity surface of ρ_B for a thicker film ($H = 17$). Two layers of core-shell cylinders can be seen. In thicker films we often observe a coexistence of half-open and full cylinders in the top layer. Both simulation results, half and full cylinders, are compatible with the experimental observation where these two situations cannot be distinguished.

In the previous work of Lyakhova *et al.*, half-open structures at the surfaces were identified as a structured wetting layer. In contrast to the findings for ABC systems, these wetting layers always developed as a completely disconnected layer from the bulk of the film, with a fixed thickness.

The cylinders in Fig. 4(g) are hexagonally packed, but there are some interconnections between the two layers. The arrows in Figure 4(g) mark another important finding: the cylinder radius is quite flexible and adjusts itself to different thicknesses. Lyakhova *et al.* have recently reported about this phenomenon for a cylinder forming ABA system with asymmetric surface interaction: they have found that cylinders can even adjust their shapes.²¹ This explains why we find cylinders in a large thickness range. In the experiments the same tendency is observed: while cylinders appear over a large thickness range at steps between terraces, the PL phase appears only at well-defined film thicknesses.³² In accordance to previous publications^{23,24,25,26} we can conclude that PL are less deformable than cylinders.

- *Comparison to the phase behavior of cylinder-forming ABA systems*

Recently Knoll *et al.* and Horvat *et al.* have presented a comparison of the phase diagram for thin films of a cylinder-forming poly(styrene)-*b*-poly(butadiene)-*b*-poly(styrene) triblock copolymer and simulations of a corresponding $A_3B_{12}A_3$ triblock copolymer film, where the interfaces preferentially attract the B-component.^{23,24,25} With increasing film thickness, both experiments and calculations show the same sequence of thin film phases: a disordered film (dis) for the smallest film thickness, very short upright cylinders (C_{\perp}), A-cylinders oriented parallel to the film plane ($C_{\parallel, 1}$), a perforated A-lamella (PL), parallel oriented A-cylinders with an elongated cross section and necks, perpendicular oriented A-cylinders and finally two layers of two parallel oriented A-cylinders ($C_{\parallel, 2}$). An orientation of the microdomains parallel to the film plane is dominant in films with surfaces having a preference for one of the blocks of the copolymer.¹⁹ At incommensurate film thicknesses, however, C_{\perp} is formed.

Our observations are in qualitative agreement with the main conclusions of the cylinder-forming ABA system. For a system forming a core-shell gyroid structure in bulk, we observe in thin films analogous core-shell PL and C_{\parallel} surface structures with the same sequence of surface structures as function of the film thickness. The PL appears at commensurate film thicknesses, at intermediate film thicknesses (in experiments at the slopes between neighboring terraces), C_{\parallel} form which can be

either half or full cylinders. In thicker films the parallel-oriented cylinders are hexagonally packed, but they show interconnections between layers of cylinders, which is indicative for the gyroid structure in bulk. In very thin films we observe a liquid-like distribution of isolated microdomains both in the experiments and the simulations, which is analogous to the very short upright cylinders (C_{\perp}) observed in the cylinder-forming ABA systems, where the packing was better ordered.

All these findings are illustrative of the fact that the thin film phase behavior of ABC triblock terpolymers is analogous, but more complex than that of ABA block copolymers.

Influence of surface field

We further study the influence of the surface field on the surface structures as a function of the film thickness. We again consider the system which forms a core-shell gyroid structure in the bulk ($\epsilon = (7.0, 8.0, 6.0)$). As the phase behavior is very complex, we restrict ourselves to a rather limited region of the phase diagram around the parameter values that we fitted to the experimental data. Starting from these component-surface interactions we vary the interactions ϵ_{AM_0} and ϵ_{BM_0} of the A- and B-component with the top surface. As we already mentioned, changing the interactions of the components with the substrate has little influence on the thin film structures due to the wetting layer and its screening effect. Additionally, we consider the case with symmetric walls where no wetting layer is formed at the substrate.

Figure 5(b) and (e) show the sequence of surface structures observed in the simulations and in the experiments as function of the film thickness, respectively, for the system investigated in the previous subsection of this paper ($\epsilon_{M_0} = 5.0$, $\epsilon_{M_1} = -5.0$). The experimental H axis was scaled such to match the H scale of the simulations. Some of the surface structures have been presented in Figure 2(c), 3 and 4. The interaction parameters in the simulations have been chosen such that the sequence of phases of the model and the experiments match very well.

A decrease of the repulsion of component A and B from the top surface to $\epsilon_{M_0} = 3.0$ leads to the following sequence of surface structures: dis, C_{\parallel} , PL_1 , C_{\parallel} , coexistence of C_{\parallel} and PL_2 , and C_{\parallel} (Fig. 5(a)). Compared to the phase diagram of Fig. 5(b), two effects occur as a result of the weaker surface field: At $H = 7$, C_{\perp} disappears, and the stability region of C_{\parallel} grows, leading to the disappearance of the coexistent C_{\parallel}/PL phase in thinner films at $H = 10$ and $H = 14$. Furthermore the PL phase in thicker films, at $H = 19$, coexists with C_{\parallel} .

Stronger repulsion of A and B from the top surface ($\epsilon_{M_0} = 7.0$) leads to the sequence of surface structures shown in Fig. 5(c): dis, coexistence of C_{\perp} and C_{\parallel} , C_{\parallel} , L, PL_1 , coexistence of PL_1 and C_{\parallel} ,

C_{\parallel} , PL_2 , C_{\parallel} , and PL_3 . We observe a significant increase of the stability region of PL. Additionally, in thinner films a lamella phase is formed between the C_{\parallel} and PL_1 phases, at $H=9$. Figure 6(a) shows the corresponding depth profiles of the different components for $H=9$. On top of the wetting layer at the substrate, a lamella is formed within which the A- and B-components are mixed. Such a lamella is also found in the experiments: A thin film of $S_{17}V_{22}T_{61}^{132}$ on mica exhibits C_{\parallel} and L between the disordered region and PL_1 .

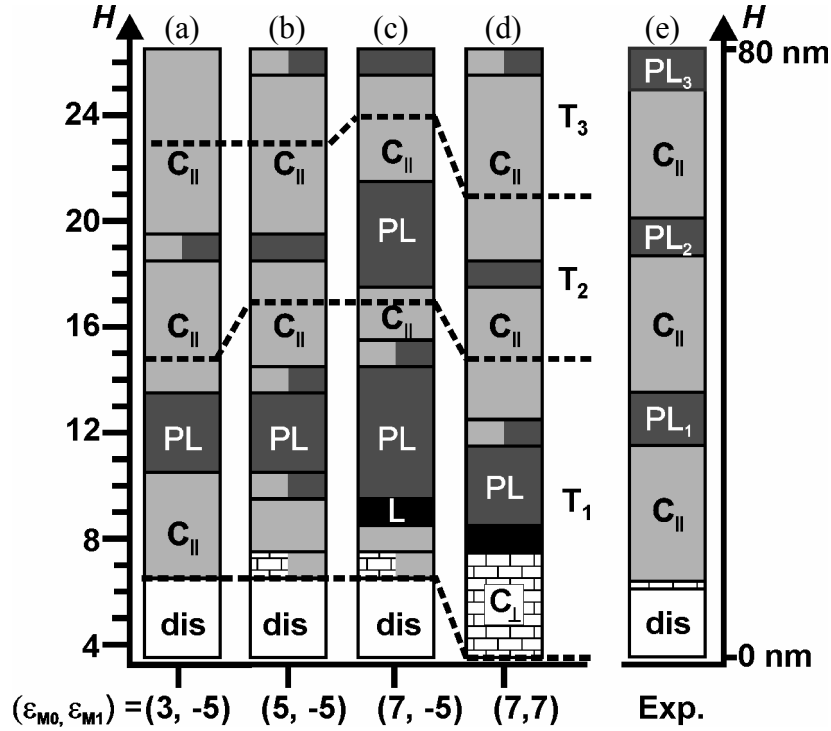
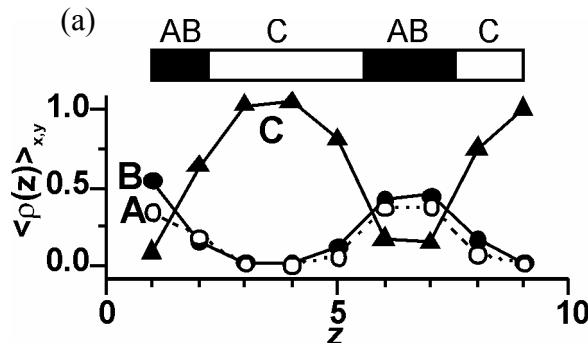


Figure 5. Influence of surface field. Surface structures (close to the free surface) as function of the film thickness and the interaction parameters with the walls $(\epsilon_{M_0}, \epsilon_{M_1})$. Color code: white: dis; light grey: C_{\parallel} ; dark grey: PL; black: L; tiled: C_{\perp} . The dashed lines indicate the transition from one (two) layer(s) of microdomain structures to two (three) layers. The interaction parameters between the components are set to $\epsilon = (7.0, 8.0, 6.0)$. The interaction parameters with the walls are $(\epsilon_{M_0}, \epsilon_{M_1}) = (3.0, -5.0)$ in (a); $(5.0, -5.0)$ in (b); $(7.0, -5.0)$ in (c); $(7.0, 7.0)$ in (d).

(e): Experimental phase diagram of $S_{17}V_{22}T_{61}^{132}$, corresponding to Fig. 1(b).



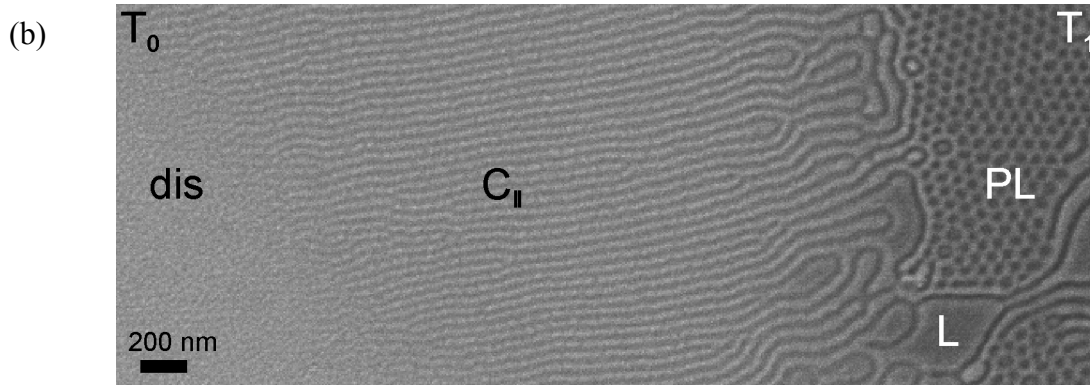


Figure 6. Details and evidence for the lamella phase in the phase diagram of Fig. 5(c). (a): Depth profiles of the laterally averaged densities ρ_A , ρ_B , and ρ_C for $H = 9$. (b): Experiment: Scanning electron micrograph of $S_{17}V_{22}T_{61}$ ¹³² prepared on a mica substrate.

Regarding the three phase diagrams (Fig. 5(a), (b), and (c)) we can identify general tendencies. We observe a complex interplay between the surface fields, prominent in the case of very thin films due to the additivity, and confinement effects such as commensurability, which lead to PL structures at film thicknesses that are a multiple amount of natural domain distances. In films with $H > 9$ grid points, only $C_{||}$ and PL are stable surface structures. With increasing surface field at the top surface the stability region of the PL phase increases and $C_{||}$ are suppressed. In very thin films ($H < 9$) the effect of the surface field has a stronger influence on the surface structures. Increasing the surface field leads to the formation of C_{\perp} between dis and $C_{||}$ (Fig. 5(c)) and to the formation of an AB-mixed lamella L between $C_{||}$ and PL. In this lamella, mixing of the A and B-component is due to a very high repulsion of these blocks from the top surface. The existence of L next to PL has already been observed in two-component systems.^{21,22,23,25,26} The fact that the L and the C_{\perp} phase are only observed for thinner films is attributed to the additivity of the surface fields of both surfaces, leading to a combined surface field that exceeds some threshold value necessary for the formation of these structures. This effect is most prominent in thin films, as the surface field extends into the film with a decay length of about one domain distance.²³

Symmetric boundary conditions

In order to investigate the influence of the wetting layer at the substrate, we also consider a phase diagram for equal component-surface interactions at both walls. Both walls attract the C-component and the surface fields are quite high ($\varepsilon_{M_0} = \varepsilon_{M_1} = 7.0$). With increasing film thickness we observe the following surface structures: C_{\perp} , $L_{||}$, PL_1 , coexistence of PL_1 and $C_{||}$, $C_{||}$, PL_2 , $C_{||}$, coexistence of PL_3 and $C_{||}$. We note that the phase diagram is rather similar to Fig. 5(c), except for very thin films, and

that the phase boundaries are shifted to lower values of H . In very thin films no C_{\parallel} appear, and the C_{\perp} phase is found in a rather large region of thicknesses, from $H = 4$ to 7. The high surface fields additionally lead to the formation of an AB-mixed lamella phase, similar to that of Fig. 5(c). PL and C_{\parallel} are again observed in the upper part of the phase diagram, with the difference that these structures have much less defects than the structures observed for films with a wetting layer at the substrate.

Comparing Fig. 5(c) and (d), we see a clear example of the screening effect: the phase behavior in the presence of a wetting layer and for the system with both surfaces attracting the C-component (the symmetric case) is rather similar. In case when the wetting layer is present, it was shown to terminate in a C-rich layer (Fig. 3(a)). When we disregard this wetting layer, the remaining part of the film experiences a confinement between two surfaces with a strong preference for the C-component. The shift of phase boundaries in the symmetric case is approximately 2 grid points which is smaller than the thickness of the wetting layer amounting to $\sim 4 - 5$ grid points.

The exact effective interactions cannot be determined, as the nature of the additivity of surface fields is yet unknown and the microdomain structures can adjust to different film thicknesses. The thickness of the wetting layer also vary. From the coexistence of C_{\perp} and C_{\parallel} in Fig. 5(b) and (c) we see that the surface field value in those cases is just above or at the threshold necessary for the formation of the C_{\perp} structure.

Influence of interaction parameters and the effect of confinement

In all thin films studied until now, we have used a fixed triple $\boldsymbol{\varepsilon} = (7.0, 8.0, 6.0)$ for the component-component interactions. We showed that in the bulk a core-shell gyroid structure appears to be quite robust in a wide range around this set of parameters. We now turn to the question how the thin film phase behavior is influenced by the strength of the interaction between the polymer components. The surface interactions are kept constant at $\varepsilon_{M_0} = 7$ and $\varepsilon_{M_1} = -5$, resulting in a strong preference of the C-component both to the top surface and to the wetting layer at the substrate. Slight changes of the $\boldsymbol{\varepsilon}$ interaction parameters lead to major changes in the surface structures and their stability regions (Fig. 7). As a reference, the phase diagram for the set of parameters of the previous sections $\boldsymbol{\varepsilon} = (7.0, 8.0, 6.0)$ is shown in Fig. 7(a), which is the same as in Fig. 5(c).

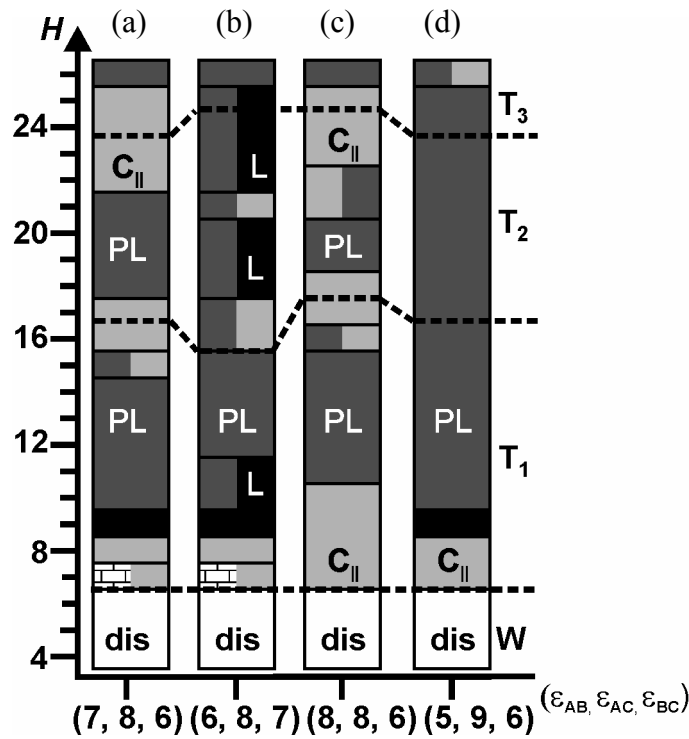


Figure 7. Influence of component-component interaction parameters ϵ on thin film structures as function of the film thickness. Color code: white: dis; light grey: $C_{||}$; dark grey: PL; black: L; tiled: C_{\perp} . The interaction parameters with the walls are set to: $\epsilon_{M_0} = 7.0$ and $\epsilon_{M_1} = -5.0$. The interaction parameters between the components are $\epsilon = (7.0, 8.0, 6.0)$; in (a); $(6.0, 8.0, 7.0)$ in (b); $(8.0, 8.0, 6.0)$ in (c); and $(5.0, 9.0, 6.0)$ in (d).

- $\epsilon = (6.0, 8.0, 7.0)$, Fig. 7(b): Exchanging the value of the interaction parameter between A and B with that between B and C leads to surface structures that are very similar in very thin films ($H < 9$). However, in thicker films, perforated lamellae form even at intermediate film thicknesses. At commensurate film thicknesses, an AB-mixed lamella coexists with PL.
- $\epsilon = (8.0, 8.0, 6.0)$, Fig. 7(c): Increasing the repulsion between the A- and the B-component leads to a phase diagram that is quite similar to the reference phase diagram (a). The phase boundaries are slightly shifted and a coexistence of PL and $C_{||}$ is more favored in thicker films. Both, the C_{\perp} and the L phase are not found. At $H = 15$ and $H = 16$ the wetting layer at the substrate is laterally not continuous. Apparently the attraction of the B-component to the substrate is not strong enough to compensate the repulsion between A and B.
- $\epsilon = (5.0, 9.0, 6.0)$, Fig. 7(d): Reducing the repulsion between the A- and B-component, and increasing the repulsion between A and C leads to a phase diagram that is dominated by the PL phase. Apparently, the $C_{||}$ surface reconstruction is no longer favored. For very thin films, the behavior is similar to the reference system, except that C_{\perp} is not found.

Although in the bulk the same microdomain structure is observed for different interaction parameters, the presence of confining walls leads to significant changes in the phase diagram and shifts of phase boundaries. As a function of the slit width and interaction parameters between the different components a zoo of surface structures is induced.

We already discussed this phenomenon of triblock terpolymers in the accompanying experimental paper.³² In the experiments the situation is even more complex as the structure formation process takes place in concentrated solutions. Tiny differences in the vapour pressure of the solvent and the nature of the solvent have proven to significantly vary the microdomain structures in thin films, while in bulk the same structure was observed. Figure 10 in the experimental paper³² shows for example four different types of cylindrical microdomain structures in thin films: core-shell cylinders, spheres-at-cylinders, cylinders-at-cylinders, and helices-at-cylinders.

Surface reconstructions: AB-mixed microdomain structures

Finally, we concentrate on a system with $\epsilon = (6.4, 5.0, 4.5)$, where all component-component interaction parameters are smaller than in our reference system ($\epsilon = (7, 8, 6)$), confined between symmetric walls attracting the C-block with $\epsilon_{M_0} = \epsilon_{M_1} = 4.75$. In the bulk, this system also forms a core-shell gyroid structure, where all three components are microphase separated (Table 2). The choice for this system is inspired by the finding of AB-mixed structures in bulk, upon decreasing the interaction parameter between A and C. Our results show that the surface field can also have an impact on the microphase separation of A and B. Figure 8(a) schematically shows the dependence of the surface structures on the film thickness: with increasing film thickness we find: L, C_{\perp} , L_{\parallel} , coexistence of L_{\parallel} and PL_1 , PL_1 , C_{\parallel} , coexistence of C_{\parallel} and PL_2 , PL_2 , coexistence of C_{\parallel} and PL_2 , C_{\parallel} , and coexistence of C_{\parallel} and PL_3 . The phase diagrams are quite similar to those shown in Fig. 5(a), (b), (c) and 7, however, no wetting layer is formed at the substrate.

Besides the AB-mixed lamellae at $H = 4$, the main difference to the phase diagrams in Figs. 5 and 7 is that also other structures show mixing of A and B next to the surfaces. A typical example of this phenomenon is displayed in Fig. 8(b), where the isodensity surface of B is shown for $H = 25$. At both surfaces, the thickness of the surface structures is much smaller than that of the center structure, which shows a well-developed core-shell structure. A general rule seems to be that if the microdomain structures fit a certain film thickness, microphase separation occurs for all three components; if not, the microdomain structures next to the surfaces exhibit mixing of A and B. These structures are marked in the phase diagram. This interesting finding reveals the complex interplay between interaction parameters and confinement effects. We interpret this effect as a new type of surface reconstruction, in which the surface field not only induces a certain type of

microdomain structure, but also affects the degree of microphase separation of the block components. It leads to the mixed situation of apparent diblock microdomain structures close to the surface and core-shell triblock microdomain structures in the middle of the film.

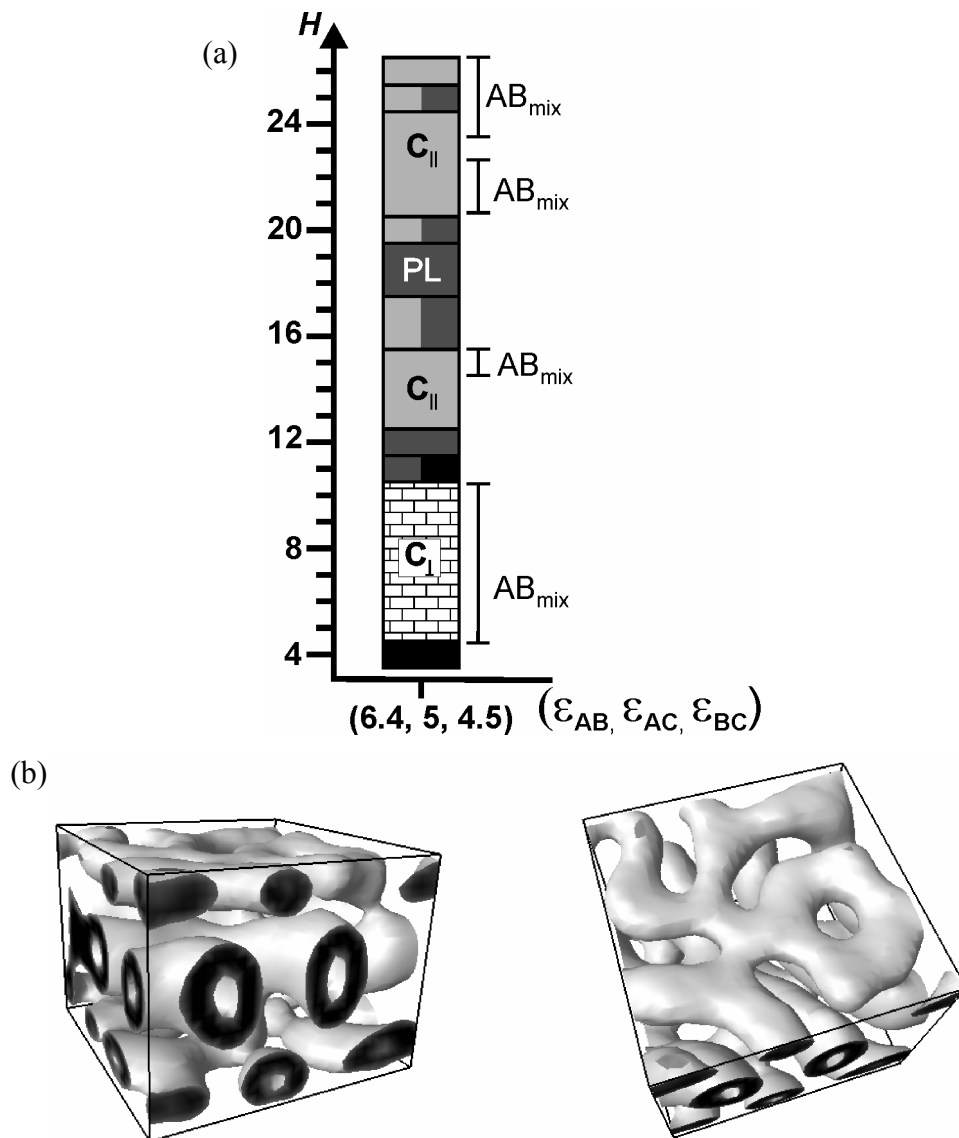


Figure 8. Surface reconstructions. The interaction parameters are $\epsilon = (6.4, 5.0, 4.5)$, $\epsilon_{M_0} = 4.75$, and $\epsilon_{M_1} = 4.75$.

(a): Surface structures as function of the film thickness. Color code: white: dis; light grey: C_{\parallel} ; dark grey: PL; black: L; tiled: C_{\perp} . (b): The isodensity surface of the B-density is shown for $H = 25$.

3.2.2. Conclusion

We described the complex phase behavior of a specific ABC triblock terpolymer system confined between two walls. Based on the experimental results³² we were able to determine the interaction parameters between the components, and the interaction parameters between the components and the interfaces. With this parameterization, a detailed match was found between the experimental results and our simulations based on SCF theory. Even details, like specific defect structures of the experiments, were found in the simulations. With increasing film thickness we observed a wetting layer (W), cylinders oriented perpendicular to the film plane (C_{\perp}), parallel cylinders (C_{\parallel}), perforated lamellae (PL) and again C_{\parallel} . In analogy with earlier work on a two-component system^{23,24,25} we identified these structures as surface reconstructions of the core-shell gyroid structure in bulk. In particular, the core-shell PL structure can be seen as analogue to the PL surface reconstruction of cylinder-forming AB and ABA systems.

Like in thin films of the two-component systems, the film thickness is modulating the stability region of the different phases via additivity of surface fields and commensurability effects. The phase behavior is much more complex in thin films of ABC triblock terpolymers due to the larger number of degrees of freedom. Confined systems are much more sensitive to small changes in the energetic interaction between the different components A, B, and C. While we observe a core-shell gyroid structure for a wide range of interaction parameters in bulk, confinement leads to a large variety of phases depending on the film thickness. In the presence of a wetting layer at one side of the film, the surface field is screened at that side, leading to microdomain structures that are rather independent of the interaction with the wall at the side where the wetting layer is present. In this case the morphology is mostly influenced by the variation of the surface field at the surface that is not covered by a wetting layer. Especially in thin slits the two surface fields interfere. A difference to two-component systems is the formation of AB-mixed L, PL, and C_{\perp} surface reconstructions.

Simulations like this might be used for rational design of desired material properties and for identification of important experimental control parameters. In particular a combinatorial approach could provide a deeper insight in the complex interplay between surface field, interaction parameters, and confinement effects in thin films of triblock terpolymers.

Acknowledgements

We thank N. Rehse and A. Horvat for fruitful discussions and help. We acknowledge support from the Deutsche Forschungsgemeinschaft (SFB 481), the VolkswagenStiftung, and the NWO-DFG bilateral program.

References

- (1) Mansky, P.; Chaikin, P.; Thomas, E. L. *J. Mater. Sci.* **1995**, 30, 1987.
- (2) Park, M.; Harrison, C.; Chaikin, P. M.; Register, R. A.; Adamson, D. H. *Science* **1997**, 276, 1401.
- (3) Park, C., Yoon, J., Thomas, E. L. *Polymer* **2003**, 44, 6725.
- (4) Anastasiadis, S. H.; Russell, T. P.; Satija, S. K.; Majkrzak, C. F. *Phys. Rev. Lett.* **1989**, 62, 1852.
- (5) Walton, D. G.; Kellogg, G. J.; Mayes, A. M.; Lambooy, P.; Russell, T. P. *Macromolecules* **1994**, 27, 6225.
- (6) Kellogg, G. J.; Walton, D. J.; Mayes, A. M., Lambooy, P.; Russell, T. P.; Gallagher, P. D., Satija, S. K. *Phys. Rev. Lett.* **1996**, 76, 2503.
- (7) Matsen, M. W. *Curr. Opin. Coll.* **1998**, 3, 40.
- (8) Binder, K. *Adv. Polymer. Sci.* **1999**, 138, 1.
- (9) Fasolka, M. J.; Mayes, A. M. *Annu. Rev. Mat. Res.* **2001**, 31, 323.
- (10) Qi, S. Y.; Wang, Z. G. *Polymer* **1998**, 39, 4639.
- (11) Chen, H.; Chakrabati, J. *J. Chem. Phys.* **1998**, 39, 4639.
- (12) Feng, J.; Liu, H.; Hu, Y. *Macromol. Theory Simul.* **2002**, 11, 556.
- (13) Brown, G.; Chakrabarti, A. *J. Chem. Phys.* **1994**, 101, 3310.
- (14) Brown, G.; Chakrabarti, A. *J. Chem. Phys.* **1995**, 102, 1140.
- (15) Wang, Q.; Yan, Q. L.; Nealy, P. F.; de Pablo, J. J. *J. Chem. Phys.* **2000**, 112, 450.
- (16) Wang, Q.; Nealy, P. F.; de Pablo, J. J. *Macromolecules* **2001**, 34, 3458.
- (17) Szamel, G.; Müller, M. *J. Chem. Phys.* **2003**, 118, 905.
- (18) Sevink, G. J. A.; Zvelindovsky, A. V.; van Vlimmeren, B. A. C.; Maurits, N. M.; Fraaije, J. G. E. M. *J. Chem. Phys.* **1999**, 35, 16.
- (19) Huinink, H. P.; Brokken-Zijp, J. C. M.; van Dijk, M. A.; Sevink, G. J. A. *J. Chem. Phys.* **2000**, 112, 2452.
- (20) Sevink, G. J. A.; Zvelindovsky, A. V.; van Vlimmeren, B. A. C.; Maurits, N. M.; Fraaije, J. G. E. M. *J. Chem. Phys.* **1999**, 110, 2250.
- (21) Huinink, H. P.; van Dijk, M. A.; Brokken-Zijp, J. C. M.; Sevink, G. J. A. *Macromolecules* **2001**, 34, 5325.
- (22) Sevink, G. J. A.; Fraaije, J. G. E. M.; Huinink, H. P. *Macromolecules* **2002**, 35, 1848.
- (23) Knoll, A.; Horvat, A.; Lyakhova, K. S.; Krausch, G.; Sevink, G. J. A.; Zvelindovsky, A. V.; Magerle, R. *Phys. Rev. Lett.* **2002**, 89, 035501-1.

- (24) Knoll, A.; Magerle, R.; Krausch, G. *J. Chem. Phys.* **2004**, 120, 1105.
- (25) Horvat, A.; Lyakhova, K. S.; Sevink, G. J. A.; Zvelindovsky, A. V.; Magerle, R. *J. Chem. Phys.* **2004**, 120, 1117.
- (26) Lyakhova, K. S.; Sevink, G. J. A.; Zvelindovsky, A. V.; Horvat, A.; Magerle, R. *J. Chem. Phys.* **2004**, 120, 1127.
- (27) Pickett, G. T.; Balazs, A. C. *Macromol. Theory Simul.* **1998**, 7, 249.
- (28) Feng, J.; Ruckenstein, E. *Polymer* **2002**, 43, 5775.
- (29) Chen, H.-Y.; Fredrickson, G. H. *J. Chem. Phys.* **2002**, 116, 1137.
- (30) Ludwigs, S.; Böker, A.; Abetz, V.; Müller, A. H. E.; Krausch, G. *Polymer* **2003**, 44, 6815.
- (31) Ludwigs, S.; Böker, A.; Voronov, A.; Rehse, N.; Magerle, R.; Krausch, G. *Nature Materials* **2003**, 2, 744.
- (32) Ludwigs, S.; Schmidt, K.; Stafford, C.; Fasolka, M.; Karim, A.; Amis, E.; Magerle, R.; Krausch, G. *submitted to Macromolecules*.
- (33) Elbs, H.; Fukunaga, K.; Stadler, R.; Sauer, G.; Magerle, R.; Krausch, G. *Macromolecules* **1999**, 32, 1204.
- (34) Elbs, H.; Abetz, V.; Hadziioannou, G.; Drummer, C.; Krausch, G. *Macromolecules* **2001**, 34, 7917.
- (35) Elbs, H.; Drummer, C.; Abetz, V.; Krausch, G. *Macromolecules* **2002**, 35, 5570.
- (36) Fukunaga, K.; Elbs, H.; Magerle, R.; Krausch, G. *Macromolecules* **2000**, 33, 947.
- (37) Fukunaga, K.; Hashimoto, T.; Elbs, H.; Krausch, G. *Macromolecules* **2002**, 35, 4406.
- (38) Fukunaga, K.; Hashimoto, T.; Elbs, H.; Krausch, G. *Macromolecules* **2003**, 36, 2852.
- (39) Fraaije, J. G. E. M. *J. Chem. Phys.* **1993**, 99, 9202.
- (40) Fraaije, J. G. E. M.; van Vlimmeren, B. A. C.; Maurits, N. M.; Postma, M.; Evers, O. A.; Hoffmann, C.; Altevogt, P.; Goldbeck-Wood, G. *J. Chem. Phys.* **1997**, 106, 4260.
- (41) Zvelindovsky, A. V.; Sevink, G. J. A.; Fraaije, J. G. E. M. *Phys. Rev. E* **2000**, 62, R3063.
- (42) Henkee, C. S.; Thomas, E. L.; Fetters, L. J. *J. Mater. Sci.* **1988**, 23, 1685.

3.3. Self-assembly of functional nanostructures from ABC triblock copolymers

Sabine Ludwigs, Alexander Böker, Andrej Voronov, Nicolaus Rehse, Robert Magerle, and Georg Krausch*

Lehrstuhl für Physikalische Chemie II and Bayreuther Zentrum für Kolloide und Grenzflächen (BZKG), Universität Bayreuth, 95440 Bayreuth, Germany

**e-mail: georg.krausch@uni-bayreuth.de*

Published in *Nature Materials* 2003, 2, 744.

The spontaneous formation of nanostructured materials by molecular self assembly of block copolymers is an active area of research, driven both by its inherent beauty and by a wealth of potential technological applications.¹⁻⁴ Thin films of block copolymers have attracted increasing interest in the recent past, particularly in view of possible applications in the area of nanotechnology.⁵⁻⁹ Although much of the current work has concentrated on block copolymers consisting of *two* components, the insertion of a third block widely enlarges the structural diversity and allows incorporation of additional chemical functionality.^{10,11} Here we describe a highly ordered hexagonally perforated lamella structure based on a ternary ABC triblock copolymer thin film. By suitable choice of the three blocks a versatile structure is formed: The perforated lamella can serve as a lithographic mask, it can be chemically converted into an amphiphilic structure without losing its order, and after selective removal of one of its constituents it could be used as a responsive membrane. Intriguingly, the particular choice of the blocks ensures that the structure is formed irrespective of the chemical nature of the solid substrate. The experimental results are supported by mesoscale computer simulations.

Most of the studies on block copolymer thin films have focused on binary systems, i.e. on block copolymers composed of two different materials *A* and *B*. For nanolithographic applications, both spherical and cylindrical mesostructures have been used. In the latter case, the cylinders tend to orient parallel to the boundary surfaces and quite some effort has been taken to overcome this tendency and stabilize a perpendicular orientation, which is desired for many applications.^{12,13} The cores of perpendicular cylinders can be removed by selective degradation of the core material thereby leaving a high aspect ratio mask for further etching, material deposition, etc.^{6,14}

If three, instead of two, different polymeric components are linked together to what is then referred to as an ABC triblock copolymer, the structural variety is significantly increased.¹⁰ Although potentially more versatile than binary block copolymers due to the increased chemical complexity, these materials have been much less studied in the context of the nanotechnology applications mentioned above.

Here, we describe the thin film self-assembly of a linear polystyrene-*block*-poly(2-vinylpyridine)-*block*-poly(*tert*-butyl methacrylate) (PS-P2VP-PtBMA) triblock copolymer. The polymer has been synthesised via anionic polymerization following standard procedures.¹⁵ The overall molecular weight of the polymer is $M_w = 140$ kDa, the polydispersity amounts to $M_w/M_n = 1.02$ and the volume fractions of the three blocks are 16%, 21%, and 63% for the PS, P2VP, and PtBMA blocks, respectively. In the bulk, the material exhibits a structure of hexagonally packed cylinders embedded within the PtBMA matrix material.¹⁶ The experimental data are compatible with the notion of a core-shell structure, where the minority PS block forms a cylindrical core surrounded by a P2VP shell. Thin films of this material were prepared on various substrates (native oxide covered silicon wafers, carbon coated silicon wafers, NaCl surfaces) by spin-coating from chloroform solution. To further induce mobility and facilitate equilibration, the samples were annealed in a well-controlled atmosphere of chloroform vapor. After drying, the thin film microdomain structure was investigated by field-emission scanning electron microscopy (FE-SEM), transmission electron microscopy (TEM), and scanning force microscopy (SFM), respectively. For TEM investigations, films were prepared on NaCl substrates, which were subsequently dissolved in water. The freely floating films were picked up onto a TEM grid for further investigation.

Figures 1(a) and (b) show FE-SEM images of a PS-P2VP-PtBMA film (thickness: 37 ± 3 nm) after storage in chloroform atmosphere and subsequent drying. The images are characterised by a hexagonal arrangement of dark dots with a characteristic nearest neighbour distance of some (70 ± 5) nm. The large scale image shown in Figure 1(b) shows that this structure is formed with only a limited number of defects over an area of about $12 \times 4 \mu\text{m}^2$. This impressive degree of order is also reflected in the Fourier transform Fig. 1(c).

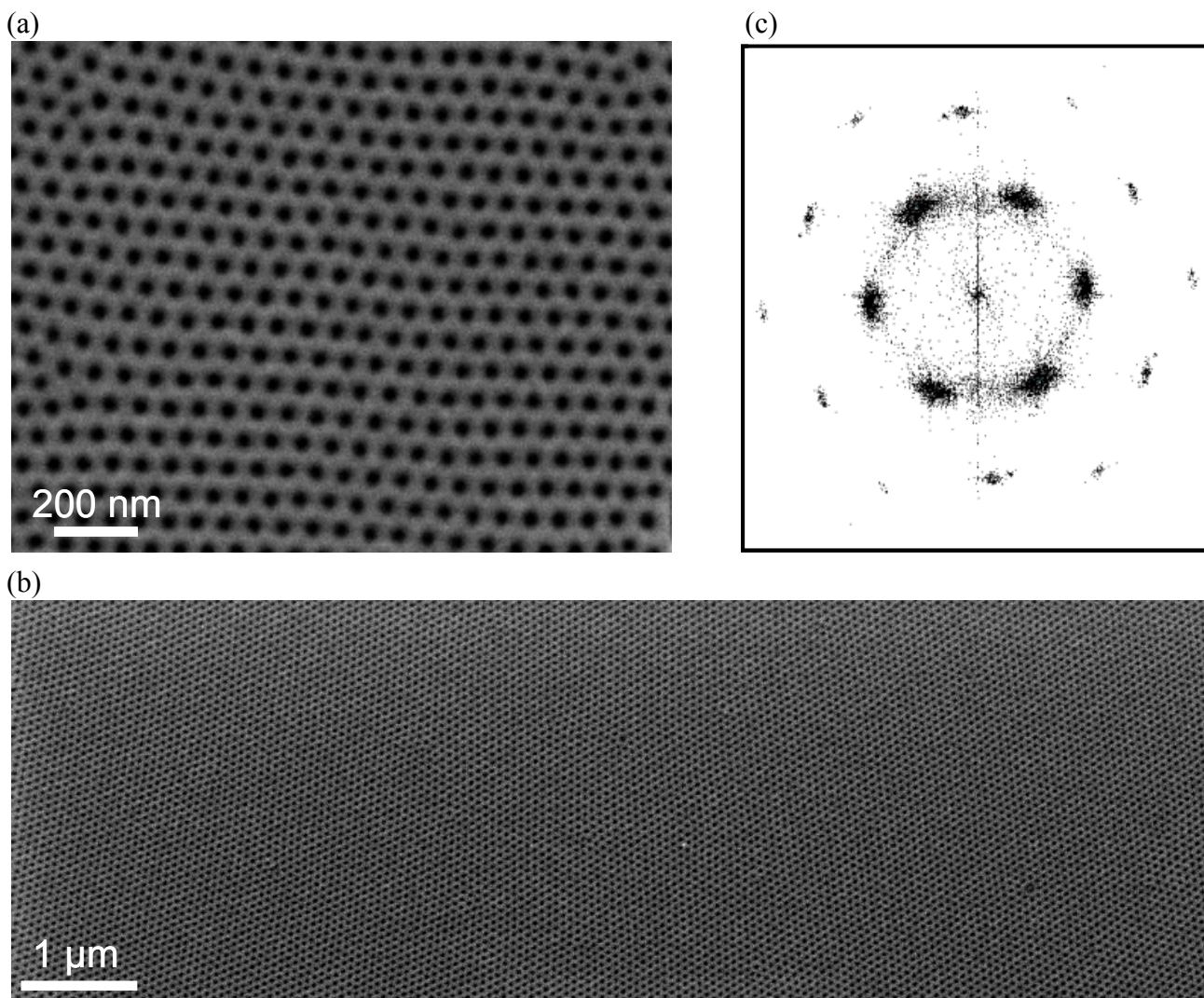


Figure 1. Highly ordered microstructure of a block copolymer. (a), (b): FE-SEM images of a 37 nm thick PS-P2VP-PtBMA film after solvent vapor treatment (partial pressure p_{CHCl_3} was reduced from $0.94 p_{\text{sat}}$ to below $0.3 p_{\text{sat}}$ within 100 h) and subsequent drying. (c): Fourier transform of an FE-SEM image of size $5 \times 5 \mu\text{m}^2$.

To establish the microdomain structure responsible for the hexagonal array of dots observed in the FE-SEM images, the samples were investigated by nanotomography¹⁷ (not shown here). In short, the sample was eroded in an oxygen plasma and AFM images were taken after each erosion step. The results of these experiments are consistent with a perforated lamella (PL) structure within the thin film. This structure can be visualized as a P2VP/PS/P2VP sheet perforated by PtBMA channels, which connect between two outer PtBMA layers (see Figure 2(e) for a sketch of the structure). Further experimental evidence for this model is given in Figure 2(a) and 2(b), where we show two AFM images of a thin PS-P2VP-PtBMA film prior to and after selective removal of the PtBMA matrix phase by UV irradiation (UV-B, 150 W, 60 min), respectively. This treatment is known to preferentially remove the acrylate phase. Indeed, on UV irradiation the originally rather flat surface develops a highly ordered hexagonal array of holes, as the PtBMA is removed from the perforations in the P2VP/PS/P2VP layer.

The latter finding indicates potential use of the PL structure for lithographic applications similar to the case of perpendicularly oriented poly(methyl methacrylate) (PMMA) cylinders in PS-PMMA block copolymer thin films.^{6,14} However, while the perforated layer remaining after PtBMA removal consists of the PS core, its surface is covered by a layer of P2VP, which can easily be modified chemically. In particular, quaternization of P2VP will lead to a water soluble coverage of the PS core, thereby circumventing well-known wettability problems, occurring when the holes in the polymer structure are to be filled in a subsequent electrochemical processing step.^{8,14} Moreover, the thickness of the quaternized layer will depend on the pH of the surrounding medium suggesting that the resulting structure could be of use as a (pH-) responsive membrane. We note that the limited aspect ratio of the PL structure may be a disadvantage in lithographic applications. It is, however, desirable in membrane applications, where a high density of well-defined nanoscopic holes within a ≈ 50 nm thick sheet are needed for optimal permeability. Since free standing films are needed for membrane applications the mechanical stability of the latter will be a crucial issue. We have therefore studied thin films prepared on polished NaCl substrates. After preparation, the substrates are dissolved in water and the free standing block copolymer films are picked up onto TEM grids. Figure 2(c) shows a TEM image taken from such a film, clearly showing that both the quality of the nanostructure is preserved and that the mechanical stability is sufficient to handle free standing films, which contain a single layer of perforated lamella.

Alternative to PtBMA removal by UV radiation, the matrix phase can be converted into poly(methacrylic acid) (PMAA) by hydrolysis in HCl. Figure 2(d) shows an AFM image of a copolymer film, which was prepared on a polished silicon wafer as described above and subsequently exposed to an atmosphere of HCl and water vapor ($\text{HCl}_{\text{conc.}}$ at 60 °C) for hydrolysis. SEM images (not shown here) indicate that the overall nanostructure is not affected by this treatment. If the film surface is imaged in water, we observe however a hexagonal array of protrusions (height: some 15 nm). Since PMAA swells considerably in water, the protrusions will form on top of the perforations of the P2VP/PS/P2VP lamella, where more PMAA material is present. It is interesting to note that the mechanical stability of the PS core is large enough to withstand the forces exerted on the majority PMAA blocks during swelling in water. Again, the height of the protrusions is expected to vary with the pH resulting in a responsive nanostructure.

The PL phase is generally believed not to be a bulk equilibrium phase in binary block copolymer systems.¹⁸ However, recent experimental and simulation results on binary systems¹⁹ show that the PL phase can be stabilized by surface interactions in thin films of cylinder forming block copolymers. If both boundary surfaces prefer the majority phase, cylinders tend to orient parallel to the boundary surfaces. In case of strong enough preference, the bulk of the thin film may be

sufficiently depleted of the majority component and the cylindrical cores of the minority phase may connect to a perforated sheet.²⁰ For the ternary copolymer studied here, the bulk equilibrium structure is also a hexagonally packed cylindrical structure. The PtBMA majority phase has indeed the lowest surface energy and therefore is attracted to the free surface of the film. If the substrate attracted the PtBMA majority phase as well, one would expect the stabilization of a perforated lamella similar to the binary cylindrical systems mentioned above.¹⁹ In case of a polar substrate like SiO_x , on the other hand, strong physisorption of the polar P2VP middle block is expected.²¹ Due to the particular stoichiometry of the block copolymer, however, such a physisorbed layer will exhibit a PtBMA-rich surface. In consequence, a perforated lamella would again be stabilized between two surfaces both preferentially attracting the PtBMA majority phase. It is a particularly intriguing property of the material under study that the perforated lamella phase is stabilized irrespective of the chemical nature of the substrate, as any polar substrate will self-adjust its surface energy by firm physisorption of a thin block copolymer layer terminated by PtBMA as soon as the surface is brought into contact with the copolymer solution, i.e. prior to film formation. This notion is in line with our experiments. Three different substrate materials have been used (SiO_x : Figs. 1 and 2 (a),(b); NaCl: Fig. 2(c); carbon-coated silicon wafer: not shown here) and in all cases the PL phase was formed. Moreover, experiments with varying film thickness (not shown here) clearly show the existence of an adsorbed layer underneath the perforated lamella.

In addition, the concept of a self-adjusting surface energy of the substrate was visualized by dynamic density functional theory (DDFT) simulations using the MesoDyn code.²²⁻²⁴ The polymer was modeled as an $\text{A}_3\text{B}_4\text{C}_{12}$ triblock copolymer confined between symmetric walls attracting the C-block (see Caption to Figure 2 for details on the simulation). Figure 2(e) shows a result of such a simulation. The core/shell perforated lamella is clearly seen in the center of the film, which is terminated by continuous C-layers (transparent) at both boundary surfaces. For comparison, in Figure 2(f) we show the results of a MesoDyn simulation with all parameters kept the same as in Figure 2(e), except that the bottom boundary now attracts the B middle block and the film thickness is 5 grid points thicker. As a result, a thin B wetting layer is formed at the bottom boundary (red), which terminates with a C-rich layer (transparent), on which again the perforated lamella structure is formed. Indeed, the perforated lamella is formed irrespective of the preference of the substrate. This property establishes a major advantage over other systems, where quite some experimental effort is needed to adjust the substrate surface energy in order to achieve the desired orientation of the nanostructure.¹²

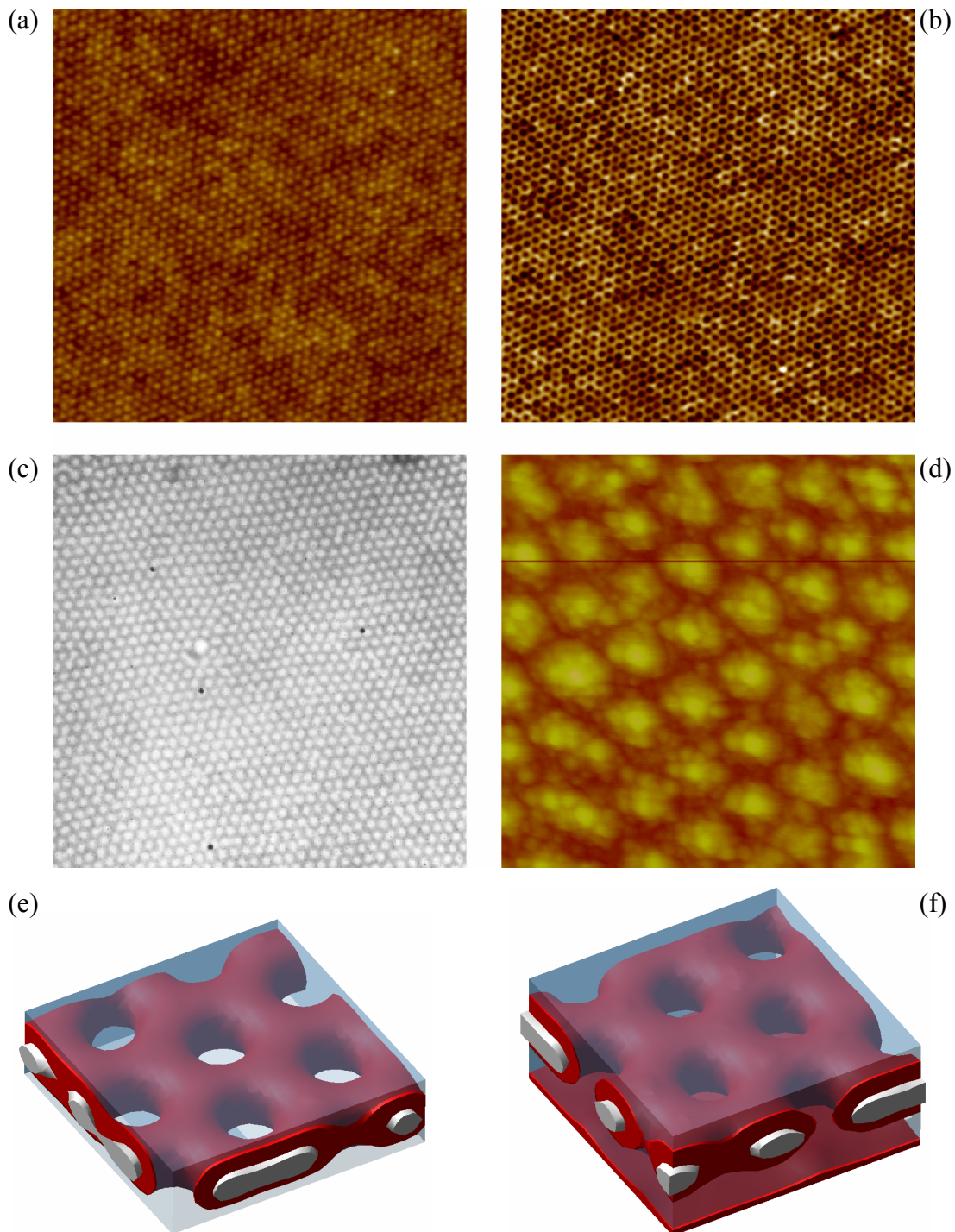


Figure 2. Exploring the microstructure of block copolymer films. (a), (b): Tapping Mode SFM topography images of the block copolymer film (a) prior to and (b) after exposure to UV radiation ($3 \times 3 \mu\text{m}^2$, same film as in Fig. 1). (c): TEM image of a block copolymer film prepared on a polished NaCl substrate, floated onto $\text{H}_2\text{O}_{\text{bidest}}$, and picked up onto a TEM grid ($2 \times 2 \mu\text{m}^2$; preparation: $p_{\text{CHCl}_3} = 0.9 p_{\text{sat}}$, $t = 15$ hrs). (d): Tapping Mode SFM image of a block copolymer film after hydrolysis of the PtBMA blocks into PMAA. The image was taken in H_2O using the liquid cell of the Multimode SFM ($0,5 \times 0,5 \mu\text{m}^2$). (e), (f): Results of MesoDyn simulations assuming symmetric (e) and asymmetric (f) boundary conditions. The block copolymer was modelled by an $A_3B_4C_{12}$ Gaussian chain with interaction parameters $\varepsilon_{AB} = 7.0$, $\varepsilon_{AC} = 8.0$, $\varepsilon_{BC} = 6.0$ (all in kJ/mol). The film interfaces were treated as hard walls with interaction parameters $\varepsilon_{AM,1} = 8.0$ (4.0 in (f)), $\varepsilon_{BM,1} = 6.0$ (6.0), $\varepsilon_{CM,1} = 0$ (-2.0), $\varepsilon_{AM,2} = 8.0$ (6.0), $\varepsilon_{BM,2} = 6.0$ (-8.0) and $\varepsilon_{CM,2} = 0$ (4.0) ($M,1$ indicates free surface, $M,2$ indicates substrate). The size of the simulation box is $32 \times 32 \times (H + 2)$ with walls at $z = 0$ and $H + 1$. The film thickness $H = 9$ and 14 grid points in (e) and (f), respectively. All other parameters are as reported elsewhere¹⁹.

We finally turn to the rather high degree of order formed spontaneously in the PS-P2VP-PtBMA perforated lamella structure. No particular measures (as, e.g. topographic patterning of the substrate surface²⁵) have been undertaken to improve the order. It is known that suitable solvent treatment can indeed improve the order of a block copolymer mesostructure.²⁶ It is interesting to note, though, that whenever our PS-P2VP-PtBMA films do *not* show the PL structure (e.g. due to different thickness) they do not exhibit the same degree of long range order. We are therefore led to assume that the bicontinuous nature of the PL phase is essential for the long range order to occur in this system. Indeed, since the PL phase is continuous in all three components, chain diffusion within the film should be highly facilitated. In consequence, defect removal via diffusion should be considerably enhanced as compared to other, non-continuous microdomain structures. We note that this finding is in agreement with our own results on other block copolymer systems as well as with earlier results by others (see: Wiesner, U. personal communication, 2002).

Acknowledgements

We thank the *Deutsche Forschungsgemeinschaft* for financial support (SFB 481), and A. Knoll, G. J. A. Sevink, C. Abetz and M. Hund for help. A modified version of the MesoDyn Code for asymmetric boundary conditions was kindly provided by G. J. A. Sevink and A. V. Zvelindovsky. A. V. acknowledges financial support through the Humboldt Foundation and R. M. acknowledges financial support through the VolkswagenStiftung.

Correspondence and requests should be addressed to G. K.

References

- (1) Bates, F. S. & Fredrickson, G. H. Block copolymer thermodynamics: theory and experiment *Ann. Rev. Phys. Chem.* **41**, 525-57 (1990).
- (2) Klok, H. A. & Lecommandoux, S. Supramolecular materials via block copolymer self-assembly *Adv. Mater.* **13**, 1217-1229 (2001).
- (3) Adrington, A. C. *et al.* Polymer-based photonic crystals *Adv. Mater.* **13**, 421-425 (2001).
- (4) Bockstaller, M., Kolb, R. & Thomas, E. L. Metallodielectric photonic crystals based on diblock copolymers *Adv. Mater.* **13**, 1783-1786 (2001).
- (5) Mansky, P., Chaikin, P. & Thomas, E. L., Monolayer films of diblock copolymer microdomains for nanolithographic applications *J. Mater. Sci.* **30**, 1987-1992 (1995).
- (6) Park, M. *et al.* Block copolymer lithography: Periodic arrays of similar to 10(11) holes in 1 square centimeter *Science* **276**, 1401-1404 (1997).
- (7) Cheng, J. Y. *et al.* Formation of a cobalt magnetic dot array via block copolymer lithography *Adv. Mater.* **13**, 1174-1178 (2001).
- (8) Jeoung, E. *et al.* Fabrication and characterization of nanoelectrode arrays formed via block copolymer self-assembly *Langmuir* **17**, 6396-6398 (2001).
- (9) Kim, H.-C. *et al.* A route to nanoscopic SiO₂ posts via block copolymer templates *Adv. Mater.* **13**, 795-797 (2001).
- (10) Bates, F. S. and Frederickson, G. H. Block copolymers: designer soft materials *Phys. Today* **52**, 32-38 (1999).
- (11) Krausch, G. & Magerle, R. Nanostructured thin films via self-assembly of block copolymers *Adv. Mater.* **14**, 1579-1583 (2002).
- (12) Mansky, P. *et al.* Controlling polymer-surface interactions with random copolymer brushes *Science* **275**, 1458-1460 (1997).
- (13) Thurn-Albrecht, T. *et al.*, Overcoming interfacial interactions with electric fields *Macromolecules* **33**, 3250-3253 (2000).
- (14) Thurn-Albrecht, T. *et al.* Ultrahigh-density nanowire arrays grown in self-assembled diblock copolymer templates *Science* **290**, 2126-2129 (2000).
- (15) Giebeler, E. & Stadler, R. ABC triblock polyampholytes containing a neutral hydrophobic block, a polyacid and a polybase *Macromol. Chem. Phys.* **198**, 3815-3825 (1997).
- (16) Ludwigs, S. *et al.* Phase behavior of linear polystyrene-*block*-poly(2-vinylpyridine)-*block*-poly(*tert*-butyl methacrylate) triblock terpolymers *Polymer* **44**, 6815-6823 (2003).
- (17) Magerle, R. Nanotomography *Phys. Rev. Lett.* **85**, 2749-2752 (2000).

- (18) Hajduk, D. A. *et al.* Stability of the perforated layer (PL) phase in diblock copolymer melts *Macromolecules* **30**, 3788-3795 (1997).
- (19) Knoll, A. *et al.* Phase behavior in thin films of cylinder-forming block copolymers *Phys. Rev. Lett.* **89**, 035501 (2002).
- (20) Huinink, H. P. *et al.* Asymmetric block copolymers confined in a thin film *J. Chem. Phys.* **112**, 2452-2462 (2000).
- (21) Tassin, J. F. *et al.* Kinetics of adsorption of block copolymers revealed by surface plasmons *J. Phys. Chem.* **93**, 2106-2111 (1989).
- (22) Fraaije, J. G. E. M. Dynamic density functional theory for microphase separation kinetics of block copolymer melts *J. Chem. Phys.* **99**, 9202-9212 (1993).
- (23) Fraaije, J. G. E. M. *et al.* The dynamic mean-field density functional method and its application to the mesoscopic dynamics of quenched block copolymer *J. Chem. Phys.* **106**, 4260-4269 (1997).
- (24) Sevink, G. J. A. *et al.* Dynamics of surface directed mesophase formation in block copolymer melts *J. Chem. Phys.*, **110**, 2250-2256 (1999).
- (25) Segalman, R. A., Yokoyama, H. & Kramer, E. J. Graphoepitaxy of spherical domain block copolymer films. *Adv. Mater.* **13**, 1152-1155 (2001).
- (26) Kim, G. & Libera, M. Morphological development in solvent-cast polystyrene-polybutadiene-polystyrene (SBS) triblock copolymer thin films. *Macromolecules* **31**, 2569-2577 (1998).

3.4. pH-dependent nanostructures in thin films

S. Ludwigs*, K. Schmidt, and G. Krausch

Physikalische Chemie II, Universität Bayreuth, D-95440 Bayreuth, Germany

Corresponding author: sabine.ludwigs@uni-bayreuth.de

Tel: 0921-552756, Fax: 0921-552059.

To be submitted to *Macromolecules*

Abstract

We present a novel route to prepare pH-dependent nanostructures from highly ordered thin film microdomain structures of poly(styrene)-*block*-poly(2-vinylpyridine)-*block*-poly(*tert*-butyl methacrylate) triblock terpolymers (SVT). Using a polymer-analogous reaction we modify the chemical nature of the block components without altering the overall structure. In particular, we perform an acid-catalyzed hydrolysis of the poly(*tert*-butyl methacrylate) block to poly(methacrylic acid) in a microphase separated perforated lamella (PL) structure. Scanning force microscopy in aqueous environment is used to follow structural changes of the PL phase as function of the pH-value.

Introduction

Thin films of incompatible block copolymers self-assemble into highly ordered surface patterns with characteristic length scales in the range between 5 and 100 nm.^{1,2,3} While block copolymers usually show a random distribution of microdomain orientations in bulk and solution, large-scale alignment and stabilization of non-bulk structures can be induced in thin films. In thin films, additional driving forces for structure formation exist: The microdomain structures have to adjust to two boundary surfaces and a certain film thickness which is comparable to the characteristic bulk domain spacing. Only recently a variety of different novel surface structures was found.⁴

A well-defined patterning in thin films can for example be used to prepare smart molecules to serve as functional devices on a nm scale. Stimuli-responsive, smart or intelligent polymer systems are materials which can react to slight changes in the environmental variables such as pH, temperature, and ionic strength with swelling. Charged macromolecules which change their conformation as a function of the pH-value are well-known in nature: DNA is a polyelectrolyte chain containing negatively charged groups, while proteins and poly(amino acids) are polyampholyte polymers which carry both positive and negative charges. The swelling behavior of synthetic homopolyelectrolytes, especially of polyacids containing carboxyl groups has been intensively investigated in the last decades.^{5,6,7,8,9,10,11} While at low degrees of ionization a compact coiled conformation of the macromolecules is favored, with increasing charge density long-range interactions resulting from electric charges located at the macromolecular chains overcome the attractive forces and induce a conformational change to the expanded state. Synthetic polyelectrolytes can be used as model systems as well as in sewage treatment, flocculation, powder coating design, and paper production,^{12,13,14,15,16,17} synthetic polyampholytes can be used for example as drug delivery systems.¹⁸

Numerous groups have focused on the solution behavior of amphiphilic block copolymers, which contain at least one polyelectrolyte block.^{19,20,21,22,23,24,25} Usually, precursor polymers are synthesized, e.g. with anionic polymerization, which are subsequently chemically modified via polymer-analogous reactions to polyacids or polybases. In most cases the amphiphilic block copolymer molecules self-associate into micelles that consist of a core formed by an insoluble hydrophobic block and a shell of water-soluble blocks.^{26,27} A review about block copolymer micelles has been recently published by Hamley.²⁸

Interesting microdomain structures, as formed in non-hydrolyzed systems both in bulk and in thin films via self-assembly, can usually not be obtained by amphiphilic block copolymers because of strongly different solubility of the block components. In order to avoid micelle formation, we use

self-assembly of a precursor triblock terpolymer to prepare defined microdomain structures in thin films and subsequently perform a polymer-analogous reaction which modifies the chemical nature of the block terpolymer, but does not effect the overall structure.

Polymer-analogous reactions on preformed /prestructured thin films provide a facile pathway to well-defined structures in films of polyelectrolytes. Langmuir Blodgett films of cellulose^{29,30,31} and PMAA^{32,33} have recently been regenerated under acidic hydrolysis conditions. Liu *et al.* have prepared thin films with nanochannels from a blend of triblock terpolymers consisting of polyisoprene, poly(2-cinnamoyl ethyl methacrylate) and poly(*tert*-butyl acrylate) mixed with small amounts of poly(*tert*-butyl acrylate).³⁴ Via extracting the homopolymer from the films and hydrolysing the poly(*tert*-butyl acrylate) block to poly(acrylic acid) after structure formation, they obtained membranes that showed to be gas, but not liquid permeable.

Recently we have presented a rather versatile structure in thin films: a perforated lamella which is formed in thin films of a cylinder-forming poly(styrene)-*block*-poly(2-vinylpyridine)-*block*-poly(*tert*-butyl methacrylate) triblock terpolymer.^{35,36} Both the bulk and the solution behavior of the hydrolyzed polymers was studied by Giebeler *et al.*^{37,38}

By exposing the perforated lamella structure to a vapor atmosphere of hydrochloric acid, poly(*tert*-butyl methacrylate) is converted to poly(methacrylic acid) without altering the overall structure. Using scanning force microscopy in aqueous solutions we investigate the morphology and the degree of swelling as function of the pH-value.

Experimental Section

Thin films of PS-*b*-P2VP-*b*-PtBMA triblock terpolymers

Poly(styrene)-*block*-poly(2-vinylpyridine)-*block*-poly(*tert*-butyl methacrylate) triblock terpolymers were synthesized and characterized as reported previously.³⁹ In this contribution we focus on a polymer which shows a core-shell cylindrical structure in bulk. The overall molecular weight is $M_w = 140$ kDa, the polydispersity amounts to $M_w/M_n = 1.02$ and the volume fractions are $\phi_{PS} = 0.16$, $\phi_{P2VP} = 0.21$, and $\phi_{PtBMA} = 0.63$.

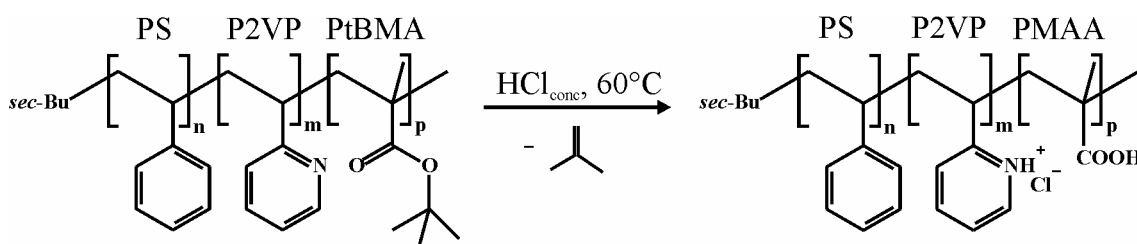
Thin films of this material were prepared on polished silicon wafers by spincoating from 5 mg/ml chloroform solutions. To further induce mobility and to facilitate equilibration the samples were annealed in a well-controlled atmosphere of chloroform vapor for 20 h ($p_{CHCl_3} = 0.9 p_0$, with p_0 being the vapor pressure of saturated chloroform). During annealing terraces of well-defined film thickness are formed which correspond to energetically preferred microdomain structures. The

resulting microdomain structures were quenched via fast solvent removal. Terraces with a film thickness of (37 ± 3) nm display a highly ordered perforated lamella structure. A systematic investigation of the thin film behavior of PS-*b*-P2VP-*b*-PtBMA triblock terpolymers has been recently performed.³⁶

Acid-catalyzed hydrolysis of prestructured films

Acid-catalyzed hydrolysis of PS-*b*-P2VP-*b*-PtBMA was accomplished by heating the prestructured films together with a reservoir of approximately 3 ml of HCl_{conc} for 12-15 h at a temperature of 60°C. The films were subsequently dried in vacuum. The reaction yields the corresponding SVA triblock copolymer with a poly(methacrylic acid) (PMAA) polyelectrolyte block without altering the thin film structure. The driving force of this reaction is the elimination of gaseous isobutylene. Besides hydrolyzing the PtBMA the reaction also yields the hydrochloride of the amine functionality of poly(2-vinylpyridine) (Scheme 1).

A similar post-transfer approach has been recently shown for Langmuir-Blodgett films of PtBMA and poly(*tert*-butyl acrylate) with a hydrolysis to PMAA and poly(acrylic acid), respectively. The elimination of gaseous isobutylene did not destroy their layered structures.^{32,33}



Scheme 1. Acid-catalyzed hydrolysis of PS-*b*-P2VP-*b*-PtBMA to PS-*b*-P2VP-H⁺-*b*-PMAA.

Characterization of hydrolyzed films of PS-*b*-P2VP-H⁺-*b*-PMAA triblock terpolymers

The degree of conversion can be determined by FTIR spectroscopy. For a quantitative IR analysis the amount of material in the thin films was not sufficient. We therefore prepared thicker films and transferred the results to the thinner films. Only for this purpose, homogeneous films with a thickness between 1 and 5 μm were cast onto silicon wafers with a blade technique and subsequently hydrolyzed in the manner described above (without annealing in chloroform vapor). IR spectra of unhydrolyzed and hydrolyzed films have been directly taken on the silicon substrate, as Si does not show absorption in the region of interest ($1000 - 4000 \text{ cm}^{-1}$), Figure 1.

Between 3500 cm^{-1} and 2400 cm^{-1} the typical broad bands of the O-H valence vibration are obtained. The C=O absorption band at 1724 cm^{-1} is broadened and shifted to 1718 cm^{-1} . Hydrolysis also leads to a shift of C-O valence vibrations from 1254 cm^{-1} and 1138 cm^{-1} to 1248 cm^{-1} and 1162

cm^{-1} , respectively. Due to the acidic conditions during the preparation the pyridinium groups are protonated as can be seen by the N-H absorption band at 2560 cm^{-1} and the absorption bands of the aromatic vibrations which are shifted from 1589 cm^{-1} and 1568 cm^{-1} to 1616 cm^{-1} and 1541 cm^{-1} , respectively. In addition, new bands appear at 994 cm^{-1} , 952 cm^{-1} and 618 cm^{-1} . The disappearance of the *tert*-butyl double absorption band at 1394 cm^{-1} and 1368 cm^{-1} is most characteristic and can be used for a quantitative analysis.

The degree of hydrolysis has been determined to approximately 91%. We assume that the degree of hydrolysis is higher in the thinner films as less material needs to be hydrolyzed.

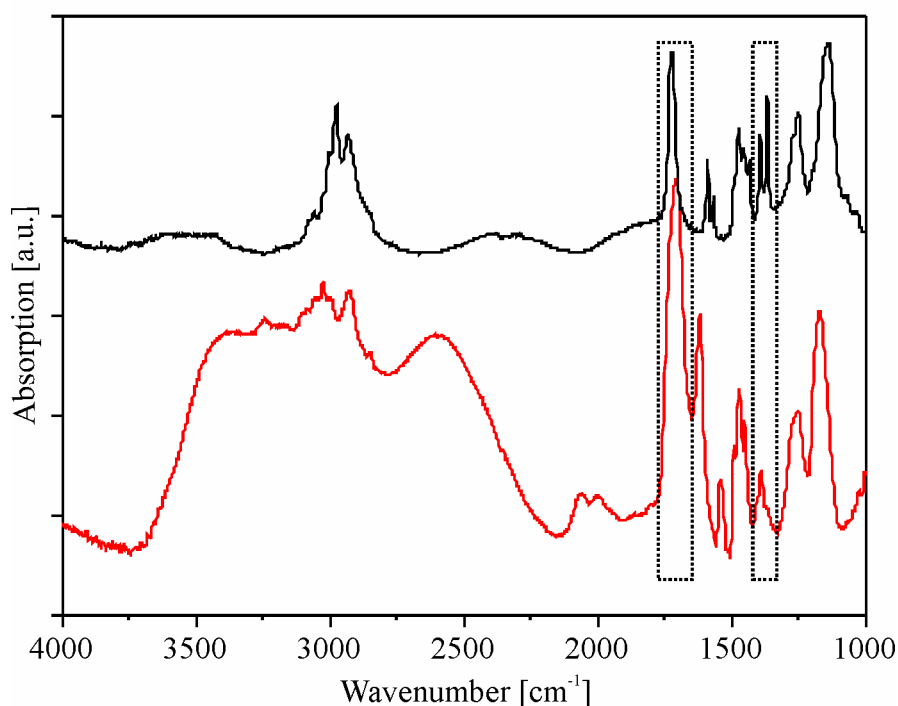


Figure 1. Hydrolysis of a $3 \mu\text{m}$ film of $\text{PS-}b\text{-P2VP-}b\text{-PtBMA}$ to $\text{PS-}b\text{-P2VP-}b\text{-PMAA}$. FTIR spectra before (black curve) and after hydrolysis (red curve).

Scanning force microscopy in aqueous environment

Thin films of $\text{PS-}b\text{-P2VP-}b\text{-PMAA}$ on silicon wafers were investigated in the fluid cell of a Multi Mode scanning force microscope (from Digital Instruments, Veeco Group). We used contact-mode tips (Veeco NP-S tips consisting of silicon nitride, spring constant $k = 0,58 \text{ N/m}$). All experiments were performed in the tapping mode (resonance frequency $\omega \approx 10 \text{ kHz}$). The water was filled into the liquid cell with a micropipette.

For the pH-dependent measurements we exchanged the water in the chamber with buffer systems. To avoid effects due to different counterions and ionic strengths⁴⁰ we have chosen sodium-phosphate buffers ($\text{H}_3\text{PO}_4 / \text{NaH}_2\text{PO}_4 / \text{Na}_2\text{HPO}_4 / \text{Na}_3\text{PO}_4$) which allow tuning the pH in the range

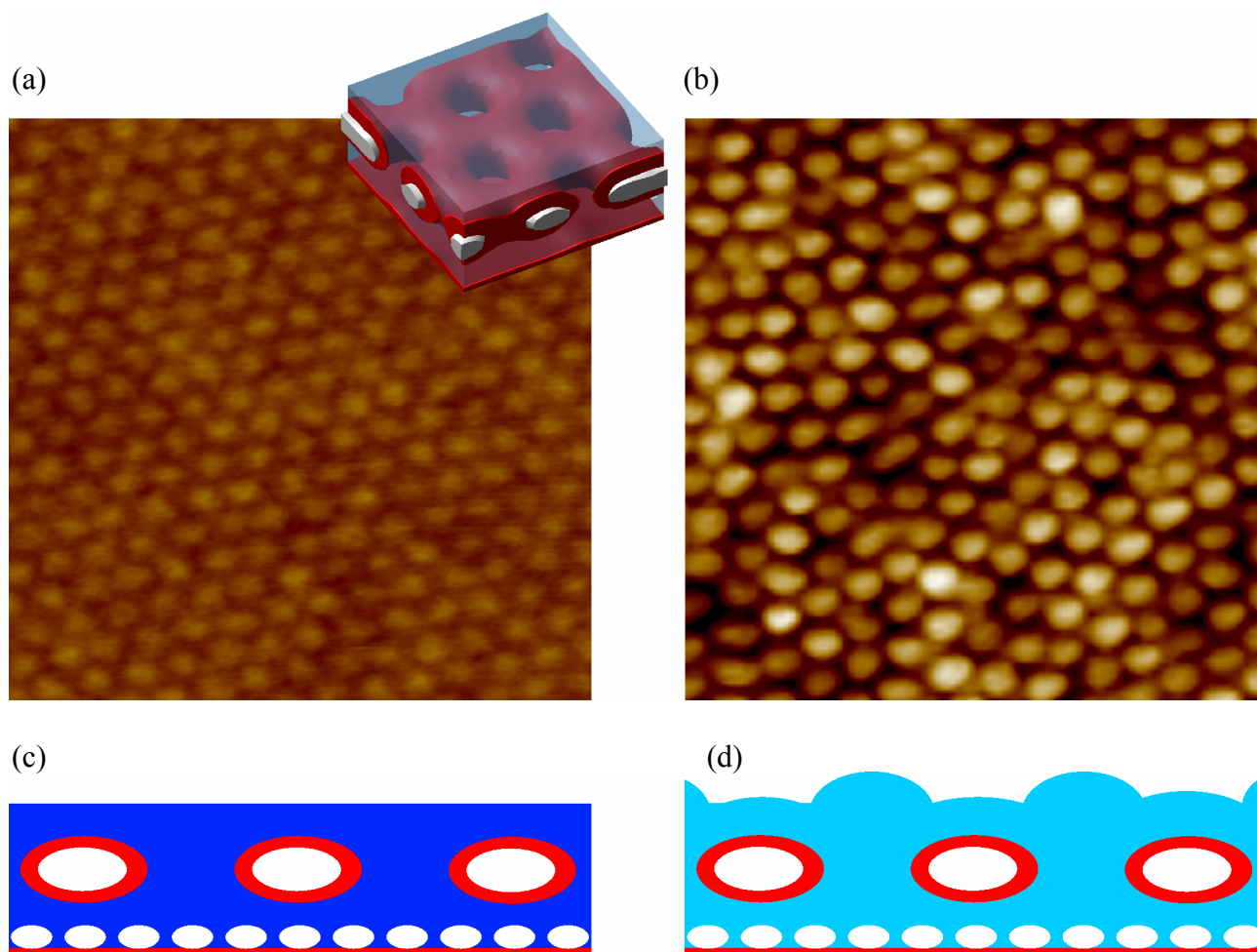
from 2 to 10.

For film thickness measurements scratches with a needle were made onto the sample after hydrolysis. The thickness of the film was determined relative to the substrate.

3.4.1. Results and discussion

Morphology after hydrolysis

Figures 2(a) and (b) show SFM images of a terpolymer film before and after acid-catalyzed hydrolysis. The unhydrolyzed film shows a rather smooth surface topology with a hexagonal pattern of bright dots, which are assigned to perforated lamellae (PL). The height difference between protrusions and valleys amounts to 2 nm. The inset in Figure 2(a) shows the sketch of a PL phase: Sheets of P2VP/PS/P2VP are perforated by channels of the majority component PtBMA which are connected between two outer layers of PtBMA, one of which is located at the air surface. Further details about the PL phase are provided in reference (35) and (36).



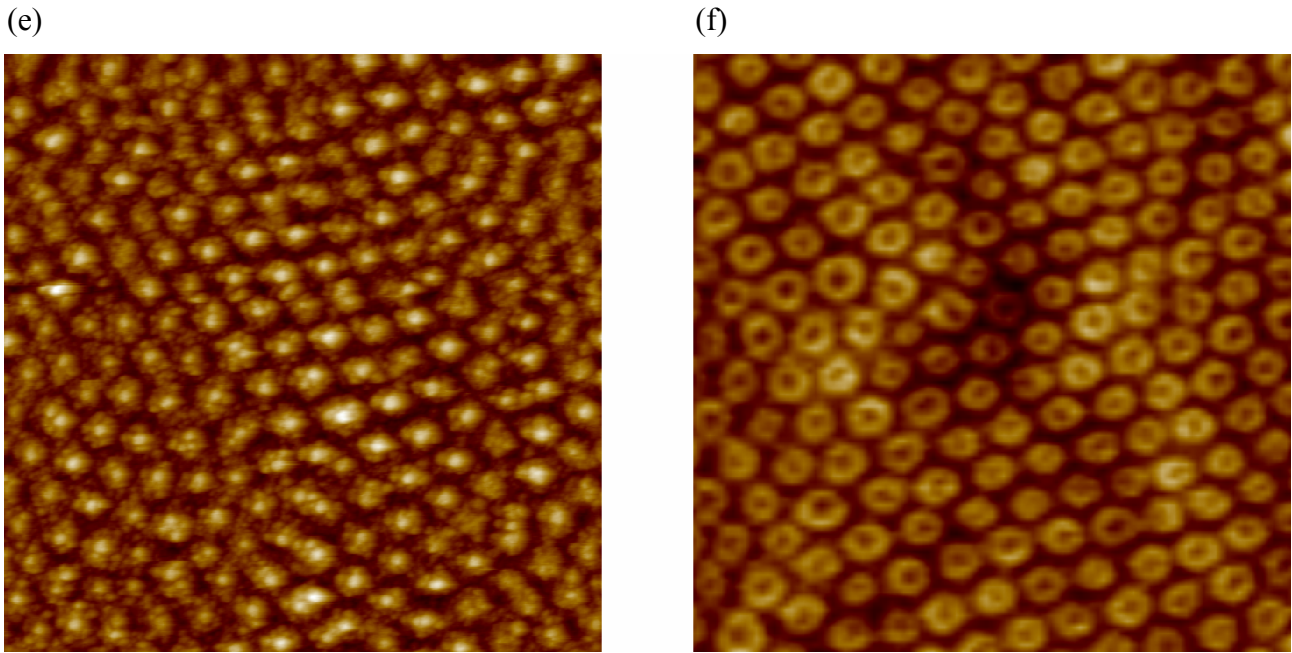


Figure 2. SFM images of the perforated lamella structure (PL) before (a) and after hydrolysis (b). The sketch in (a) corresponds to a MesoDyn simulation^{35,41} of the first terrace of PL; the phases can be assigned to PS (white phase), P2VP (red phase) and PtBMA (blue phase). (c) and (d): Schematic cross-sections of a PL phase before and after hydrolysis. (e) and (f): SFM images of the PL structure after hydrolysis, taken in aqueous solutions. The image size of the SFM images is $1 \times 1 \mu\text{m}^2$. The height scale for (a) and (b) is $\Delta z = 0\text{-}10 \text{ nm}$ and for (e) and (f) $\Delta z = 0\text{-}30 \text{ nm}$.

After hydrolysis a hexagonal arrangement of protrusions is clearly visible with the height difference between protrusions and valleys amounting to $\sim 15 \text{ nm}$. The overall structure is not affected by the HCl treatment. During hydrolysis the P2VP block is protonated and the majority component PtBMA is modified to PMAA. Since PMAA is rather hygroscopic, the film swells even at ambient conditions. Figure 2(c) and (d) represent the corresponding sketches of the microdomain structure before and after hydrolysis. The protrusions of the acid component form on top of the perforations of the P2VP/PS/P2VP lamella, where more PMAA material is present. These results are consistent with our previous observations of the PL phase: Selective removal of the PtBMA component with UV-light or oxygen plasma exhibits holes at the same places, where we find protrusions after hydrolysis.³⁵ Film thickness measurements reveal an overall shrinkage of the film thickness after acid saponification. Before any treatment the thickness of the first terrace of PL amounts to $d_{SVT} \sim (37 \pm 2) \text{ nm}$, after hydrolysis the film thickness is about $d_{SVA} \sim (26 \pm 2) \text{ nm}$. As the films swell due to the water content in the air, the theoretical film thickness of a SVA film should be even smaller and can be determined with the following equation:

$$d_{SVA}^{calc} = \frac{d_{SVT} \cdot \rho_{PtBMA} \cdot M_{PMAA}}{\rho_{PMAA} \cdot M_{PtBMA}} \cdot \frac{1}{U} \quad (1)$$

where d_{SVA}^{calc} is the theoretical film thickness after hydrolysis; d_{SVT} the film thickness of an unhydrolyzed film, d_{SVA} the film thickness of a hydrolyzed film in the dry state, d_{SVA}^{aqua} the film thickness of a hydrolyzed film in an aqueous medium, and U the degree of hydrolysis. The densities of PtBMA and PMAA amount to $\rho_{PtBMA} = 1.022 \text{ g/cm}^3$ and $\rho_{PMAA} = 1.170 \text{ g/cm}^3$, respectively. The molecular weights of these polymers are $M_{PtBMA} = 142 \text{ g/mol}$ and $M_{PMAA} = 86 \text{ g/mol}$, respectively.

With a degree of hydrolysis of $U \sim 98\%$, the theoretical film thickness amounts to $d_{SVA}^{calc} = (20 \pm 2)$ nm. The degree of swelling can therefore be determined to $d_{SVA} / d_{SVA}^{calc} = 1.4$ for films measured at ambient conditions.

We observe higher film thicknesses when investigating the surface structure with scanning force microscopy in the aqueous phase. Typical values of in water swollen SVA are $d_{SVA}^{aqua} (43 \pm 3)$ nm. The degree of swelling relative to the theoretical film thickness then amounts to $d_{SVA}^{aqua} / d_{SVA}^{calc} = 2.1$ and relative to the measured film thickness in air $d_{SVA}^{aqua} / d_{SVA} = 1.5$.

Again the protrusions consisting of PMAA become thicker. Typical images of PS-*b*-P2VP-H⁺-*b*-PMAA films swollen in water are shown in Figure 2(e) and (f). Both Figures show the hexagonal arrangement of protrusions. While Figure 2(e) exhibits a granular structure with the highest thickness being in the middle of the protrusions, Figure 2(f) shows protrusions with indentations on top. We assume that the differences may be due to the quality of the SFM tip. For the measurements in the aqueous phase we have used contact mode tips which are generally much softer than tips used for tapping mode SFM at air conditions. The indentations on top of the PMAA protrusions may be explained by an indentation of the tip into the material, since these positions are the most swollen and therefore the softest.

pH-dependence of the PL phase

In the following section we study the influence of the pH-value of the aqueous solution on the morphology and the film thickness of a hydrolyzed film.

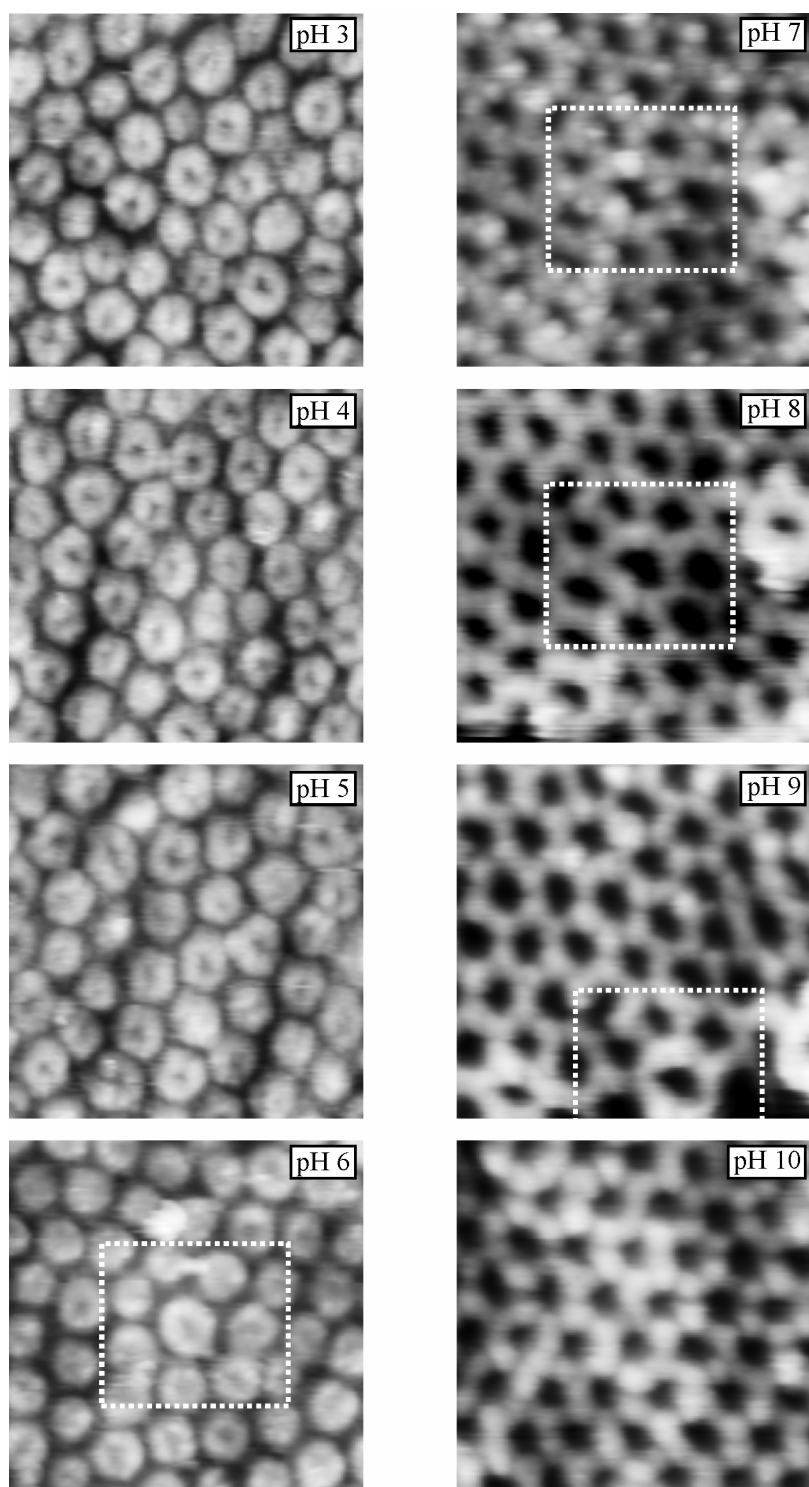


Figure 3. SFM images of one layer of perforated lamellae at different pH-values of the buffer solution. The image size is $500 \times 500 \text{ nm}^2$. The height scale for pH 3-6 is $\Delta z = 0\text{-}30 \text{ nm}$, and $\Delta z = 0\text{-}80 \text{ nm}$ for pH 7-10. The white box marks the same sample position.

In Figure 3 SFM images at different pH-values are displayed. Between pH 6 and pH 9 the same sample region has been measured, for visualization purposes we have marked a typical defect of the hexagonal pattern: a “seven-ring”. The surface morphology remains the same up to pH-values of 6 (for a larger surface region, please compare Figure 2(f)), at higher pH-values the pattern changes:

holes appear at the positions of the protrusions, but interestingly the hexagonal arrangement of the pattern does not change. As the length scales are also identical (protrusion-to-protrusion and hole-to-hole distance: $L = (80 \pm 5)$ nm) we assume that the skeleton of the perforated lamellae, consisting of PS and P2VP, does not change during the pH-treatment.

The film thickness simultaneously increases with increasing pH, Figure 4 shows the degree of swelling as function of the pH-value. The data points correspond to different samples and the degree of swelling has been always calculated relative to the thickness observed for the particular sample after hydrolysis in the dry state. Below pH 6 the film thickness does not change, while between pH 6 and 8 we find a sharp increase in the film thickness with a plateau at a maximum degree of swelling of $(d_{SVA}^{aqua} / d_{SVA}) \sim 7.5$ fold at $\text{pH} > 8$. For pH-values around 10 we could not get reliable data because of imaging problems.

We have further reduced the pH-value towards the starting point, displayed by the red triangles in the graph. The film thickness reaches a minimum value which is in good accordance to the original film thickness.

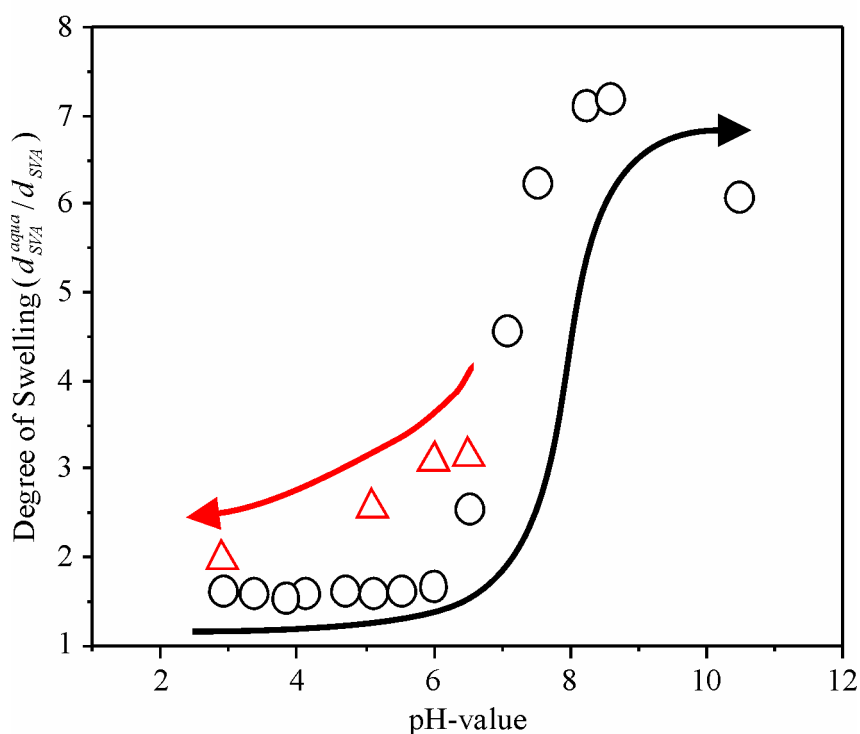


Figure 4. Degree of swelling as function of the pH-value. After having reached the maximum pH-value (curve of black circles), the pH was decreased to the starting point (red triangles).

Regarding the different block components and their behavior at distinct pH-values, poly(2-vinylpyridine) should respond to the pH at low pH-values ($\text{pH} < 5$).^{42,43} The homopolymer is hydrophobic and insoluble in water at $\text{pH} > 5$, but ionized and water-soluble in acidic aqueous

solutions at $\text{pH} < 5$. As neither the film thickness nor the morphology undergo a transition at low pH-values ($\text{pH} < 6$) we assume that the role of P2VP is negligible for the present investigations. Although P2VP should be protonated and therefore in a swollen state at low pH due to the acidic conditions during the saponification process, the effect of deswelling with increasing pH – as found for the homopolymer - is not observed. One possible explanation may be that the volume fraction of P2VP amounts only to $\phi_p = 20\%$ and that our method is not sensitive enough to detect resulting deswelling / swelling effects. Additionally P2VP forms the shell of the PL phase and can only shrink / expand when the majority component PMAA has enough mobility (PS does not respond to pH changes at all). We assume that P2VP is screened from pH-changes of the solution.

Homo[poly(methacrylic acid)] is known to undergo a transition from a contracted to an expanded state at $\text{pH} = \text{pK}_a = 5$ in solution. The conformational change is induced by the repulsion between the increasing amount of carboxylate anion groups. The chains resist expansion before a critical charge density is attained. This fact has been interpreted as being due to a hypercoiled conformation of PMAA in the unionized state which is stabilized through hydrophobic interactions between the methyl substituents of PMAA and hydrogen bonding forces.^{5,6,7,9}

The sharp increase in the film thickness and the structural changes from protrusions to holes indicate a change at $\text{pH} > 6$ for our system, which is well above the pK_a of PMAA. Apparently the results of the solution behavior of the homopolymer can only be transferred to some extent to our observations. At pH-values less than 6 the PMAA seems not to respond to any changes of the surrounding medium. Probably methyl-methyl and hydrogen-bonding forces have a stabilizing effect on the PMAA chains, but additionally the particular structure plays an important role: We have chemically modified a frozen surface structure which is confined to a certain film thickness. Only at a certain degree of ionization, higher than the pK_a , the PMAA chains can undergo a rearrangement from the contracted form, which is given by the dimensions of the PL phase, to an extended form. While at low charge densities the chain entropy and the confinement of the material tend to keep the polymer configuration as close to the Gaussian statistics as possible, at a certain charge density stretching of the coils is favoured. Probably similar to the homopolymer in solution, first free COOH groups are ionized which are mainly located at external regions of the coil and/or at the top surfaces of the film. The deprotonation of the inner groups can be regarded as the inset of the transformation.⁶ Up to pH 6 water is hindered to enter the film (constant film thickness), at $\text{pH} > 6$, the water uptake and the mobility of the polymer chains increase which is indicated by the strong increase of the film thickness (by orders of magnitude).

Figure 5(a) and (b) show sketches of the PL phase at $\text{pH} < 6$ and $\text{pH} > 6$, respectively. No lateral changes occur during the variations of the pH-value. The films swell in z-direction with the skeleton

of the PL phase remaining unchanged. Since the first two blocks are hydrophobic in a basic environment and do not swell, the PMAA chains can only stretch to a certain value. We assume that the holes appear in the swollen case because the chains can only stretch to a certain radius, which is indicated by the circle in the sketch (Fig. 5(b)).

The mechanical stability of the first two blocks PS and P2VP is apparently large enough to withstand the forces exerted on the majority PMAA blocks during swelling in water. These two blocks act as skeleton for the overall structure and prevent a breaking of the structure.

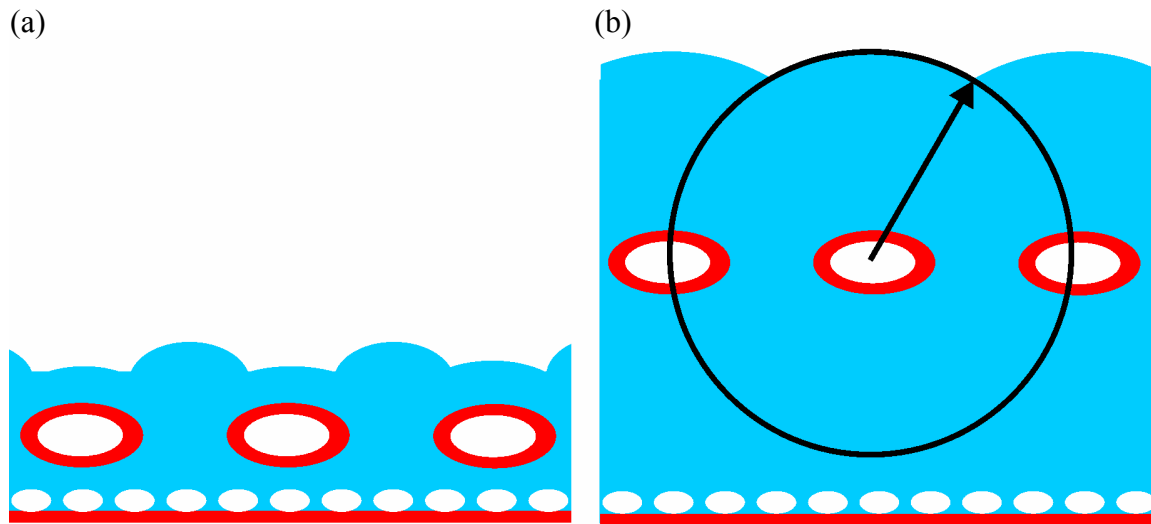


Figure 5. Sketches of the PL phase at $pH < 6$ (a) and $pH > 6$ (b).

Figure 6 shows the degree of swelling as function of the time at pH 7. The following equation can be used to fit the fractional water uptake (M_t/M_∞) as function of the time:

$$\frac{M_t}{M_\infty} = k \cdot t^n \quad (2)$$

where M_t is the mass of water absorbed at time t , M_∞ is the mass of water absorbed at equilibrium, k is a characteristic constant of the material, and n is a characteristic exponent describing the mode of the penetrant transport mechanism. For a film, $n = 0.5$ indicates Fickian diffusion, $n > 0.5$ indicates non-Fickian or anomalous transport and $n = 1$ implies case II (relaxation controlled) transport. We assume a Fickian behavior, which shows the following dependence for short times:

$$\frac{M_t}{M_\infty} = \sqrt{\frac{16D}{l^2\pi}} \cdot \sqrt{t} \quad (3)$$

where D is the diffusion coefficient and $l = (d_0 + d_\infty)/2$ the thickness of the film with d_0 (d_{SVA}) being the original film thickness and $d_\infty = 130$ nm, the film thickness which can be determined with

graphical extrapolation. Due to

$$\frac{d}{d_0} - 1 = \frac{M_t}{M_\infty} \cdot \left(\frac{d_\infty}{d_0} - 1 \right) \quad (4)$$

with d (d_{SVA}^{aqua}) being the measured film thickness at times t , we have plotted $(d/d_0 - 1)$ as function of t in Figure 6. The continuous line indicates the fit of the data by equation 4. Though we have used a rather rough model to describe the diffusion behavior of water in thin films, the Fickian curve fits the data quite well. The diffusion coefficient can be determined to $D = (1,7 \cdot 10^{-14} \pm 1 \cdot 10^{-14}) \text{ cm}^2/\text{sec}$. For a more accurate evaluation it has to be taken into consideration that both the diffusion coefficient and the film thickness in thin films are not independent of the concentration, which is anticipated by the equations used above.

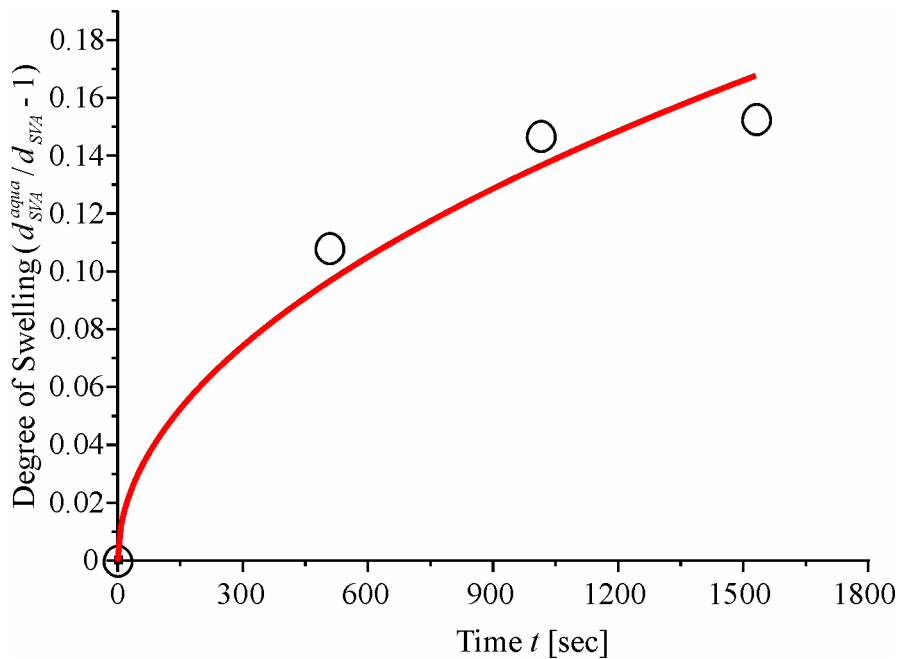


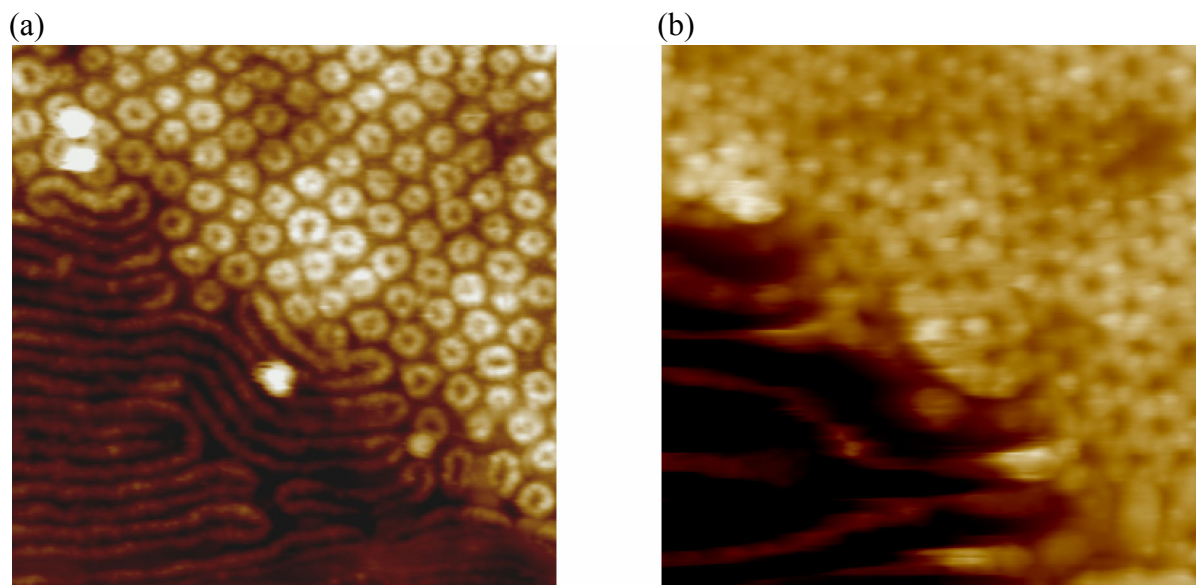
Figure 6. Degree of swelling at different times t at $\text{pH} = 7$. The data points are fitted with equation 4.

pH-dependence of cylinder structures

In this section we discuss the stability of cylinders oriented parallel to the interfaces as a function of pH. Figure 7(a) shows a SFM image of the transition between a perforated lamella structure and core-shell cylinders oriented parallel to the substrate after hydrolysis at pH-values ≤ 6 . Similar to the above described PL phase, the hydrolysis has apparently not altered the microdomain structure.

Figure 7(b) and (c) show the corresponding SFM images at pH 6.5 and pH 7, respectively, at the same spot of the sample. While the PL phase remains stable and undergoes the structural changes described in the previous section, the cylinders become unstable and finally disappear. In contrast to the perforated lamella structure, where PS and P2VP act as skeleton for the overall structure, the core-shell cylinders are single objects embedded in a matrix of the strongly swollen PMAA. Due to the strong swelling of PMAA around pH 7 the cylinders may be solubilised, and even parts of the PL phase are broken away.

Figure 7(d) exhibits a thin disordered layer beneath the $C_{||}$ phase. We assume that this layer can be attributed to a wetting layer which is attached to the silicon substrate via the polar poly(2-vinylpyridine) block. These observations are in coincidence with our former discussions about the wetting layer next to the substrate in thin films of the unhydrolyzed triblock terpolymer.^{35,36} We have found that irrespective of the chemical nature of the substrate a PtBMA rich layer of about 10 nm thickness is found beneath the higher terraces. We can transfer the previous results to the hydrolyzed films, as we have shown that the acid saponification did not change the overall structure.



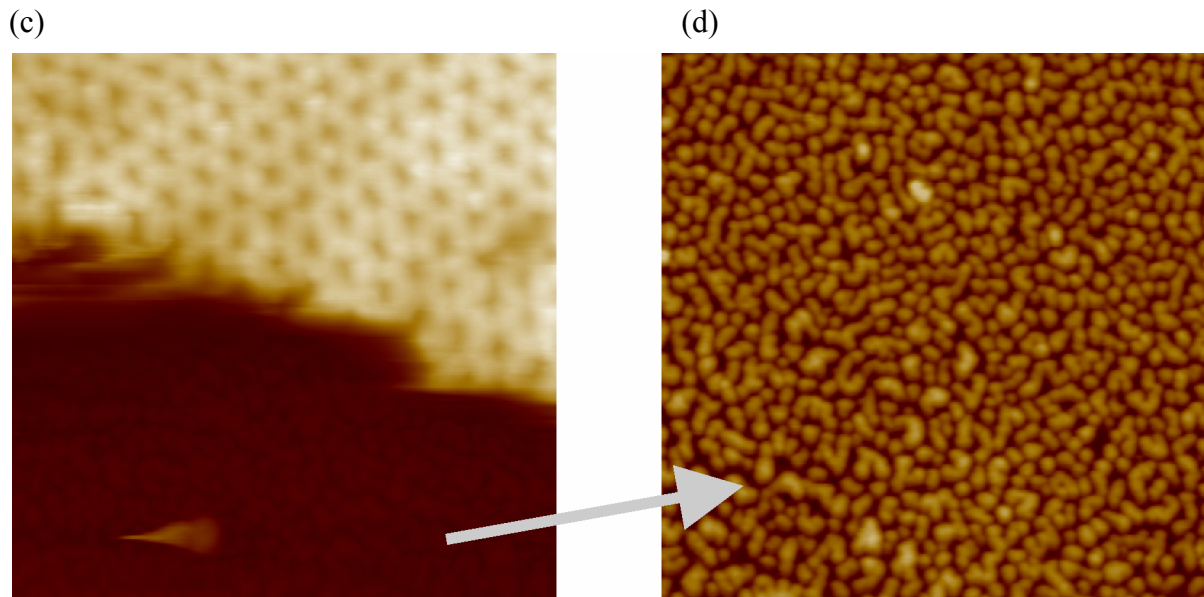


Figure 7. SFM images (aqueous phase) of a transition between perforated lamellae (PL) and cylinders oriented parallel to the surfaces ($C_{||}$) at pH 6 (a), pH 6.5 (b) and pH 7 (c). The image size is $1 \times 1 \mu\text{m}^2$. The height scales are $\Delta z = 0\text{-}30 \text{ nm}$ (a), $\Delta z = 0\text{-}160 \text{ nm}$ (b) and $\Delta z = 0\text{-}500 \text{ nm}$ (c). (d) shows the structure of a wetting layer next to the substrate after removal of $C_{||}$.

3.4.2. Conclusion

Via acid-catalyzed hydrolysis we perform a polymer-analogous reaction of a prestructured thin film surface structure: a perforated lamella structure consisting of poly(styrene), poly(2-vinylpyridine) and poly(*tert*-butyl methacrylate) is modified to a triblock terpolyampholyte consisting of poly(styrene), protonated poly(2-vinylpyridine) and poly(methacrylic acid). The hydrolysis does not alter the overall perforated lamella structure.

We study the influence of the pH-value on this perforated lamella structure. Upon changing the pH of the surrounding medium we observe a strong swelling of the original film thickness at $\text{pH} > 6$ to a maximum degree of swelling of 7.5-fold. In the same pH region we find a change in the surface pattern: at $\text{pH} > 6$ holes appear at the positions where the protrusions of the perforated lamella have been. The hexagonal arrangement of the pattern is not affected. We assume that a conformational change of the majority component PMAA takes place in this pH region: while the PMAA chains are Gaussian chain like and confined as matrix phase of the perforated lamellae at $\text{pH} < 6$, we enhance the freedom of the chains with increasing pH-value of the solution. The chains begin to swell and reach an expanded state at pH-values > 8 . The PMAA chains can only swell to a certain value as they are chemically linked to P2VP which is immobile at these pH-values. We emphasize that the first two blocks PS and P2VP act as skeleton of the PL phase which withstands the mechanical forces exerted on the strongly swollen PMAA. In contrast to the PL phase core-shell cylinders

oriented parallel to the interfaces cannot withstand these forces and are solubilised at high pH-values.

With this contribution we show that the perforated lamella phase is a rather versatile surface structure which can easily be modified to a pH-tunable material.

Acknowledgement

We thank M. Lysetska for her help with the MultiMode SFM and R. Magerle for fruitful discussions. We acknowledge financial support from the Deutsche Forschungsgemeinschaft (SFB 481).

References

- (1) Matsen, M. W. *Curr. Opin. Coll.* **1998**, 3, 40.
- (2) Binder, K. *Adv. Polym. Sci.* **1999**, 138, 1.
- (3) Fasolka, M. J.; Mayes, A. M. *Annu. Rev. Mat. Res.* **2001**, 31, 323.
- (4) Krausch, G.; Magerle, R. *Adv. Mater.* **2002**, 14, 1579.
- (5) Arnold, R. *J. Colloid. Sci.* **1957**, 12, 549.
- (6) Dong, J.; Tsubahara, N.; Fujimoto, Y.; Ozaki, Y.; Nakashima, K. *Appl. Spect.* **2001**, 55, 1603.
- (7) Morawetz, H. *Macromolecules* **1996**, 29, 2689.
- (8) Chu, D.-Y.; Thomas, J.-K. *Macromolecules* **1984**, 17, 2142.
- (9) Nakashima, K.; Fujimoto, Y.; Anzai, T.; Dong, J.; Sato, H.; Ozaki, Y. *Bull. Chem. Soc. Jpn.* **1999**, 72, 1233.
- (10) Bednar, B.; Trnena, J.; Svoboda, P.; Vajda, S.; Fidler, V.; Prochazka, K. *Macromolecules* **1991**, 24, 2054.
- (11) Soutar, I.; Swanson, L. *Macromolecules* **1994**, 27, 4304.
- (12) Böhm, N.; Kulicke, W.-M.; *Colloid Polym. Sci.* **1997**, 275, 73.
- (13) Duivenvoorde, F. L.; van Nostrum, C. F.; van der Linde, R. *Prog. Org. Coat.* **1999**, 36, 225.
- (14) Claesson, P. L.; Dahlgren, M. A. G.; Erikson, L. *Coll. Surf. A* **1994**, 93, 293.
- (15) Buchhammer, H.-M.; Petzold, G.; Lunckwitz, K. *Langmuir* **1999**, 15, 4306.
- (16) Dautzenberg, H.; Jaeger, W.; Kötz, J.; Philipp, B.; Seidel, C.; Stscherbina, D. *Polyelectrolytes*; Hanser: Munich, **1994**; pp. 272.
- (17) Musabekov, K. B.; Tusupbaev, N. K.; Kudaibergenov, S. E. *Macromol. Chem. Phys.* **1998**, 199, 401.
- (18) Makino, K.; Miyauchi, E.; Togawa, Y.; Ohshima, H.; Kondo, T. *Polym. Repr.* **1992**, 33, 476.
- (19) Kamachi, M.; Kurihara, M.; Stille, J. K. *Macromolecules* **1972**, 5, 161.
- (20) Ramireddy, C.; Tuzar, Z.; Prochazka, K.; Webber, S. E.; Munk, P. *Macromolecules* **1992**, 25, 2541.
- (21) Patrickios, C. S.; Hertler, W. R.; Abbott, N. L.; Hatton, T. A. *Macromolecules* **1994**, 27, 930.
- (22) Bronstein, L. M.; Sidorov, S. N.; Valetsky, P. M. *Langmuir* **1999**, 15, 6256.
- (23) Gohy, J.-F.; Antoun, S.; Jérôme, R. *Macromolecules* **2001**, 34, 7435.
- (24) Qin, S.-H.; Qiu, K.-Y. *J. Polym. Sci. Part A Polym. Chem.* **2001**, 39, 1450.
- (25) Bieringer, R.; Abetz, V.; Müller, A. H. E. *Eur. Phys. J. E* **2001**, 5, 5.
- (26) Förster, S.; Schmidt, M.; *Adv. Polym. Sci.* **1995**, 120, 53.

- (27) Kassapidou, K.; Jesse, W.; Kuil, M. E.; Lapp, A.; Egelhaaf, S.; van der Maarel, J. R. C. *Macromolecules* **1997**, 30, 2671.
- (28) Hamley, I. W. *The Physics of Block Copolymers*; Oxford University Press: Oxford, 1998.
- (29) Buchholz, V.; Adler, P.; Bäcker, M.; Hölle, W.; Simon, A.; Wegner, G. *Langmuir* **1997**, 13, 3206.
- (30) Buchholz, V.; Wenz, G.; Wegner, G.; Stein, A.; Klemm, D. *Adv. Mater.* **1996**, 8, 399.
- (31) Staub, M.; Wenz, G.; Wegner, G.; Stein, A.; Klemm, D. *Adv. Mater.* **1993**, 5, 919.
- (32) Esker, A. R.; Mengel, C.; Wegner, G. *Science* **1998**, 280, 892.
- (33) Mengel, C.; Esker, A. R.; Meyer, W. H.; Wegner, G. *Langmuir* **2002**, 18, 6365.
- (34) Liu, G.; Ding, J.; Stewart, S. *Angew. Chem. Int. Ed.* **1999**, 38, 835.
- (35) Ludwigs, S.; Böker, A.; Voronov, A.; Rehse, N.; Magerle, R.; Krausch, G. *Nature Materials* **2003**, 2, 744.
- (36) Ludwigs, S.; Schmidt, K.; Stafford, C.; Fasolka, M.; Karim, A.; Amis, E.; Magerle, R.; Krausch, G. *submitted to Macromolecules*.
- (37) Giebeler, E.; Stadler, R. *Macromol. Chem. Phys.* **1997**, 198, 3815.
- (38) Giebeler, E. PhD Thesis, Mainz, 1996.
- (39) Ludwigs, S.; Böker, A.; Abetz, V.; Müller, A. H. E.; Krausch, G. *Polymer* **2003**, 44, 6815.
- (40) Jeon, C. H.; Makhaeva, E. E.; Khokhlov, A. R. *Macromol. Chem. Phys.* **1998**, 199, 2665.
- (41) Ludwigs, S.; Zvelindovsky, A. V.; Sevink, G. J. A.; Krausch, G.; Magerle, R. *submitted to Macromolecules*.
- (42) Puterman, M.; Koenig, J. L.; Lando, J. B. J. *Macromol. Sci.-Phys.* **1979**, B16, 89.
- (43) Martin, T. J.; Prochazka, K.; Munk, P.; Webber, S. E. *Macromolecules* **1996**, 29, 6071.

4. Summary

The thin film phase behavior of poly(styrene)-*block*-poly(2-vinylpyridine)-*block*-poly(*tert*-butyl methacrylate) (PS-*b*-P2VP-*b*-PtBMA) triblock terpolymers with volume fractions $\phi_{\text{PS}} : \phi_{\text{P2VP}} : \phi_{\text{PtBMA}} = 1 : 1.2 : x$, with x ranging from 3.05 to 4, is studied with a combinatorial gradient approach (Chapter 3.1). Gradients in film thickness are prepared via thin film flow coating of dilute solutions in chloroform. Upon controlled annealing in nearly saturated solvent vapor the films form terraces of well-defined step height. The dependence between morphology and film thickness is studied with optical microscopy, tapping mode scanning force microscopy, and scanning electron microscopy.

Though showing different morphologies in the bulk, the same sequence of surface structures is found with increasing film thickness for the whole range of compositions: a disordered phase in the thinnest regions, a liquid-like distribution of upright standing cylinders, cylinders oriented parallel to the film, and finally a hexagonally ordered perforated lamella structure (PL) on the first terrace with a thickness of $d = (37 \pm 3)$ nm. Higher terraces also exhibit perforated lamellae as surface structures. Due to the chemical nature of the block components and the particular stoichiometry of the polymer a wetting layer with a PtBMA-rich top layer is formed next to the substrate.

By imposing an additional gradient in substrate surface energy, orthogonal to the gradually increasing film thickness, the perforated lamella is shown to be a stable phase, regardless of the chemical nature of the substrate, which makes this structure and methodology robust for application in nanotechnology.

The nature of the solvent used for annealing has a significant influence on the structure formation. Using the same preparation procedure as with chloroform, the use of tetrahydrofurane leads to terraces exhibiting cylinders oriented parallel to the surfaces (C_{\parallel}). This phenomenon is explained with a different selectivity of the solvents to the different blocks.

Additionally, the importance of a well-controlled sample preparation is emphasized. As the structure formation process takes place in highly concentrated polymer solutions even slight changes in concentration may induce phase transitions between neighboring morphologies. Thin films of triblock terpolymers exhibit a wealth of structures due to the delicate interplay between the large number of block-block and block-surface interactions.

The complex phase behavior observed in thin films is supported by mesoscale computer simulations based on dynamic density functional theory (Chapter 3.2). Thin films of the above mentioned triblock terpolymers are modeled as a melt of $A_3B_4C_{12}$ Gaussian chains which is confined in a slit with film thickness H . By adjusting the interaction parameters between the polymer components and the surfaces, the experimentally observed sequence of surface structures as function of the film

thickness can be successfully modeled. At well-defined film thickness the perforated lamella structure is formed. In analogy with earlier work on a two-component system these structures are identified as surface reconstructions of the bulk structure. In particular, the core-shell PL can be seen as analogue to the PL surface reconstruction of cylinder-forming AB and ABA systems.

The influence of film thickness, surface field, and the interaction parameters between the different polymer components on the phase behavior is also explored. A large spectrum of surface structures is observed in analogy to the experiments.

Further attention has been given to the perforated lamella structure. This structure can be visualized as P2VP/PS/P2VP lamellae which are perforated by channels of PtBMA interconnecting between two outer layers of PtBMA (Chapter 3.3). A highly ordered perforated lamella structure could be prepared with a very small number of defects over an area of about $12 \times 4 \mu\text{m}^2$. Because of the special functionalities of the triblock terpolymer a rather versatile nanostructure was produced. By selective UV-depolymerization of the PtBMA matrix phase, the PL phase might potentially be used for lithographic applications similar to the case of perpendicularly oriented poly(methyl methacrylate) (PMMA) cylinders in PS-*b*-PMMA block copolymer thin films. Furthermore, a responsive membrane can be created by selective removal of the matrix phase. The remaining perforated lamella has a P2VP shell which might be either switched via the pH-value or loaded with metal components.

A polymer-analogous reaction of the matrix phase of the perforated lamella to poly(methacrylic acid) via acid-catalyzed hydrolysis leads to a pH-responsive nanostructure without altering the overall structure (Chapter 3.4). With scanning force microscopy in aqueous environment structural changes of the PL phase are studied as function of the pH-value. Upon changing the pH of the surrounding medium a strong swelling of the original film thickness is observed at pH-values > 6 to a maximum degree of 7.5-fold swelling. This swelling is explained with a conformational change of the matrix phase poly(methacrylic acid). The hexagonal arrangement of the pattern is not affected. The first two blocks PS and P2VP act as skeleton of the PL phase which withstands the mechanical forces exerted on the strongly swollen PMAA. In contrast to the PL phase core-shell cylinders oriented parallel to the interfaces cannot withstand these forces and are solubilised at high pH-values.

In summary, an in-depth understanding of the structure formation process in thin films of ABC triblock terpolymers is provided. Essential control parameters are identified which are indispensable

to fully exploit the potential of these materials and to create tailor-made nanostructured thin films. The combinatorial approach of the sample preparation enables a systematic analysis of the film phase behavior with one specimen. In addition to rapidly providing a comprehensive map of the phase behavior, such techniques reduce the problems of reproducibility since processing parameters are held constant. The simulations are useful for the understanding of experimental results. They have successfully been used to identify important experimental control parameters, and might be also used for a rational design of material properties. It has been shown within this thesis, that a modification of the chemical nature of thin film structures by selective removal of specific components or by polymer-analogous reactions leads to tailored nanostructures which might be used as lithographic masks, responsive membranes, or pH-responsive nanostructures.

Zusammenfassung

In der vorliegenden Doktorarbeit wird das Phasenverhalten von Polystyrol-*block*-Poly(2-Vinylpyridin)-*block*-Poly(*tert*-Butylmethacrylat) Dreiblock-Terpolymeren in dünnen Filmen mit Hilfe kombinatorischer Präparationsmethoden untersucht (Kapitel 3.1). Die Volumenanteile der untersuchten Polymere betragen $\phi_{PS} : \phi_{P2VP} : \phi_{PtBMA} = 1 : 1.2 : x$ (mit x zwischen 3,05 and 4). Proben mit Dickengradienten werden aus verdünnten Polymerlösungen in Chloroform mittels einer Rakeltechnik präpariert. Durch geeignete Behandlung im Lösungsmitteldampf (nahe des Sättigungsdampfdrucks des Lösungsmittels) bilden diese Filme Terrassen mit bestimmter Stufenhöhe aus. Der Zusammenhang zwischen Morphologie und Filmdicke konnte mit Lichtmikroskopie, Rasterkraftmikroskopie im TappingMode und Rasterelektronenmikroskopie aufgeklärt werden.

Im gesamten, oben genannten Zusammensetzungsbereich, das heißt unabhängig von der Volumenstruktur, findet man eine definierte Abfolge von Dünnsfilmstrukturen als Funktion der Filmdicke: die dünnsten Bereiche der Probe zeigen eine sehr ungeordnete Struktur, gefolgt von unregelmäßig angeordneten senkrecht stehenden Zylindern, liegenden Zylindern und schließlich einer hexagonal geordneten perforierten Lamellenstruktur auf der ersten Terrasse, die eine Filmdicke von (37 ± 3) nm aufweist. Aufgrund der chemischen Natur der Polymerblöcke und der speziellen Zusammensetzung des Dreiblock-Terpolymers bildet sich eine dünne, am Substrat haftende Polymerschicht unterhalb der Oberflächenstrukturen aus. Dieser sogenannte 'wetting layer' ist bedeckt mit der Majoritätskomponente Poly(*tert*-Butylmethacrylat) (PtBMA). Mit Hilfe von Oberflächenenergiegradienten, die sich orthogonal zur graduell ansteigenden Filmdicke erstrecken, konnte festgestellt werden, dass sich die perforierte Lamellenstruktur unabhängig von der chemischen Natur des Substrates ausbildet. Diese Eigenschaft kann für mögliche Anwendungen von Nutzen sein.

Darüberhinaus muss Wert auf eine kontrollierte Probenpräparation gelegt werden. Da die Strukturbildung in hochkonzentrierten Polymerlösungen stattfindet, können auch kleinste Veränderungen in der Konzentration Phasenübergänge zwischen benachbarten Morphologien induzieren. Aufgrund der großen Anzahl der Wechselwirkungen zwischen den Blöcken untereinander und zu den Filmoberflächen zeigen dünne Filme aus Dreiblock-Terpolymeren eine Vielzahl von unterschiedlichen Morphologien.

Die experimentellen Untersuchungen werden durch Computersimulationen unterstützt, die auf einer Dichtefunktionaltheorie basieren. Dünne Filme der oben genannten Polymere werden dabei als Schmelze aus $A_3B_4C_{12}$ Ketten modelliert, die in einer Dimension geometrisch eingeschränkt (Filmdicke) ist. Durch Anpassen der Wechselwirkungsparameter zwischen den Polymerkomponenten und den Filmgrenzflächen konnte die experimentell beobachtete Abfolge von Dünnsfilmstrukturen als Funktion der Filmdicke erfolgreich nachgeahmt werden. Bei definierten Filmdicken findet man perforierte Lamellen als Oberflächenstruktur. In Übereinstimmung mit Arbeiten über zweikomponentige Systeme werden diese Strukturen als Oberflächenrekonstruktionen der Volumenstruktur identifiziert. Die gefundene perforierte Lamelle mit Kern-Schale Struktur kann dabei als direktes Analogon zur perforierten Lamelle in dünnen Filmen aus ABA Dreiblockcopolymeren betrachtet werden.

Der Einfluß der Filmdicke, der Grenzflächen und der Wechselwirkung zwischen den einzelnen Polymerkomponenten wird ebenfalls intensiv untersucht. In den Simulationen findet man, ähnlich wie im Experiment, eine Vielzahl verschiedenartiger Oberflächenstrukturen.

Besonderes Interesse wurde weiterhin auf die Struktur der perforierten Lamelle gelegt, auch im Hinblick auf mögliche Anwendungen. Bildlich kann man sich diese Struktur als Lamellen aus Polystyrol (PS) und Poly(2-Vinylpyridin) (P2VP) vorstellen, die durch hexagonal angeordnete Kanäle der Matrixphase PtBMA perforiert sind. Im Rahmen der Doktorarbeit konnte ein Film hergestellt werden, der über eine Fläche von $12 \times 4 \mu\text{m}^2$ nahezu defektfrei ist. Aufgrund der besonderen chemischen Zusammensetzung der untersuchten Dreiblock-Terpolymere lässt sich die Struktur der perforierten Lamelle weiter chemisch modifizieren. Durch selektive Depolymerisation des Esterblockes ließe sich beispielsweise eine lithographische Maske herstellen. Ein ähnliches Prinzip wurde schon erfolgreich für senkrecht stehende Zylinder aus Polystyrol-*block*-Poly(Methylmethacrylat) Zweiblockcopolymeren gezeigt. Desweiteren könnten auch schaltbare Membranen hergestellt werden: nach Depolymerisation des Esterblockes entsteht aus der perforierten Lamellenstruktur eine nanoporöse Membran, deren Oberfläche noch mit P2VP bedeckt

ist. Dieses Polymer kann sowohl auf pH-Änderungen reagieren als auch mit Metallen beladen werden.

Eine polymeranaloge Umsetzung der Esterkomponente mittels säurekatalysierter Hydrolyse zu Poly(Methacrylsäure) führt zu einer pH-abhängigen Nanostruktur. Die Gesamtmorphologie ändert sich bei dieser Behandlung nicht. Die Änderung der Struktur wurde mittels Rasterkraftmikroskopie in wässriger Umgebung bei veränderlichem pH-Wert in situ verfolgt.

Bei Erreichen eines pH-Wertes von etwa 6 quillt der Film um das 7,5-fache seiner ursprünglichen Filmdicke an. Dieser Effekt wird durch eine Konformationsänderung der Poly(Methacrylsäure) erklärt. Die hexagonale Anordnung der Kanäle bleibt dabei erhalten, da sowohl Polystyrol als auch Poly(2-Vinylpyridin) als hydrophobes Skelett agieren. Auch starke mechanische Kräfte, die aus dem starken Schwellgrad resultieren, zerstören die Struktur nicht. Im Gegensatz zur perforierten Lamelle, werden liegende Zylinder bei ähnlicher Behandlung aufgelöst und weggeschwemmt.

Zusammenfassend betrachtet bietet diese Arbeit einen wichtigen Beitrag zum Verständnis der Strukturbildung in dünnen Filmen aus ABC Dreiblock-Terpolymeren. Auf der Basis entsprechender grundlegender Erkenntnisse können maßgeschneiderte, nanostrukturierte Filme hergestellt werden. Der kombinatorische Ansatz der Probenpräparation ermöglicht eine systematische und schnelle Analyse des Phasenverhaltens dünner Filme anhand einer einzelnen Probe. Ein weiterer Vorteil dieser Technik ist die Reproduzierbarkeit, da entscheidende Parameter konstant gehalten werden können. Simulationsmessungen helfen dabei, die experimentellen Resultate besser zu verstehen; so lassen sich einerseits wichtige experimentelle Einflußgrößen finden, andererseits könnten Simulationen auch dazu eingesetzt werden, gezielt Materialeigenschaften maßzuschneidern. Sowohl durch Depolymerisation bestimmter Blöcke als auch durch polymer-analoge Umsetzungen konnte eine chemische Modifizierung einer bestimmten Dünnschichtstruktur erreicht werden, die als aussichtsreiches Material für lithographische Masken, schaltbare Membranen oder pH-abhängige Nanostrukturen eingeschätzt werden kann.

5. Appendix

5.1. Publication on the bulk phase behavior of the investigated polymers

Phase behavior of linear poly(styrene)-*block*-poly(2-vinylpyridine)-*block*-poly(*tert*-butyl methacrylate) triblock terpolymers

Sabine Ludwigs^a, Alexander Böker^{a,b}, Volker Abetz^{b*}, Axel H.E. Müller^{b,c}, and Georg Krausch^{a,c*}

^a*Physikalische Chemie II*, ^b*Makromolekulare Chemie II*,

^c*Bayreuther Zentrum für Kolloide und Grenzflächen (BZKG), Universität Bayreuth, D-95440 Bayreuth, Germany*

Corresponding authors: volker.abetz@uni-bayreuth.de, Tel.: 0921-553395 and georg.krausch@uni-bayreuth.de, Tel: 0921-552751, Fax: 0921-552059.

Published: *Polymer* 2003, 44, 6815.

Abstract

Using sequential living anionic polymerization we synthesized well-defined linear ABC triblock terpolymers from poly(styrene) (PS), poly(2-vinylpyridine) (P2VP), and poly(*tert*-butyl methacrylate) (PtBMA). The length of the PtBMA block was systematically increased at constant block length ratios of the PS and P2VP blocks. The microdomain structures were characterized by transmission electron microscopy (TEM) and small angle X-ray scattering (SAXS). With increasing PtBMA block size we observe a systematic change in the bulk structure of the block terpolymers.

Keywords:

Anionic polymerisation, triblock terpolymers

Introduction

In recent years ternary triblock terpolymers have attracted increasing interest owing to their rich variety of bulk morphologies [1,2,3]. The latter is due to the large number of independent molecular parameters characterizing these materials. In addition to the degree of polymerization and the different mutual segmental interactions also the composition and the chain topology control the phase behavior in the melt. Ternary triblock terpolymers may form core-shell analogs of the well-known diblock copolymer morphologies, where the middle block forms a layer between the two outer blocks [3,4,5]. Alternatively, the middle block may form spheres or cylinders between the two outer blocks [1,6]. In addition, structures with the middle block forming the matrix around cylinders or spheres of the outer blocks [4] or systems where only one outer block forms dispersed domains in a lamella of the middle block are known [7]. Among the most fascinating morphologies is a helical morphology, in which one end block forms a cylinder, which is helically surrounded by cylindrical midblock domains, both embedded in a matrix of the other end block [6]. Finally, a core-shell double gyroid structure has been observed, in which one end block forms the two gyroids, which are surrounded by shells of the midblock and the other outer block fills the space between these two core-shell gyroids [3,5,8,9].

We have recently reported on first experiments investigating the thin film behavior of ABC triblock terpolymers [10,11,12,13,14]. In the presence of boundary surfaces and confined to a thickness comparable to the characteristic bulk spacing, the microdomain structures of block terpolymers can significantly differ from the respective bulk structures. Both large scale alignment of the microdomains as well as the formation of novel microdomain structures has been observed [15,16]. For the particular case of a poly(styrene)-*block*-poly(2-vinylpyridine)-*block*-poly(*tert*-butyl methacrylate) (SVT) triblock terpolymer with volume fractions $\phi_S : \phi_V : \phi_T$ scaling as 1 : 1.4 : 3 a particularly rich variety of thin film structures was found. In order to be able to study these phenomena more systematically, we have synthesized two series of triblock terpolymers which exhibit a certain constant ratio between the PS and P2VP blocks, while the volume fraction of the PtBMA block was stepwise increased within each series. The goal of this procedure is to systematically explore certain regions of the ternary phase diagram. Here, we summarize our synthetic results and describe the bulk structures found for the various materials as a function of composition. While a systematic variation of the length of the middle block requires the complete synthesis procedure for each block copolymer [1,4], in the case of the variation of the last block a sequential addition of the last monomer can lead to a series of block copolymer having exactly the same diblock copolymer precursor [17].

Our approach is based on earlier work by Giebeler *et al.* who first synthesized SVT block

terpolymers [18] aiming at the investigation of their amphiphilic behavior after the hydrolysis of the PtBMA block, which leads to a block polyelectrolyte.

Experimental Section

Synthesis of SVT triblock terpolymers

The linear SVT triblock terpolymers were synthesized via sequential living anionic polymerization in THF using *sec*-butyl lithium as initiator [18]. Both after polymerization of the PS block and of the P2VP block, 1,1-diphenylethylene was added to end-cap the living ends of the anions. In this way crossover steps and transfer reactions due to too high nucleophilicity could be suppressed. During the polymerization of the PtBMA block, samples were taken from the reactor after different polymerization times and were precipitated into degassed methanol. Thus we could obtain a series of polymers with constant ratio of the PS and P2VP blocks, but with increasing length of the PtBMA end block.

We synthesized two series with the above-described procedure, one series with volume fractions $\phi_S : \phi_V : \phi_T = 1 : 1.2 : x$ (x increasing) and the other with $\phi_S : \phi_V : \phi_T = 1 : 1.4 : x$ (x increasing). Gel permeation chromatography (GPC) measurements were performed on a set of 30 cm SDV-gel columns of 5 μm particle size having a pore size of 10^5 , 10^4 , 10^3 and 10^2 Å with refractive index and UV ($\lambda = 254$ nm) detection. GPC was measured at an elution rate of 1 ml/min with THF as solvent. The calibration was based on narrowly distributed poly(styrene) standards. Figure 1 shows the GPC trace (RI signal) of the triblock terpolymer with the highest amount of PtBMA and its precursors PS and PS-*b*-P2VP. The number-averaged molecular weight of the poly(styrene) precursor and the molecular weight distributions of the triblock terpolymers were determined by this method. All polymers exhibit a narrow molecular weight distribution characterized by a polydispersity between 1.01 and 1.05. A quantitative evaluation of the respective peaks in the GPC trace shows that the relative amount of diblock copolymer and homopolymer is less than 1%. The polydispersity index does not include the contributions of homopolymer and diblock precursor, however, an estimate shows that due to the small amounts the actual numbers would not significantly change if the precursors would be included. Additionally, $^1\text{H-NMR}$ spectra were acquired on a 250 MHz Bruker AC spectrometer using CDCl_3 as solvent and tetramethylsilane (TMS) as internal standard. The molecular weights of the P2VP and the PtBMA blocks were calculated using the block copolymer composition determined by NMR and the poly(styrene) molecular weights from GPC. Table 1 summarizes the molecular parameters of the resulting materials.

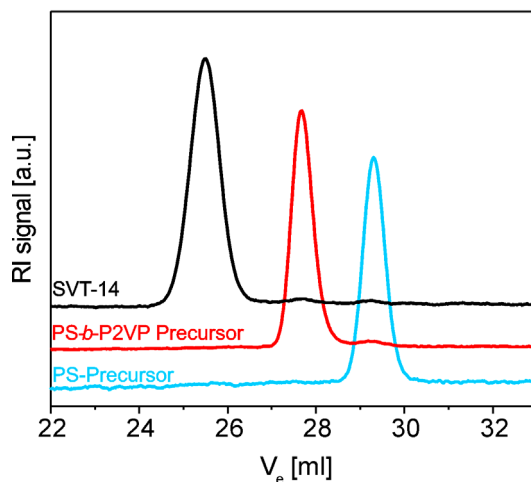


Figure 1: GPC trace (RI signal) of triblock terpolymer $S_{16}V_{21}T_{63}^{140}$ and its precursors PS and PS-b-P2VP. $M_w = 140\ 000\ \text{g/mol}$; $M_w/M_n = 1.03$.

Table 1: Block Copolymer Molecular Characteristics

Polymer ^a	M_w [kg/mol]	M_w/M_n	$\phi_{PS} : \phi_{P2VP} : \phi_{PtBMA}$	Bulk morphology ^b
$S_{16}V_{21}T_{63}^{140}$	140	1.03	1 : 1.2 : 4	CYL
$S_{17}V_{22}T_{61}^{132}$	132	1.03	1 : 1.2 : 3.65	GYR, PL
$S_{17}V_{23}T_{60}^{129}$	129	1.03	1 : 1.2 : 3.39	GYR, PL
$S_{18}V_{24}T_{58}^{124}$	124	1.03	1 : 1.2 : 3.33	GYR, PL
$S_{19}V_{25}T_{56}^{120}$	120	1.03	1 : 1.2 : 3.05	GYR, PL
$S_{25}V_{33}T_{42}^{90}$	90	1.04	1 : 1.2 : 1.76	L
$S_{27}V_{35}T_{38}^{84}$	84	1.04	1 : 1.2 : 1.39	L
$S_{30}V_{39}T_{31}^{77}$	77	1.04	1 : 1.2 : 1.13	L
$S_{30}V_{40}T_{30}^{74}$	74	1.04	1 : 1.2 : 1	GYR
$S_{32}V_{42}T_{26}^{70}$	70	1.05	1 : 1.2 : 0.82	GYR
$S_{34}V_{45}T_{21}^{66}$	66	1.05	1 : 1.2 : 0.66	GYR
$S_{35}V_{52}T_{13}^{82}$	82	1.02	1 : 1.4 : 0.39	GYR
$S_{36}V_{54}T_{10}^{80}$	80	1.02	1 : 1.4 : 0.30	UL
$S_{37}V_{55}T_8^{78}$	78	1.01	1 : 1.4 : 0.24	UL
$S_{38}V_{56}T_6^{76}$	76	1.01	1 : 1.4 : 0.15	GYR
$S_{43}V_{57}^{52}$	52	1.01	1 : 1.2	L
$S_{40}V_{60}^{72}$	72	1.01	1 : 1.4	L

^a $S_{\%S}V_{\%V}T_{\%T}^{M_w}$ with the subscripts representing the weight fractions of the respective blocks (parts in hundred), while M_w is the overall weight-averaged molecular weight in kg/mol; ^bKey: CYL, core-shell-cylinder; GYR, core-shell-gyroid; PL, perforated lamellae; L, lamellae; UL, undulated lamellae.

Structural Characterization

For structural characterization films of the SVT triblock terpolymers were cast from CHCl_3 solution by slowly evaporating the solvent for several days. The films were subsequently dried under vacuum for 4 days at 50°C . Extended annealing (several days) at temperatures well above the glass transition temperatures of the three block components did not lead to any changes in the microdomain structure. In addition to the melt samples, we have investigated the microdomain structure prior to drying in chloroform solutions with different concentrations.

For transmission electron microscopy (TEM) 30 – 60 nm thick sections were cut from the as-cast films. All TEM micrographs were taken on a Zeiss transmission electron microscope (CEM 902) operating at 80 kV in the bright field mode. In order to enhance the electron density contrast between the three phases the samples were stained with RuO_4 and I_2 , respectively. On staining with RuO_4 the PS and P2VP phases are expected to appear dark and grey, respectively, in the TEM images, while the PtBMA phase should remain unstained and appear bright. Exposure of the samples to I_2 on the other hand leads to a preferential staining of the P2VP phase. One should keep in mind, though, that staining often is not selective enough to establish an unambiguous contrast between all three polymer components. Furthermore, it is well-known that electron beam damage can lead to considerable volume shrinkage of polymethacrylate phases [19].

Small angle X-ray scattering (SAXS) measurements were performed at the ID2 beamline at the European Synchrotron Radiation Facility (ESRF, Grenoble, France). The typical photon flux obtained at the ID2 sample position is $8 \cdot 10^{12}$ photons/sec, the energy bandwidth is $\Delta E/E = 2 \cdot 10^{-4}$. All experiments were obtained at 12.5 keV corresponding to an X-ray wavelength of 0.1 nm. The scattering intensities were detected via a CCD camera. The detector system is housed in a 10 m evacuated flight tube. The scattering patterns were corrected for the beam stop and the background prior to evaluations. The calculations of the scattering intensities were obtained with the Fit2D evaluation program [20].

To estimate the scattering contrast between the three components PS, P2VP and PtBMA, we have calculated their electron densities: $\rho_e(\text{PS}) = 0.566 \text{ mol/cm}^3$; $\rho_e(\text{P2VP}) = 0.611 \text{ mol/cm}^3$ and $\rho_e(\text{PtBMA}) = 0.561 \text{ mol/cm}^3$. As the values of PS and PtBMA are very similar, we expect only a weak scattering contrast between the two end blocks of the triblock terpolymers.

Results and discussion

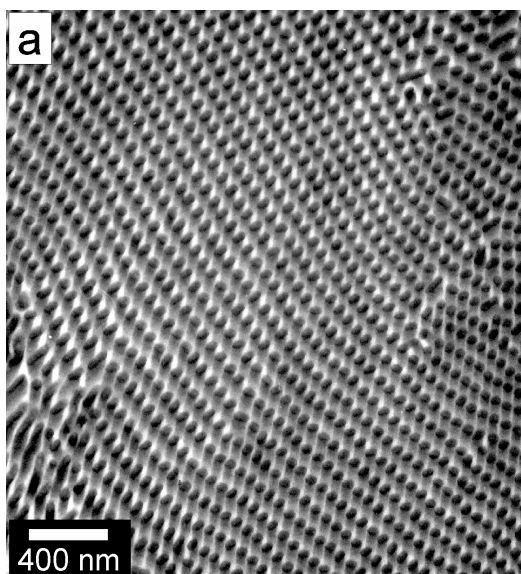
In the following we summarize the results on the microdomain structure of the materials.

Depending on the length of the PtBMA block we can identify six different regions of characteristic bulk structures in the phase diagram. We present the results obtained for six characteristic block terpolymers – the remaining materials resemble one of the six and will only briefly be discussed below. We start with the largest PtBMA volume fractions and move towards decreasing PtBMA content. We use the notation of the block terpolymers given in Table 1, i.e. we denote the polymers as $S_{\%S}V_{\%V}T_{\%T}^{M_w}$ with the subscripts representing the weight fractions of the respective blocks (parts in hundred), while M_w is the overall weight-averaged molecular weight in kg/mol.

$S_{16}V_{21}T_{63}^{140}$: Core-shell cylinders

Fig. 2a shows a transmission electron micrograph of $S_{16}V_{21}T_{63}^{140}$ after staining with I_2 . P2VP appears as dark phase. A slightly distorted hexagonal arrangement of dark cylinder heads can be recognized, which is in accordance with the SAXS data. Figure 2b shows the SAXS data for a 36wt.% SVT solution in chloroform and for a solvent-annealed dry film (prepared in the manner described above). The scattering maxima appear at relative positions of $1 : \sqrt{3} : 2 : \sqrt{7} : \sqrt{12} : \sqrt{13}$, which correspond to the [100], [110], [200], [210], [220] and [310] reflections of a hexagonal cylindrical structure. The [300] peak is not visible. The SAXS pattern of the solution clearly exhibits the peaks characteristic of a cylindrical structure, while on the dry sample the [110] and [200] reflections cannot be clearly distinguished because of peak broadening. This might be due to preparation effects. However it can be clearly seen that the peaks shift to smaller q values, which is typical for our system as the spacing of the long period is growing with increasing polymer concentration with a maximum value for the bulk structure.

Considering the volume fractions of the blocks, we assume a core-shell-cylinder-morphology with PS-core surrounded by a P2VP-shell embedded within a PtBMA matrix phase.



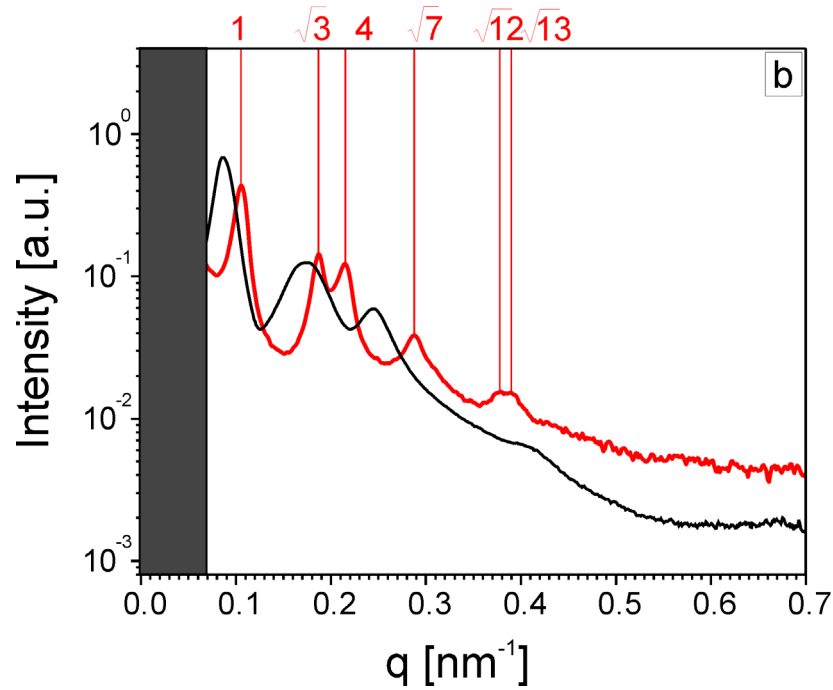


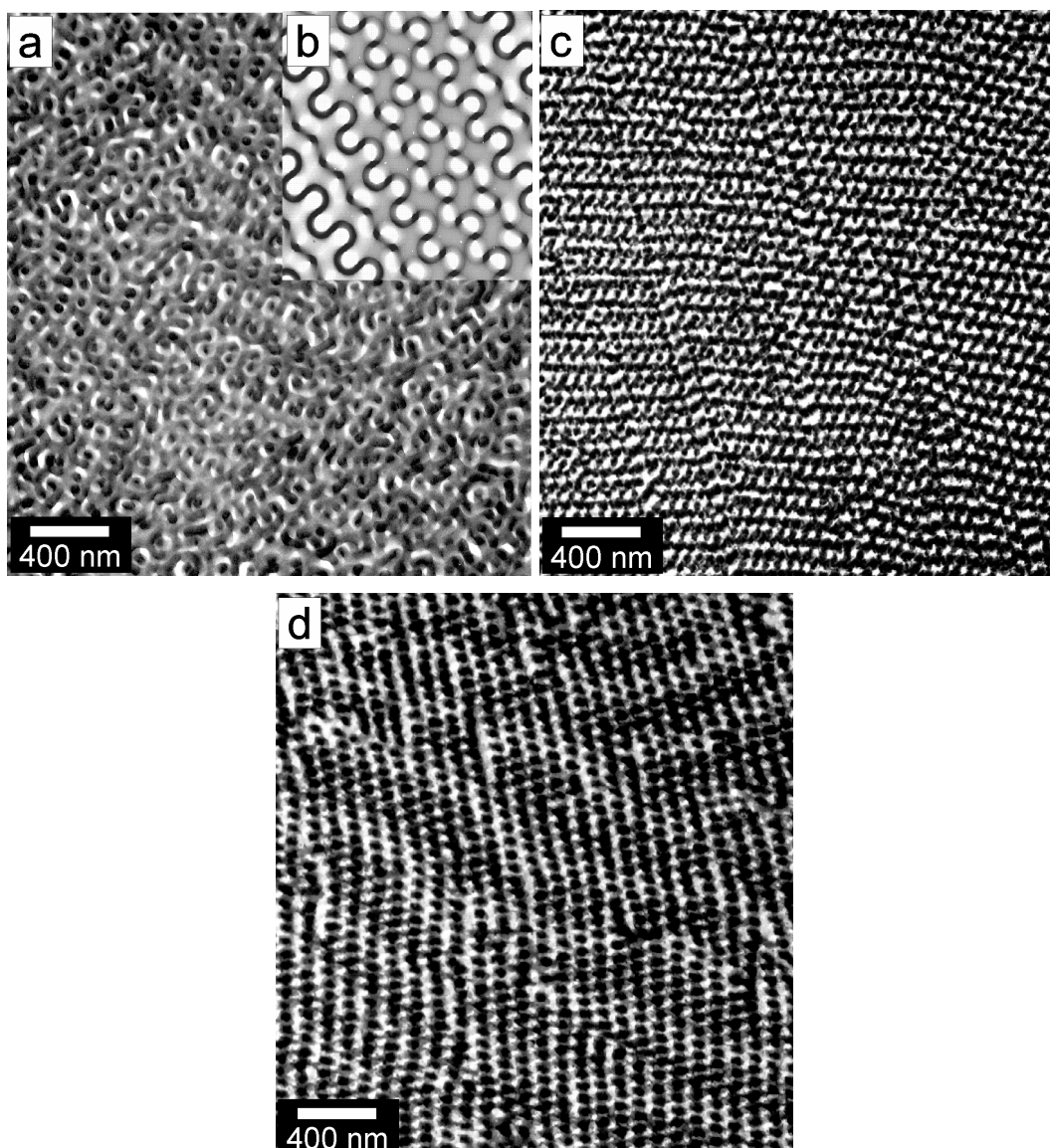
Figure 2: $S_{16}V_{21}T_{63}^{140}$ a) TEM micrograph, stained with I_2 (dark phase: P2VP); b) SAXS pattern of a 36 wt% chloroform solution (red curve) and the dry state (dark curve) ($q = 4\pi/\lambda\sin\theta$; $\lambda =$ wavelength, $2\theta =$ scattering angle), typical cylindrical reflex positions.

$S_{19}V_{25}T_{56}^{120}$: Via core-shell gyroid towards lamellae

Upon reduction of the PtBMA volume fraction, the microdomain structure changes. Fig. 3a, c and d show TEM micrographs taken at different spots of the sample. Three different structures can be identified: The structure shown in Fig. 3a can best be interpreted as a gyroid structure. For comparison, in Fig. 3b we show simulation results of the [1.08;0.84;2.04] projection of the cubic lattice of a double-gyroid structure [21,22]. Note that the presentation of the Miller indices in non-integer numbers is given to show that the observed projection is not exactly the [112] projection, but very close to that. In Fig. 3c three-fold projections (stripe-like pattern) are found while Fig. 3d shows four-fold projections (pearl-like structure). In Figures 3c and d staining was achieved with RuO_4 , while in Fig. 3a I_2 was used. In Fig. 3e, the corresponding SAXS pattern is shown. The pattern is rather complex and may be interpreted as a superposition of scattering patterns resulting from at least two coexisting structures. The three maxima with relative positions of 1 : 2 : 3 are typical for a lamellar structure. Additionally, an assignment of the scattering maxima of a gyroid morphology can be discussed under the assumption that the shoulder at the $\sqrt{3}$ -position is corresponding to the [211]-reflection. The relative ratios of the maxima of a gyroid morphology are $\sqrt{3} : \sqrt{4} : \sqrt{7} : \sqrt{10} : \sqrt{11}$. The scattering patterns of gyroid morphologies have been discussed before [23,24].

We assume that parts of the material form a core-shell-gyroid with PS-cores surrounded by P2VP

shells embedded within a PtBMA matrix. Figures 3c and d show a preferential direction of the stripe-like and pearl-like structures. This could cause the lamellar arrangement of the scattering maxima in the SAXS profile. We anticipate the coexistence of perforated lamellae with PtBMA channels (matrix component) connecting between two sheets of PtBMA in a lamellar structure. Up to now the morphology of perforated lamellae has only been found in diblock copolymers [25,26], and in blends of ABC and AD block copolymers [27]. From self-consistent field theory it follows that perforated lamellae are not stable in the case of diblock copolymers [28]. Recently, this result has been verified experimentally for a number of diblock copolymers, including poly(styrene)-*b*-polyisoprene (PS-*b*-PI), poly(styrene)-*b*-poly(2-vinylpyridine) (PS-*b*-P2VP), and poly(ethylene oxide)-*b*-poly(ethyl ethylene) (PEO-*b*-PEE) [26,29,30,31,32,33]. In these cases a transition from perforated lamellae to a bicontinuous gyroid structure was observed upon isothermal annealing. Whether the perforated lamellae may be stable in the case of ABC triblock terpolymers or not, remains unclear up to now.



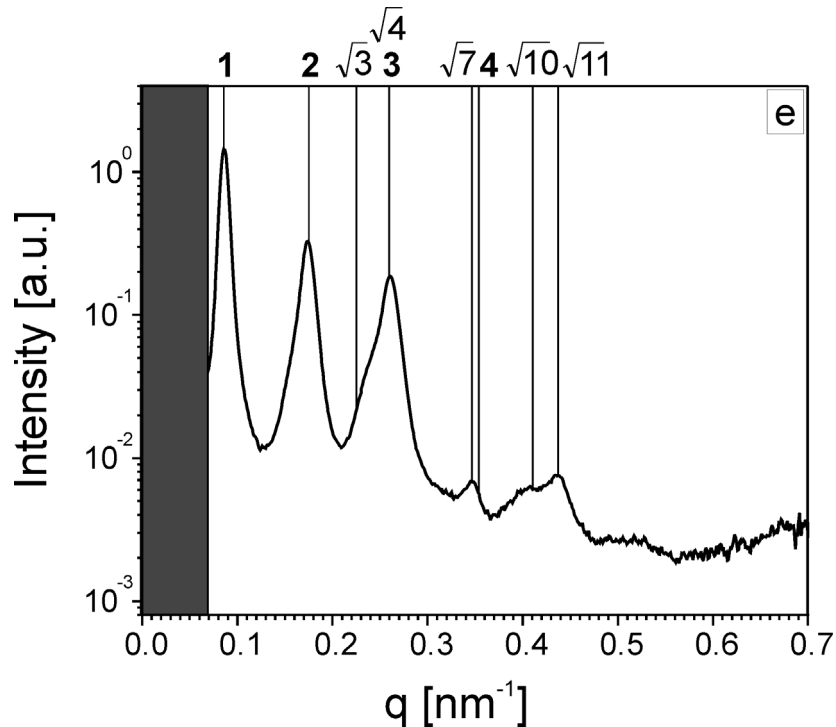


Figure 3: $S_{19}V_{25}T_{56}^{120}$ a), c) and d) TEM micrographs; a) stained with I_2 (dark phase: P2VP); c) and d) stained with RuO_4 (bright phase: PtBMA, dark phase: PS / P2VP; b) TEMsim simulation of the “[1.08;0.84;2.04]” projection (dark matrix, translation 0.48, thickness 0.35) [21,22]; e) SAXS ($q = 4\pi/\lambda \sin\theta$; $\lambda =$ wavelength, $2\theta =$ scattering angle), reflex positions typical for a lamellar (bold-faced printed figures) and a gyroid structure (as [211] reflection).

$S_{30}V_{39}T_{31}^{77}$: Lamellae

Further reduction of the PtBMA volume fraction leads to the formation of a lamellar microdomain structure. This can be seen in Fig. 4a, which shows a TEM micrograph after staining with I_2 . In this case, all three block components can be distinguished: P2VP appears as dark phase, the thick bright phase can be assigned to PS and the thinner phase can be assigned to PtBMA, as the latter is expected to shrink in volume due to damage in the electron beam. Shrinkage of methacrylate microdomains to less than half of the expected value have been reported [9]. The corresponding SAXS pattern of a $S_{30}V_{39}T_{31}^{77}$ sample is shown in Fig. 4b. Higher order reflections appear at integer multiples of the first order peak characteristic for a lamellar structure. However, the peak intensities of the first and third order peak are rather small. This may be due to the rather small electron density contrast between the two end blocks PS and PtBMA and the same domain sizes of PS and PtBMA for this composition. If PS and PtBMA were not distinguished in the SAXS measurement, the lamellar spacing would appear to be only half of the actual triblock terpolymer periodicity and peaks would appear at positions [200], [400], ... The SAXS pattern exhibited in Fig. 4b can therefore be interpreted as a superposition of the actual triblock terpolymer scattering pattern and a (stronger) “diblock copolymer” scattering pattern of only half the characteristic spacing.

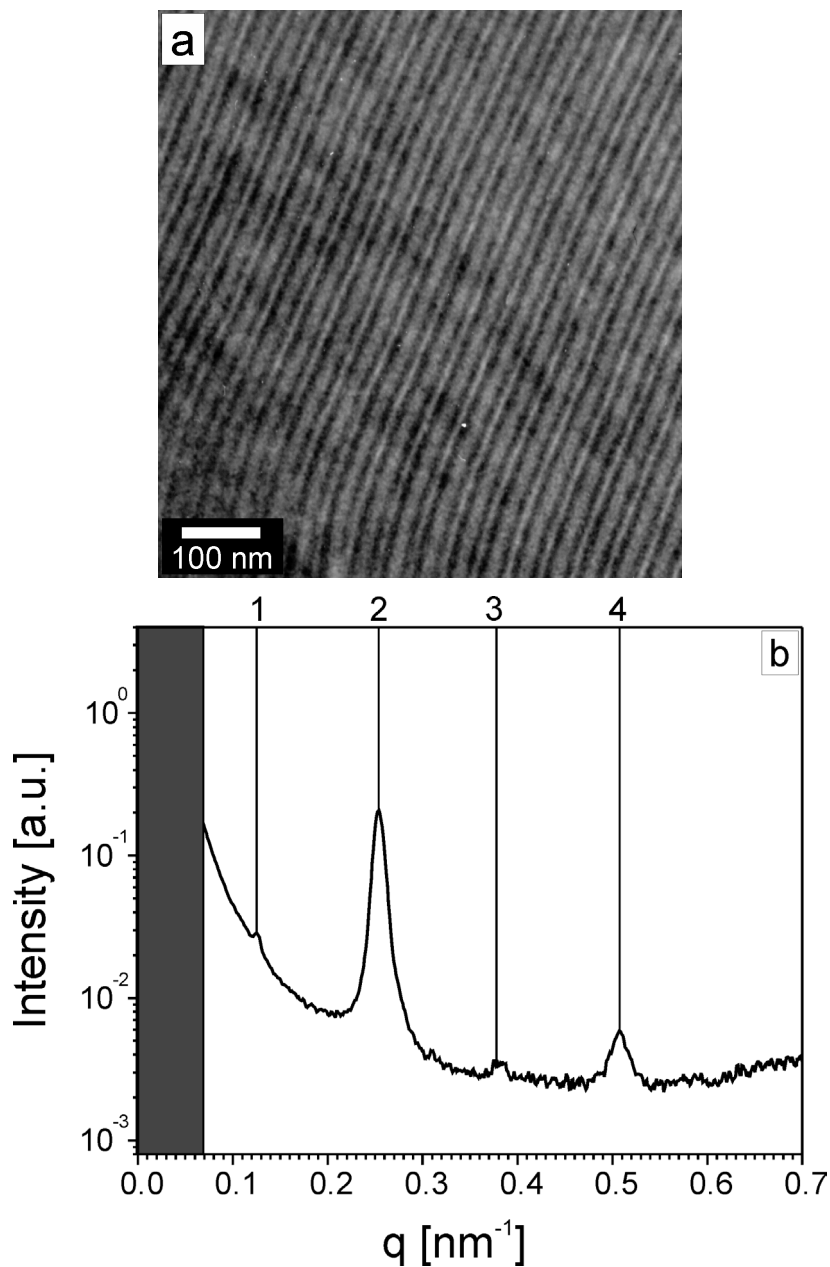


Figure 4: $S_{30}V_{39}T_{31}^{77}$ a) TEM micrograph, stained with I_2 (dark phase: P2VP); b) SAXS ($q = 4\pi/\lambda\sin\theta$; $\lambda =$ wavelength, $2\theta =$ scattering angle), typical lamellar reflex positions.

$S_{32}V_{42}T_{26}^{70}$: Gyroid

For $S_{32}V_{42}T_{26}^{70}$ both TEM and SAXS exhibit a gyroid morphology. The structure in Fig. 5a can be compared to the TEMsim simulation of the [112] projection shown in Fig. 5b [21,22]. The marked positions in the SAXS profile shown in Fig. 5c are in agreement to a cubic lattice under the assumption that the first peak corresponds to the [211] reflection. From the available data it cannot be unambiguously distinguished whether the material forms a gyroid structure consisting of interpenetrating tripod networks of the two endblocks, or if it forms yet another core-shell gyroid.

However, in view of the other structures found in this series we assume the latter: An inverse core-shell-gyroid with PtBMA cores surrounded by a P2VP shell embedded within a PS matrix.

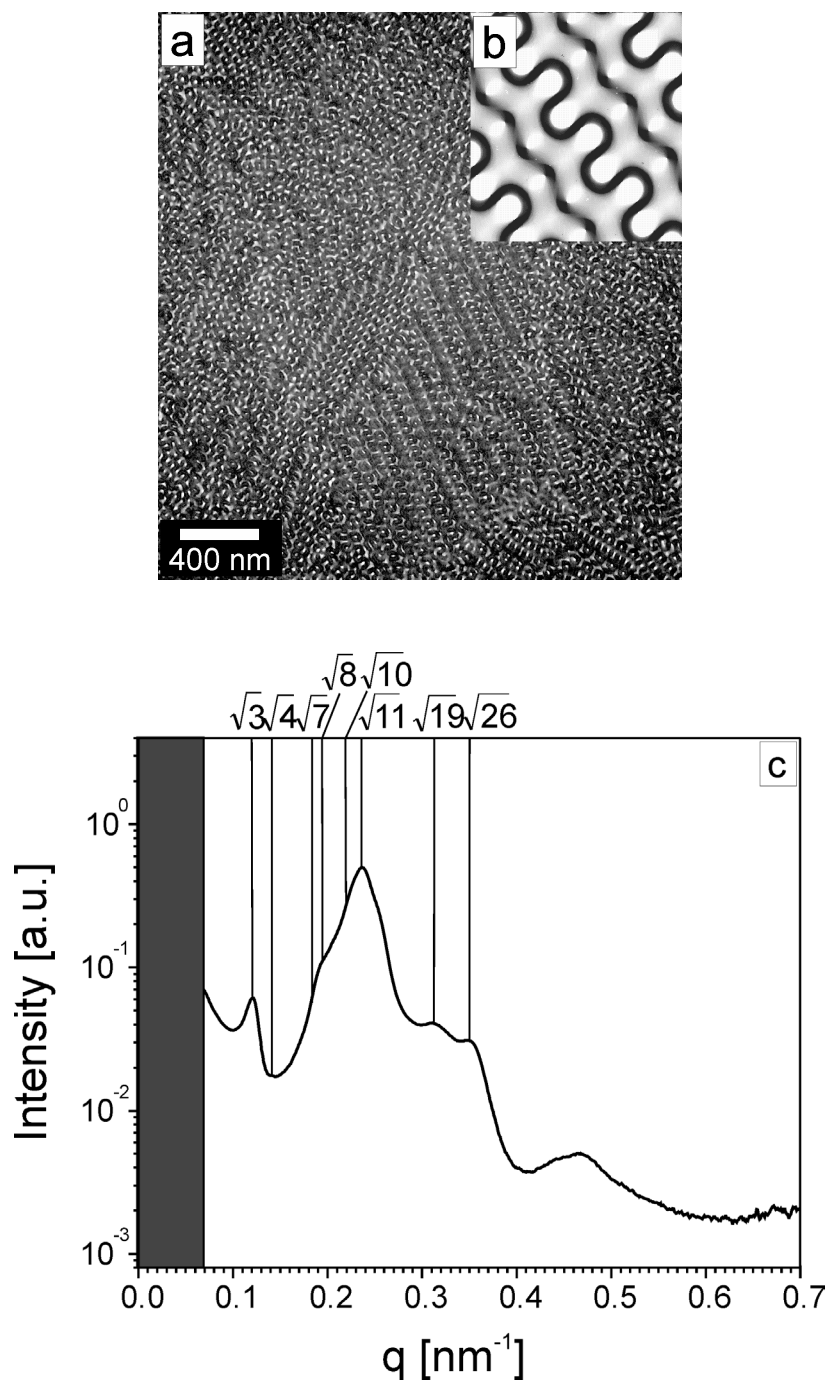


Figure 5: $S_{32}V_{42}T_{26}^{70}$ a) TEM micrograph, stained with I_2 (dark phase: P2VP); b) TEMsim simulation of the [112] projection (dark matrix, translation 0, thickness 0.33) [21,22]; c) SAXS ($q = 4\pi/\lambda \sin \theta$; $\lambda =$ wavelength, $2\theta =$ scattering angle), typical gyroid reflex positions.

$S_{37}V_{55}T_8^{78}$: Undulated lamellae

Fig. 6a shows a TEM micrograph of a $S_{37}V_{55}T_8^{78}$ sample after staining with I_2 . The dark phase corresponds to P2VP. The structure can be described as undulated lamellae. There are small bright

dots of PtBMA (minority component) within the P2VP phase, which seem to cause the undulation of the lamellae. In accordance with the SAXS pattern (Fig. 6b) which exhibit a hexagonal cylindrical structure ($1 : \sqrt{3} : 2 : \sqrt{7} : 3$), we assume that the PtBMA minority phase forms hexagonally arranged cylinders within the P2VP sheets of a lamellar phase. Note that the hexagonal packing of the cylinders is most likely due to the composition. A similar morphology was found before for a poly(ethylene-*alt*-propylene)-*block*-poly(ethyl ethylene)-*block*-poly(styrene) triblock terpolymer, where the PS cylinders were arranged on a non-hexagonal lattice [7], and in an ABC miktoarm star terpolymer [34].

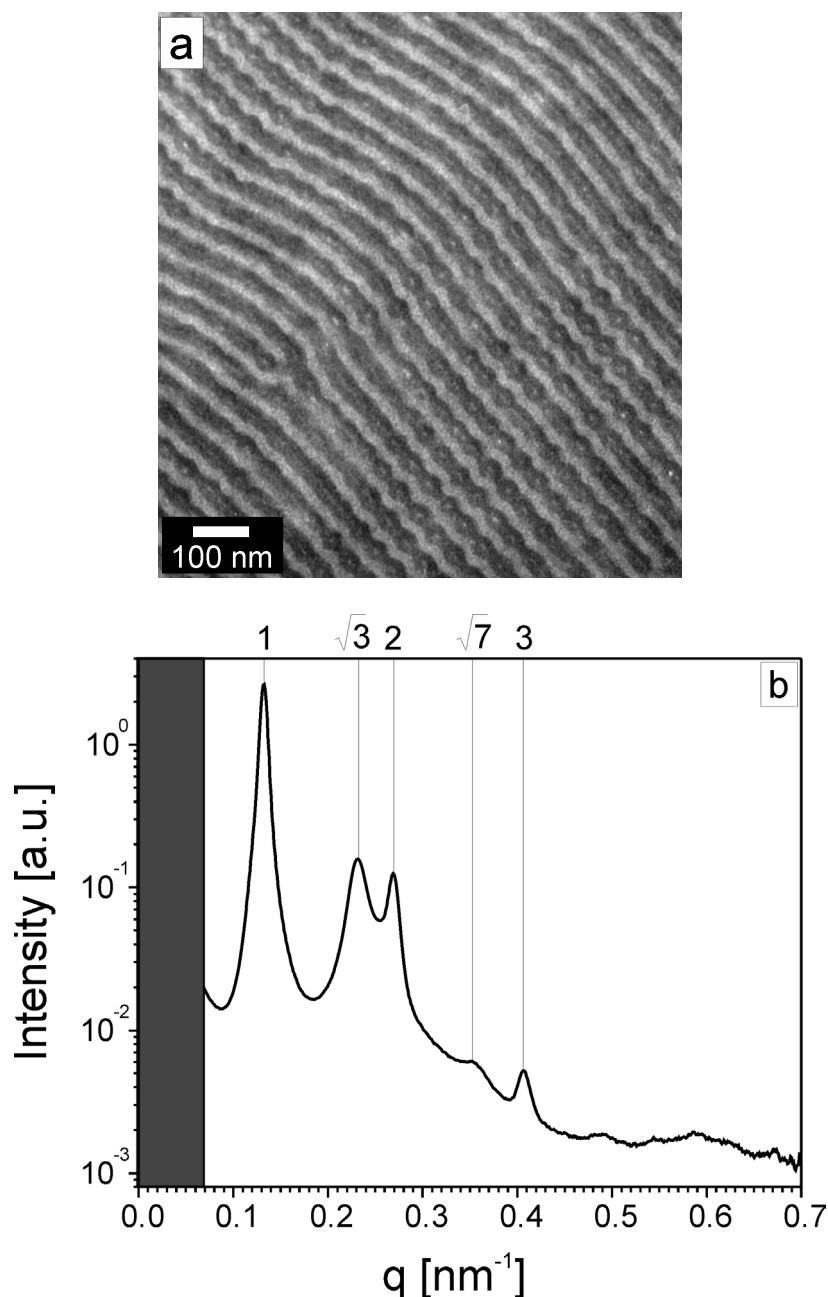


Figure 6: $S_{37}V_{55}T_8$ a) TEM micrograph, stained with I_2 (dark phase: P2VP); b) SAXS ($q = 4\pi/\lambda\sin\theta$; $\lambda =$ wavelength, $2\theta =$ scattering angle), typical lamellar and cylindrical reflex positions.

$S_{38}V_{56}T_6^{76}$: „Diblock“ Gyroid

The polymer with the smallest amount of PtBMA, $S_{38}V_{56}T_6^{76}$, again shows a gyroid morphology. The structure in the micrographs in Fig. 7a and b can be related to Fig. 5b and the SAXS profile in Fig. 7c shows two maxima in the relation of $\sqrt{3} : \sqrt{4}$. Due to the small molecular weight of PtBMA we may assume that the two endblocks mix. Table 2 summarizes the solubility parameters (δ), which are used to estimate the corresponding segmental interaction parameters (χ) according to

$$\chi_{XY} = \frac{V}{RT}(\delta_X - \delta_Y)^2$$

with V being the segmental volume (100 cm³/mol). The different χ -parameters are: $\chi_{SV} \approx 0.08$, $\chi_{ST} \approx 0.025$, $\chi_{VT} \approx 0.13$. Estimates of χN indicate that at these rather low molecular weights the block copolymer is located in the weak segregation limit WSL [35].

Table 2: Solubility (δ) parameters at 298 K

Polymer	δ [MPa ^{1/2}] [38,39]
Poly(styrene) (S)	18.5
Poly(2-vinylpyridine) (V)	20.4 [40]
Poly(<i>tert</i> -butyl methacrylate) (T)	18.0

Therefore we may assume that an AB diblock or ABA triblock-like gyroid phase forms with only two interpenetrating mixed phases of PS/PtBMA separated by P2VP. Due to the relatively short blocks of PS and PtBMA the respective χN is rather low ($\chi N_{ST} \approx 7.7$ [36]). Diblock copolymers with such a degree of incompatibility would be disordered. Due to a mixing of the outer blocks there is a gain of conformational entropy of the middle block, which leads to an additional lowering of the free energy [37]. Alternatively, also a miscibility between P2VP and PtBMA seems to be possible. Here $\chi N_{VT} \approx 63$ and the relative volume fraction of PtBMA is $\phi = 0.065$. Considering the asymmetric composition, a χN value about 70 should be expected for the transition from the disordered to an ordered phase (closely packed spheres), if we consider a free diblock copolymer [35]. However, the incompatible block (PS) should lower the limiting value of χN for the disordered phase of P2VP and PtBMA. Thus, a gyroid morphology of an AB-like block copolymer, in which P2VP and PtBMA form the mixed matrix between two interpenetrating PS tripod networks seems less likely.

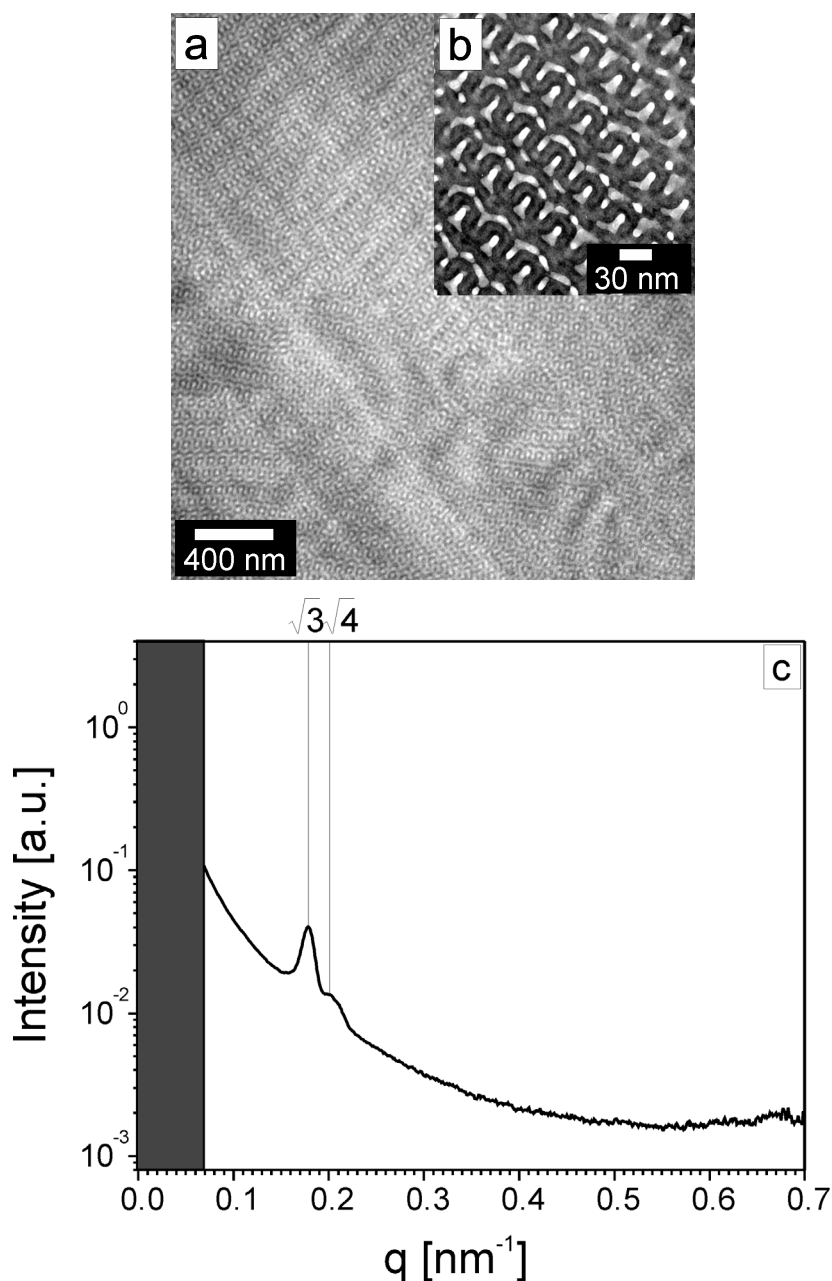


Figure 7: $S_{38}V_{56}T_6^{75}$ a) and b) TEM micrographs, stained with I_2 (dark phase: P2VP); c) SAXS ($q = 4\pi/\lambda \sin\theta$; $\lambda =$ wavelength, $2\theta =$ scattering angle), typical gyroid reflex positions.

Diblock copolymer precursor: Lamellae

In order to complete the above investigations of the systematic variation of the amount of the last block we note that TEM and SAXS data of the poly(styrene)-*b*-poly(2-vinylpyridine) precursor copolymers $S_{43}V_{57}^{52}$ and $S_{40}V_{60}^{72}$ exhibit a lamellar morphology (not shown here).

Phase Diagram of SVT triblock terpolymers

We have summarized the above results in a ternary phase diagram together with sketches of the anticipated structures (Fig. 8). The colors of these sketches were chosen such as to match the grey

values in the TEM images after staining with RuO₄: The black phase is PS, the grey phase is P2VP and the white phase is PtBMA. Along with the 6 block terpolymers discussed in detail above, all other materials have been entered into the phase diagram as well.

With decreasing PtBMA volume fraction, the morphologies change from core-shell cylinders (PS core surrounded by a P2VP shell in a PtBMA matrix) via a core-shell gyroid (in coexistence to the metastable perforated lamellar phase) to a lamellar structure. In this sequence the curvature of PS/P2VP interface decreases systematically: cylinder core - gyroid core – lamellar phase. Further reduction of the PtBMA block leads yet to another gyroid structure. We believe that a tripod network of PS in a gyroid structure with two chemically different interpenetrating networks is energetically less favourable than forming the matrix in a core-shell-gyroid with PtBMA-core in a P2VP-shell ($\chi_{SV} < \chi_{VT}$). The other argument for this structure is that even with very small molecular weights of PtBMA, like in S₃₅V₅₂T₁₃⁸² we receive the same characteristic results from TEM and SAXS investigations. The polymers with the smallest amounts of PtBMA exhibit the following morphologies: undulated lamellae (PtBMA cylinders within P2VP sheets of a lamellar structure) and a “diblock gyroid” structure. In this sequence the curvature of the P2VP-PtBMA decreases. Finally the diblock precursor shows a lamellar structure which is in accordance to previous investigations [31].

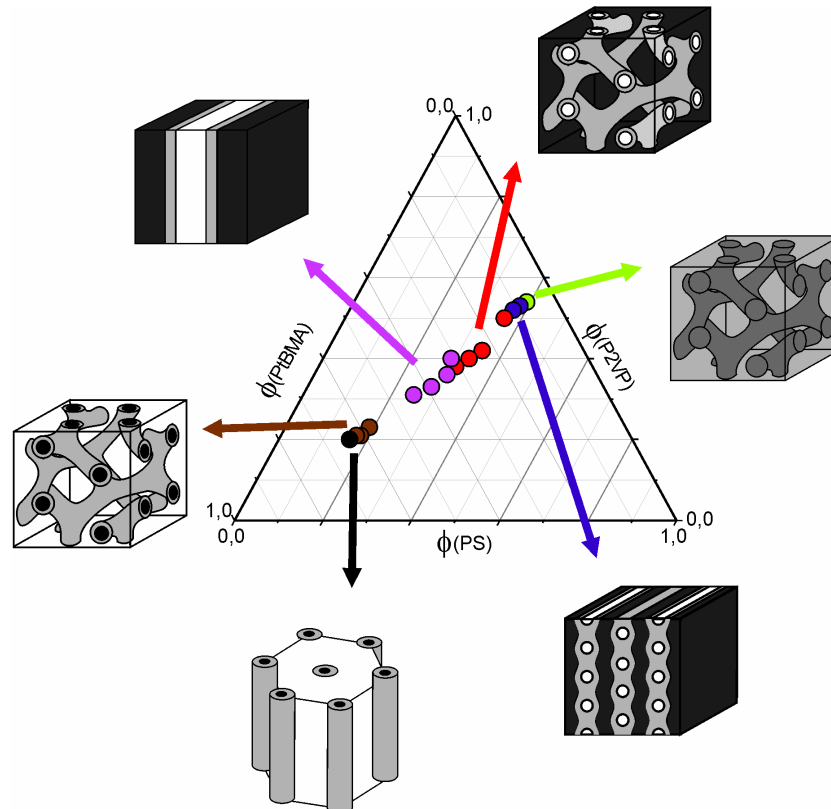


Figure 8: Phase diagram of synthesized SVT block terpolymers.

We note in passing that the well-developed inverse core shell gyroid structure observed in the $S_{32}V_{42}T_{26}^{70}$ polymer may be of potential interest for the formation of a membrane with nanoscopic pore sizes. If hydrolysis of the T cores to poly(methacrylic acid) could be achieved without altering the overall morphology of the block copolymer, a 3D continuous network of a water soluble polyelectrolyte should result. The permeability through these channels may then be controlled by the pH of the respective solution. This aspect, however, is beyond the scope of the present work.

Conclusion

The systematic variation of one block with respect to the other two blocks of an SVT triblock terpolymer reveals the following picture: Starting from a symmetric composition, i.e. all three blocks have the same length, the morphology changes from lamellae via core-shell double gyroid to core-shell cylinders upon increase of the PtBMA block. These morphologies may be considered as core-shell analogues of the corresponding diblock copolymer morphologies. Upon decrease of the PtBMA block the morphological scheme is different: A slight decrease of PtBMA leads to the formation of an inverse core-shell double gyroid, but the further decrease leads to a cylinder-in-lamellae morphology, which does not have an analogue in diblock copolymers. The reason for the formation of this morphology is most likely the asymmetry of the interactions between the adjacent blocks involved. The competition of different interactions in combination with the composition is responsible for this behavior. A similar transition from a core-shell double gyroid to a cylinder-in-lamellae morphology has also been observed for poly(ethylene-alt-propylene)-*block*-poly(ethyl ethylene)-*block*-poly(styrene) triblock terpolymer with comparable compositions. Further decrease of the PtBMA block finally leads to a morphology comparable to binary block copolymers, where only two different microphases can be distinguished. This is due to the vanishing repulsion between the two outer blocks in combination with an entropic gain of the middle block. In future work the thin film behavior of these block terpolymers will be investigated in order to set up a relationship between bulk and thin film morphologies.

Acknowledgement

The authors thank Astrid Göpfert and Carmen Kunert for their skilful help with the TEM measurements. In addition we thank Volker Urban (ESRF, Grenoble, France) for his assistance during the SAXS measurements. We thank M. Gradzielski for helpful discussions. We are grateful to the ESRF for financial support and provision of synchrotron beam time. This work was carried out in the framework of the *Sonderforschungsbereich 481* funded by the *Deutsche Forschungsgemeinschaft* (DFG).

References

- [1] Stadler R, Auschra C, Beckmann J, Krappe U, Voigt-Martin I, Leibler L. *Macromolecules* 1995; 28: 3080.
- [2] Bates FS, Fredrickson, GH. *Physics Today* 1999; 52: 32.
- [3] Abetz V. Block Terpolymers, Ternary Triblocks In: Kroschwitz, JI, editor. *Encyclopedia of Polymer Science and Technology*, John Wiley & Sons, Inc., 3rd ed., 2003, Vol. 1, p. 482-523.
- [4] Mogi Y, Nomura M, Kotsuji H, Ohnishi K, Matsushita Y, Noda I. *Macromolecules* 1994; 27: 6755.
- [5] Hückstädt H, Göpfert A, Abetz V. *Polymer* 2000; 41: 9089.
- [6] Breiner U, Krappe U, Abetz V, Stadler R. *Macromol. Chem. Phys.* 1997; 198: 1051.
- [7] Neumann C, Loveday DR, Abetz V, Stadler R. *Macromolecules* 1998; 31: 2493.
- [8] Shefelbine MA, Vigild ME, Matsen MW, Hajduk D, Hillmyer MA, Cussler EL, Bates FS. *J. Am. Chem. Soc.* 1999; 121: 8457.
- [9] Abetz V, Goldacker T. *Macromol. Rapid Commun.* 2000; 27: 6755.
- [10] Elbs H, Fukunaga K, Stadler R, Sauer G, Magerle R, Krausch G. *Macromolecules* 1999; 32: 1204.
- [11] Böker A, Müller AHE, Krausch G. *Macromolecules* 2001; 34: 7477.
- [12] Elbs H, Drummer C, Abetz V, Hadziioannou G, Krausch G. *Macromolecules* 2001; 34: 7917.
- [13] Fukunaga K, Hashimoto T, Elbs H, Krausch G. *Macromolecules* 2002; 35: 4406.
- [14] Elbs H, Drummer C, Abetz V, Krausch G. *Macromolecules* 2002; 35: 5570.
- [15] Krausch G. *Mat. Sci. Eng. Rep.* 1995; 14: 1.
- [16] Fasolka MJ, Mayes AM. *Ann. Rev. Mat. Res.* 2001; 31: 323.
- [17] Bailey TS, Pham HD, Bates FS. *Macromolecules* 2001; 34: 6994.
- [18] Giebeler E, Stadler R. *Macromol. Chem. Phys.* 1997; 198: 3815
- [19] Sawyer LC, Grubb DT. *Polymer Microscopy*, 2nd ed. London: Chapman & Hall, 1996.
- [20] Fit2D: <http://www.esrf.fr/computing/scientific/FIT2D>.
- [21] TEMsim: <http://www.msri.org/publications/sgp/jim/software/temsim/index.html>.
- [22] Hückstädt H, Goldacker T, Göpfert A, Abetz V. *Macromolecules* 1994; 27: 6755.
- [23] Matsen MW. *J.Chem.Phys.* 1998; 108: 785.
- [24] Garstecki P, Holyst R. *Phys.Rev.E* 2001; 64: 021501-1.
- [25] Hashimoto T. *Macromolecules* 1992; 25: 1433.

- [26] Förster S, Khandpur AK, Zhao J, Bates FS, Hamley IW, Ryan AJ, Bras W. *Macromolecules* 1994; 27: 6922.
- [27] Goldacker T. PhD Thesis, University of Bayreuth 1999.
- [28] Matsen MW, Bates FS. *J. Chem. Phys.* 1997; 106: 2436.
- [29] Hajduk DA, Takenouchi H, Hillmyer MA, Bates FS, Vigild ME, Almdal K. *Macromolecules* 1997; 30: 3788.
- [30] Khandpur AK, Förster D, Bates FS, Hamley IW, Ryan AJ, Bras W, Almdal K, Mortensen K. *Macromolecules* 1996; 28: 8796.
- [31] Schulz MF, Khandpur AK, Bates FS, Almdal K, Mortensen K, Hajduk DA, Gruner SM. *Macromolecules* 1996; 29: 2857.
- [32] Hillmyer MA, Bates FS, Almdal K, Mortensen K, Ryan AJ, Faiclough JPA. *Science* 1996; 271: 976.
- [33] Hillmyer MA, Bates FS. *Macromolecules* 1996; 29: 6994.
- [34] Hückstädt H, Göpfert A, Abetz V. *Macromol. Chem. Phys.* 2000; 201: 296.
- [35] Matsen MW, Bates FS. *Macromolecules* 1996; 29: 1091.
- [36] Schubert DW, Stamm M, Müller AHE. *Polymer Eng. Sci.* 1999; 39: 1501.
- [37] Abetz V, Stadler R, Leibler L. *Polymer Bulletin* 1996; 37: 135.
- [38] Barton AF. *CRC Handbook of Polymer Liquid Interaction Parameters and Solubility Parameters*, Boca Raton: CRC Press, 1990.
- [39] Brandrup J, Immergut EH. *Polymer Handbook*, 3rd ed. New York: Wiley, 1989.
- [40] Lescanec RL, Fetters LJ, Thomas EL. *Macromolecules* 1998; 31: 1680.

5.2. Curriculum vitae

Date of Birth	19 th of January 1978, in Cologne, Germany
Parents	Karin and Dr. Heinz-Walter Ludwigs one sister, 19 years old
Scholar education	1984-1988: primary school in Bayreuth 1988-1997: high school at Bayreuth (Graf-Münster-Gymnasium) 1997: final examination
Scientific background	10/97 – 02/02: study of chemistry, University of Bayreuth 09/99– 10/99: industrial training at Bayer AG, Leverkusen 06/01 – 07/01: Diploma, final examination 08/01 – 02/02: Diplomarbeit: 'Microphase behavior of poly(styrene)- <i>b</i> -poly(2-vinylpyridine)- <i>b</i> -poly(<i>tert</i> -butyl methacrylate) (SVT) triblock terpolymers'; cooperative study between physical chemistry (Prof. Dr. G. Krausch) and macromolecular chemistry (Prof. Dr. A. Müller) including several stays at the European Synchrotron Radiation Facility (ESRF, Grenoble, France); award of the 'Otto-Warburg-foundation' for the fastest studies in chemistry in 2002. since 03/02: PhD thesis at the department of physical chemistry, Prof. Dr. G. Krausch, subject: 'Complex phase behavior of SVT triblock terpolymers in thin films' 04/02 – 07/02: stay at the CNRS (Centre National de la Recherche Scientifique) Mulhouse, France; subject: 'Thin film phase behavior of poly(styrene)- <i>b</i> -poly(benzyl-L-glutamate) diblock copolymers', cooperation project with Prof. Dr. G. Reiter, CNRS Mulhouse and Prof. Dr. M. Antonietti, Max-Planck-Institut Golm/Berlin

03/03: stay at NIST Gaithersburg, USA; subject: ‘Combinatorial gradient techniques’, cooperation project with Dr. A. Karim and Dr. M. Fasolka

Languages English and French

Activities Piano, saxophone, choir;
1996 – 2003 jobbing as sales assistant for Fa. Steingraeber & Söhne, Piano
manufactory, Bayreuth

Bayreuth, May 2004

5.3. List of publications

The following publications are enclosed in this PhD thesis:

- Ludwigs, S.; Böker, A.; Voronov, A.; Rehse, N.; Magerle, R.; Krausch, G. 'Self-assembly of functional nanostructures from ABC triblock copolymers' *Nature Materials* **2003**, 2, 744.
- Ludwigs, S.; Schmidt, K.; Stafford, C.; Fasolka, M.; Karim, A.; Amis, E.; Magerle, R.; Krausch, G. 'Combinatorial mapping of the phase behavior of ABC triblock terpolymers in thin films: Experiments' *submitted to Macromolecules*.
- Ludwigs, S.; Zvelindovsky, A.V.; Sevink, G.J.A.; Krausch, G.; Magerle, R. 'Phase behavior of ABC triblock terpolymers in thin films: Simulations' *submitted to Macromolecules*.
- Ludwigs, S.; Schmidt, K.; Krausch, G. 'pH-dependent nanostructures in thin films' *to be submitted*.

Within the scope of my Diploma and my PhD thesis the following publications have been additionally published.

- Ludwigs, S.; Böker, A.; Abetz, V.; Müller, A.H.E.; Krausch, G. 'Phase behavior of linear poly(styrene)-*block*-poly(2-vinylpyridine)-*block*-poly(*tert*-butyl methacrylate) triblock terpolymers' *Polymer* **2003**, 44, 6815.
- Ludwigs, S.; Böker, A.; Abetz, V.; Müller, A. H. E.; Krausch, G. 'Self-assembly of poly(styrene)-*block*-poly(2-vinylpyridine)-*block*-poly(*tert*-butyl methacrylate) triblock copolymers in bulk and in thin films' *Polym. Prepr., Am. Chem. Soc., Div. Polym. Chem.* **2002**, 43(2), 377.
- Ludwigs, S.; Voronov, A.; Elbs, H.; Rehse, N.; Knoll, A.; Horvat, A.; Tsarkova, L.; Magerle, R.; Krausch, G. 'Selbstorganisation von ABA und ABC Dreiblockcopolymeren in dünnen Filmen' *Macr. Chem. Phys.* **2003**, 2004, F19.
- Ludwigs, S.; Krausch, G.; Losik, M.; Schlaad, H.; Antonietti, M.; Reiter, G. 'Thin film phase behavior of poly(styrene)-*block*-poly(γ -benzyl-L-glutamate) diblock copolymers' *to be submitted*.

- Böker, A.; Elbs, H.; Hänsel, H.; Knoll, A.; Ludwigs, S.; Zettl, H.; Urban, V.; Abetz, V.; Müller, A. H. E.; Krausch, G. ‘Microscopic mechanisms of electric-field induced alignment of block copolymer microdomains’ *Phys. Rev. Lett.* **2002**, 89, 1319.
- Böker, A.; Elbs, H.; Hänsel, H.; Knoll, A.; Ludwigs, S.; Zettl, H.; Zvelindovsky, A.V.; Sevink, G. J. A.; Urban, V.; Abetz, V.; Müller, A. H. E.; Krausch, G. ‘Electric field induced alignment of concentrated block copolymer solutions’ *Macromolecules* **2003**, 36, 8078.
- Böker, A.; Elbs, H.; Hänsel, H.; Knoll, A.; Ludwigs, S.; Zettl, H.; Urban, V.; Abetz, V.; Müller, A. H. E.; Krausch, G. ‘Macroscopic alignment of concentrated block copolymer solutions in electric fields’ *Polym. Prepr., Am. Chem. Soc., Div. Polym. Chem.* **2002**, 43(2), 350.

5.4. Presentations at international conferences

- DPG, Regensburg, March 2002, *poster presentation*
‘The phase behavior of PS-*b*-P2VP-*b*-PtBMA triblock copolymers in bulk and in thin films’
- Pattern Formation by Molecular Self-Organization at Interfaces, Berlin, March 2002, *poster presentation*
‘Phase behavior of PS-*b*-P2VP-*b*-PtBMA triblock copolymers in bulk and in thin films’
- Young Researchers Meeting Polynano, Mulhouse, June 2002, *oral presentation*
‘Swelling and crystallization of diblock copolymers’
- Molecular Organization for Nanosystems, Kloster Banz, February 2003, *poster presentation*
‘Nanoporous membranes from PS-*b*-P2VP-*b*-PtBMA triblock copolymers’
Poster award
- Makromolekulares Kolloquium, Freiburg, February 2003, *poster presentation*
‘Selbstorganisation von ABA und ABC Dreiblockcopolymeren in dünnen Filmen’

- DPG, Regensburg, March 2003, *poster presentations*
‘Nanoporous membranes from PS-*b*-P2VP-*b*-PtBMA triblock copolymers’
‘Structure formation of poly(styrene)-*block*-poly(γ -benzyl-L-glutamate) diblock copolymers in thin films’
- Minerva Students Symposium, Naurod, April 2003, *oral presentation*
‘Complex nanostructures from ABC triblock terpolymers in thin films’
- Bayreuther Polymer Symposium, Bayreuth, September 2003, *poster presentation*
‘Self-assembly of ABC triblock terpolymers in thin films’
- DPG, Regensburg, March 2004, *oral presentation*
‘Combinatorial mapping of PS-*b*-P2VP-*b*-PtBMA triblock copolymers in thin films’
- ACS, Anaheim, March 2004, *oral presentation in replacement of Prof. G. Krausch*
‘pH-responsive nanostructures from ABC triblock copolymers’

Danksagung

Ich möchte mich bei allen bedanken, die auf vielfältige Weise zum Gelingen dieser Arbeit beigetragen haben, insbesondere bei:

- Herrn Prof. Dr. G. Krausch für die interessante und vielseitige Aufgabenstellung, seine wertvollen Anregungen und seine stete Diskussionsbereitschaft, auch im Hinblick auf mögliche Zukunftsperspektiven. Desweiteren danke ich ihm dafür, dass er mich auf viele interessante Tagungen geschickt hat.
- Herrn Priv.-Doz. Dr. R. Magerle für unzählige Ratschläge und viele Diskussionen, vor allem bei der Auswertung der Simulationsdaten.
- Herrn Dr. A. Karim, Herrn Dr. M. Fasolka und Herrn Dr. C. Stafford für die Betreuung vor Ort am NIST, USA.
- Herrn Dr. A. V. Zvelindovsky und Herrn Dr. G. J. A. Sevink von der Universität Leiden für die Bereitstellung des MesoDyn Codes und Diskussionen über Simulationsergebnisse.
- Frau Kristin Schmidt für die gute Zusammenarbeit im Rahmen ihrer Diplomarbeit.
- Herrn Nicolaus Rehse und Frau Andriana Horvat für die Einarbeitung in die MesoDyn Software.
- Frau Marina Lysetska für die Einführung in AFM-Messungen in der wässrigen Phase.
- Herrn Dr. Armin Knoll, Herrn Nicolaus Rehse, Herrn Helmut Hänsel, Herrn Frank Schubert und Herrn Heiko Zettl für ihre stete Hilfsbereitschaft.
- Frau Clarissa Abetz für REM Messungen, Frau Carmen Kunert für TEM-Messungen, Herrn Werner Reichstein für die Einführung ins Ellipsometer und Frau Christine Thunig (PCI) für die Unterstützung bei den ODT-Messungen in CHCl_3 .
- Herrn Dr. W. Häfner und Herrn Dipl. Ing. Markus Hund für die Ratschläge beim Aufbau einer Filmdickengradientenapparatur.
- Frau Sibylle Zimmermann für die Hilfe in allen organisatorischen und bürokratischen Belangen.
- allen Mitgliedern des Arbeitskreises PCII, auch den hier nicht namentlich erwähnten, für die hervorragende Arbeitsatmosphäre.
- Herrn Prof. Dr. A. Müller und seiner Arbeitsgruppe für die Einweisung in polymerchemische Arbeitsgebiete während meiner Diplomarbeit.
- meiner Familie für ihre immerwährende Unterstützung.

Erklärung

Hiermit erkläre ich, dass ich die Arbeit selbständig verfasst und keine anderen als die angegebenen Quellen und Hilfsmittel benutzt habe.

Ferner erkläre ich, dass ich nicht anderweitig mit oder ohne Erfolg versucht habe, eine Dissertation einzureichen oder mich einer Doktorprüfung zu unterziehen.

Bayreuth, den 14. 05. 04

